UNIVERSITÀ DEGLI STUDI DI NAPOLI "FEDERICO II"

SCUOLA POLITECNICA E DELLE SCIENZE DI BASE

AREA DIDATTICA DI SCIENZE MATEMATICHE, FISICHE E NATURALI

TESI MAGISTRALE IN BIOLOGIA

An *in-vitro* study of radiation-induced DNA damage in the context of the Boron-Neutron Capture Therapy (BNCT): a comparison with X-rays on osteosarcoma and glioblastoma

Studio *in-vitro* del danno radioindotto al DNA nell'ambito della Boron-Neutron Capture Therapy (BNCT): un confronto con i raggi X su osteosarcoma e glioblastoma

Relatore:
Prof. Mimmo Turano

Candidata:
Alessia Fornaro
Matr. N92002538

Correlatori:
Prof. Lorenzo Manti
Prof.ssa Silva Bortolussi

ANNO ACCADEMICO 2023/2024

Lascia che io torni a respirare,
e mai così tanto saprò apprezzare la vita.
Il vuoto che esso mi lascerà nel petto,
lo farò occupare tutto dal cuore.

Marina Gaddi, sul cancro al seno.

Contents

INTRODUCTION

The use of radiation began in 1895 with Wilhelm Conrad Röntgen's experiments with X-rays and Marie Curie's discovery of radioactivity [1]. From that moment, it was observed that radioactive substances, as well as man-made radiation, could also find medical applications in the treatment of tumours. It was the dawn of radiotherapy.

Today, the role of radiotherapy in the treatment of tumours is widely recognized, and new approaches are requested as radiobiological studies have deepened our knowledge on the complexity of the tumour radioresponse, particularly as is the case with resistance to conventional therapies, hence to increase the patient's quality of life and expectancy of disease-free survival. One of such alternative approaches is Boron-Neutron Capture Therapy (BNCT), which is based on the idea to preferentially and selectively deliver boron-10 to tumours and then to expose the patient to a low-energy thermal neutrons beam to trigger a capture reaction. The aim is to provide a therapeutic advantage by protecting healthy tissues and increasing the efficiency of tumour cell kill compared to conventional external beam radiotherapy based on photons/electrons. In fact, the boron-neutron capture reaction, which is ^{10}B (n,α) ^{7}Li, produces four different types of ionizing radiations: γ rays, protons, Li-nuclei and alpha particles. The latter two types of charged particles are responsible for the superior ability of BNCT to induce more lethal DNA damage and, consequently, more cancer cell death compared to conventional radiotherapy [2]. In fact, Li ions and alpha-particles are so-called high Linear Energy Transfer (LET) radiations. These particles cause DNA Double-Strand Breaks (DSBs) that are more complex in nature and hence more difficult to repair than those caused by lower LET radiation, such as photons [3].

In this thesis work, boronophenylalanine (BPA) was used as boron carrier. BPA has a phenylalanine structure that can be recognized by LAT1 amino acid transporters that are over expressed on many cancer cells. This could allow efficient cellular internalization [4].

To date, BNCT has been studied clinically in a variety of disease sites, including glioblastoma multiforme and osteosarcoma, which have been the subject of this study.

Specifically, ionizing radiation-induced DNA damage was analysed through the foci assay, in which biomarkers of DNA DSBs, that is 53BP1 and γH2AX, are used to quantify DNA damage. Histone H2AX is phosphorylated at serine139 in a region of several megabase pairs in response to DSBs and forms nuclear foci. Furthermore, 53BP1 (p53-binding protein 1) is an important DSB response protein that promotes DSB repair. The combined analysis of γH2AX and 53BP1, through the foci assay and analysis by immunofluorescence microscopy, represents a reliable experimental strategy for the analysis of DSBs [5].

The main goal of this study was therefore to analyse the damage induced by BNCT on tumour lines of rat osteosarcoma (UMR-106) and human glioblastoma (U87MG) and compare it with low-LET radiation (X-rays), in order to verify the greater effectiveness of BNCT.

This work was carried out at the Radiation Biophysics Laboratory, Physical Sciences Department, University of Naples Federico II, in collaboration with the Departments of Physics and of Clinical-Surgical, Diagnostic and Pediatric Sciences, University of Pavia. The research nuclear reactor TRIGA Mark II, located at the L.E.N.A (Laboratorio Energia Nucleare Applicata) in Pavia, was used as the neutron source to perform BNCT irradiation. The photon irradiations took place in Naples at the Radiation Biophysics Laboratory and at Istituto Nazionale Tumori "Fondazione Pascale".

This thesis consists of 4 chapters:

- Chapter 1 recalls the main concepts of the interaction between biological matter and ionizing radiation, with a particular focus on the biological effects of ionizing radiation and a new approach to study the DNA repair process through the quantification of Ionizing Radiation-Induced Foci (IRIF).

- Chapter 2 focuses on the BNCT, the neutron sources and boron carriers prevalently used in this type of radiotherapy and its applications in the treatment of glioblastoma and osteosarcoma.
- Chapter 3 describes materials and methods; specifically, the experimental setup, the sample preparation, irradiation, the experimental protocols adopted, and finally the data analysis methods employing a software for the automatic identification and quantification of IRIFs. For the latter, the optimization of different classifiers for the improvement of their count is described.
- Chapter 4 illustrates the obtained results with their discussion.

Finally, conclusions and possible future developments are discussed.

1 Interaction between biological matter and ionizing radiation

Radiobiology is the study of the effects of ionizing radiation on biological matter. In biological material, the absorption of energy from radiation may lead to excitation or ionization.

By "excitation" we mean the ability of an electron to raise a higher energy level in an atom or molecule without being ejected from the atomic shell to which it belongs.

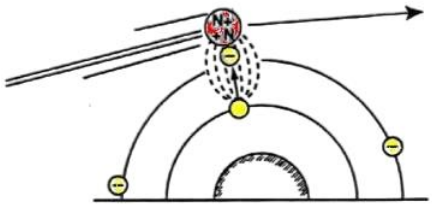

Figure 1.1 Excitation of an atom by ionizing radiation [6].

On the other hand, “ionization” is the process by which the incident radiation has sufficient energy to eject one or more electrons from the atom or molecule causing the atom to become charged (or ionized).

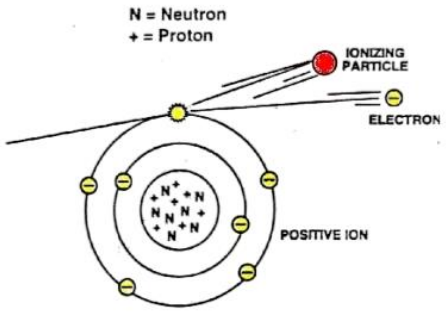

Figure 1.2 Ionization of an atom by ionizing radiation [6].

The energy dissipated per ionizing event is about 33 eV, which is more than enough to break a strong chemical bond (breakage of the commonly found C=C bond requires 4.9 eV).

Ionizing radiation includes electromagnetic radiation (X-rays and γ-rays) and particle radiation. In this work, the action of X-rays and charged particles will be analysed.

X-rays are produced in an electrical device that accelerates electrons to high energy and then stops them abruptly in a target usually made of tungsten, so that part of the kinetic energy of the electrons is converted to X-rays. X-rays may be considered as waves of electrical and magnetic energy but also as streams of photons, or "packets" of energy. The amount of energy contained in each energy packet is equal to:

$$E = h\,v$$

In which h is known as Planck's constant and v is the frequency. In radiobiology, the concept of X-rays being composed of photons is very important: in its interaction with matter, the energy is deposited in tissues and cells non-uniformly in discrete packets. Each energy packet is enough to break a chemical bond, causing biologic change. Thus, the biologic effect depends on the photon size (or packet size) of the energy [1].

Particle radiation includes electrons, protons, α-particles, neutrons, and heavy charged particles:

- *Electrons* are small and negatively charged particles that can be accelerated to high energy in electrical devices such as cyclotrons or linear accelerators and used for cancer therapy.
- *Protons* are positively charged particles. They represent a component of natural background radiation. Because of their mass, more complex accelerators are required to accelerate them. Protons have a favourable dose distribution as a function of their path in tissue, which allows them to be used in cancer therapy.
- *α-Particles* have a net positive charge and can be accelerated in large accelerators like those used for protons and they are also emitted during the decay of heavy, naturally

occurring radionuclides, such as uranium and radium. They are nuclei of helium atoms and consist of two protons and two neutrons in close association.

- *Neutrons* have no electrical charge; as a result, they cannot be accelerated in an electrical device. They are similar in mass to protons. Neutrons can be produced by the acceleration of a charged particle to high energy which then impinges on a suitable target material, but they are also emitted as a by-product of the fission of heavy radioactive atoms.
- *Heavy charged particles* are nuclei of elements, such as carbon, neon, argon, or even iron. Because some or all the planetary electrons have been stripped from them, they are positively charged and can be used in radiation therapy by accelerating them to elevated energy (thousands of millions of volts) in specialized facilities.

The process by which radiation produces damage, in its interaction with living matter, can be schematized in three different stages:

1. *Physical phase*: interaction of the particles with the electronic orbitals and consequent ionization and excitation processes. These processes are completed in extremely short times, ranging from 10^{-24} to 10^{-14}s.
2. *Chemical phase*: the ionization and excitation processes lead to a breakdown of chemical bonds with the formation of free radicals which interact with other molecules and cellular components following a series of rapid chemical reactions. These processes are completed in a few *ms* after exposure.
3. *Biological phase*: it includes all subsequent processes that affect biomacromolecules, in particular DNA, causing cellular and tissue alterations. They can manifest themselves in extremely variable times: a few hours, months, or even tens of years.

1.1 Biophysical characteristics of ionizing radiation

The biological effect of radiation depends on many factors, including radiation dose (the overall absorbed energy per unit mass) and the spatial distribution of its energy deposition events across a given volume.

The physical quantity that quantifies the energy deposition of a radiation is the *absorbed dose (D)*, defined as the ratio between the average energy ε absorbed and the mass m.

$$D = \frac{\varepsilon}{m}$$

The unit of absorbed dose is the Gray (Gy), where 1 Gy represents the unit energy absorbed per unit mass:

$$Gy = \frac{J}{kg}$$

Another important biophysical parameter is the *Linear Energy Transfer (LET)*, which measures the amount of energy (dE) transferred by an ionizing particle to the material traversed per unit distance (dl):

$$LET = \frac{dE}{dl}$$

Its units are keV/μm. Radiation can be classified into high LET (low-energy protons, α particles, and neutrons) and low LET (X-rays, γ radiation, and fast electrons). As the biological impact of radiation depends on the ionization density and its distribution along its trajectory, particles with high LET have a more deleterious impact per unit dose than the low-LET radiation, generating more complex and clustered damage.

For the same absorbed dose, the biological effect produced by the two different types of radiation is measured through the *Relative Biological Effectiveness (RBE)*, defined as follows:

$$RBE = \frac{D(reference)}{D(particle)}$$

Thus, the RBE is the ratio of the dose of the reference radiation to that of the radiation under investigation needed to induce the same level of a given effect. This parameter considers the fact that identical doses of radiation with different LET values produce different levels of biological effect (iso-effect doses).

There is a strong correlation between RBE and LET: high-LET particles, such as protons or alpha particles, have a higher RBE than low-LET radiations, like X-rays or gamma rays. This implies that high-LET particles are more effective in causing biological damage for the same absorbed physical dose.

Therefore, it is possible to make another classification of radiation, based on the damage along the track, that is between “sparsely ionizing” and "densely ionizing":

Sparsely ionizing radiation, such as x-rays and gamma rays, generates relatively few ionizations along its track. These types of radiation typically interact with matter by expelling electrons from atoms, but the ionizations are distributed over a larger volume, causing less concentrated damage along the track.

Densely ionizing radiation creates a higher density of ionizations along the track, causing more complex and clustered damage. The particles involved have a greater charge and mass compared to photons. This type of radiation tends to have a higher RBE compared to sparsely ionizing radiation, in the sense that they are more effective in causing biological damage per unit of absorbed dose. This distinction is particularly relevant in the fields of oncological radiotherapy and radioprotection.

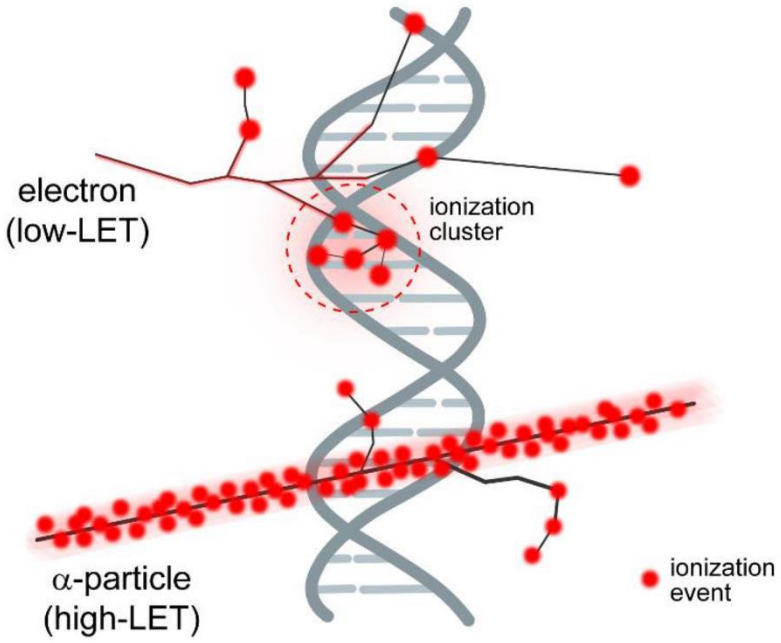

Figure 1.3 Complexity of DNA damage induced by ionizing radiation. The complexity of DNA damage induced by ionizing radiation strongly depends on the biophysical characteristics of the radiation, in particular its LET. High-LET radiation induces more complex and clustered damage than low-LET radiation [7].

1.2 Biological effects of ionizing radiation

Humans are always exposed to ionizing radiation that arise from man-made or natural sources present in the environment. The study of the effects of ionizing radiation on human health has become essential, especially with the advent of the nuclear age. Currently, radiation is extensively used in medical procedures (such as radiology, nuclear medicine, and radiotherapy), absorbed from consumer products or industrial radiation sources, and employed in various research activities. It is important to study the effects of radiation on humans so that we can use it safely.

When radiation interacts with the human body, a part or the whole of the energy may be absorbed by the cell through processes like ionization and excitation, which may impact cell normal functions. The severity of the imparted damage depends on several factors such as the nature and energy of the radiation, the total dose and dose rate, the extent of the exposed body part, the age of the exposed person, and the radiation sensitivity of the exposed organ(s). In its interaction with the human body, most of the energy from radiation is initially deposited in water molecules, and only a small part is absorbed directly by the other biomolecules. This interaction with water produces free radicals that react with biomolecules in cells, resulting in DNA and protein damage. Such damage may lead to the impairment of cell division, structural changes of the DNA visualized as chromosome aberrations, gene mutations, all such ultimately leading to cell death, defined as the loss of the cell's proliferative ability.

Radiobiological effects can be classified in terms of their occurrence likelihood as a function of dose:

- *Non-Stochastic Effects:* These include skin erythema, desquamation, necrosis, vomiting, haemorrhage, and, in extreme cases, death. These effects are deterministic in

nature and the severity increases with the increase in the dose received above a given threshold.

- *Stochastic Effects*: These effects are probabilistic and do not present a threshold dose. They may occur also as due to small exposures received over long periods of time and may lead to cancer and transmissible genetic anomalies. Their severity does not depend on dose.

Another classification of radiation effects is based on the time of their manifestation after exposure:

- *Early effects*: These may appear immediately after exposure (within a few hours to weeks). They are due to acute exposure and large doses received over a short period of time and are attributed to the depletion of cell population due to cell killing. For example, acute exposure of the whole body to around 1 Gy may lead to a reduction in lymphocyte and granulocyte counts and radiation sickness in the form of nausea and vomiting. In the dose range of 3-5 Gy, about 50% of exposed individuals may die within 60 days, showing symptoms of anaemia, infection, and high fever, knows as Haematopoietic Syndrome. At higher doses (7-10 Gy), cells in the gastrointestinal system become severely damaged leading to diarrhoea, loss of appetite, dehydration, electrolyte imbalance, weight loss and high fever, typical symptoms of Gastrointestinal Syndrome (GIS) and can cause death in 7 to 14 days. Higher doses may result in Central Nervous System (CNS) Syndrome, characterized by depression, fatigue, delirium, and coma, ultimately leading to death.
- *Late effects*: Characterized by a long latent period, these effects include condition like cancer, fibrosis in various tissues, and cataracts of the eye lens [8].

Radiation can also cause *local effects*, particularly on the skin, our body's first barrier. Immediate manifestations such as erythema and desquamation are observed, especially in radiotherapy among the most radiosensitive patients.

Additionally, radiation can induce genetic-level effects, affecting chromosomes.

1.2.1 Direct and indirect action of radiation

Radiation can be categorized as either directly or indirectly ionizing.

All charged particles are considered *directly ionizing.* If these particles have sufficient kinetic energy, they can directly alter the atomic structure of the material they are absorbed by, leading to chemical and biological changes.

On the other hand, electromagnetic radiations (such as X- and γ-rays) are *indirectly ionizing*. When absorbed by a material, they release their energy, generating charged particles capable of causing damage [1].

Radiation damage to cells can result from the direct or indirect action of radiation on DNA molecules, as illustrated in Figure 1.4:

- *Direct action* occurs when radiation directly hits the DNA molecule, ionizing and/or exciting the macromolecules in cells. This process disrupts the covalent bonds of the molecular structure, potentially leading to cell damage or death. Direct action becomes more predominant with high-LET radiations, such as α-particles, heavy ions and neutrons, and at high radiation doses [8].
- *Indirect action* involves radiation hitting water molecules and other organic molecules, producing free radicals that are able to diffuse far enough to reach and damage the critical targets [1]. Free radicals are produced by oxygen metabolism, characterized by an unpaired electron in the structure, resulting highly reactive species. The indirect

action represents most of the low-LET radiation-induced damage because water constitutes nearly 70% of the cell [8].

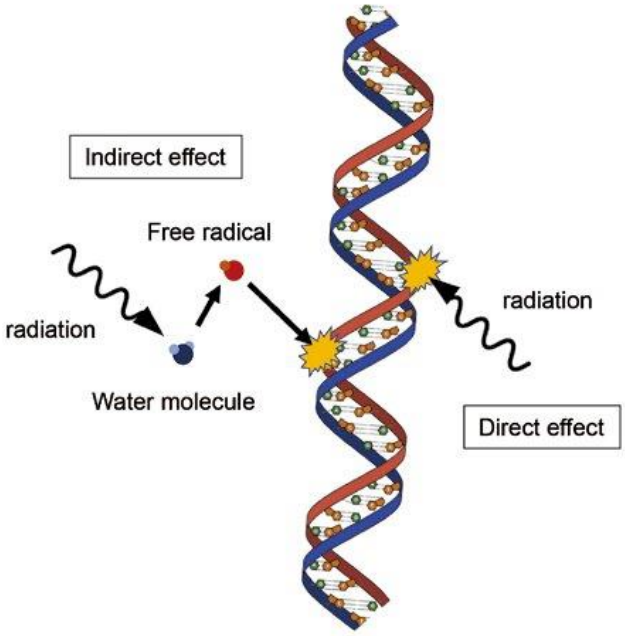

Figure 1.4 Direct and indirect action of radiation on DNA [9].

1.2.2 DNA damage induced by ionizing radiation

Deoxyribonucleic acid (DNA) is the principal target for the biologic effect of radiation. It consists of two strands held together by hydrogen bonds between the bases, forming the well-known "double helical structure". Each strand's backbone consists of alternating sugar (deoxyribose) and phosphate groups. The DNA molecule is composed of four types of nucleotides, covalently linked into a polynucleotide chain with the sugar-phosphate backbone from which the bases (A, C, G, and T) extend [9]. The bases on opposite strands must be complementary: adenine pairs with thymine, and guanine pairs with cytosine. The structure of the DNA is illustrated in Figure 1.5.

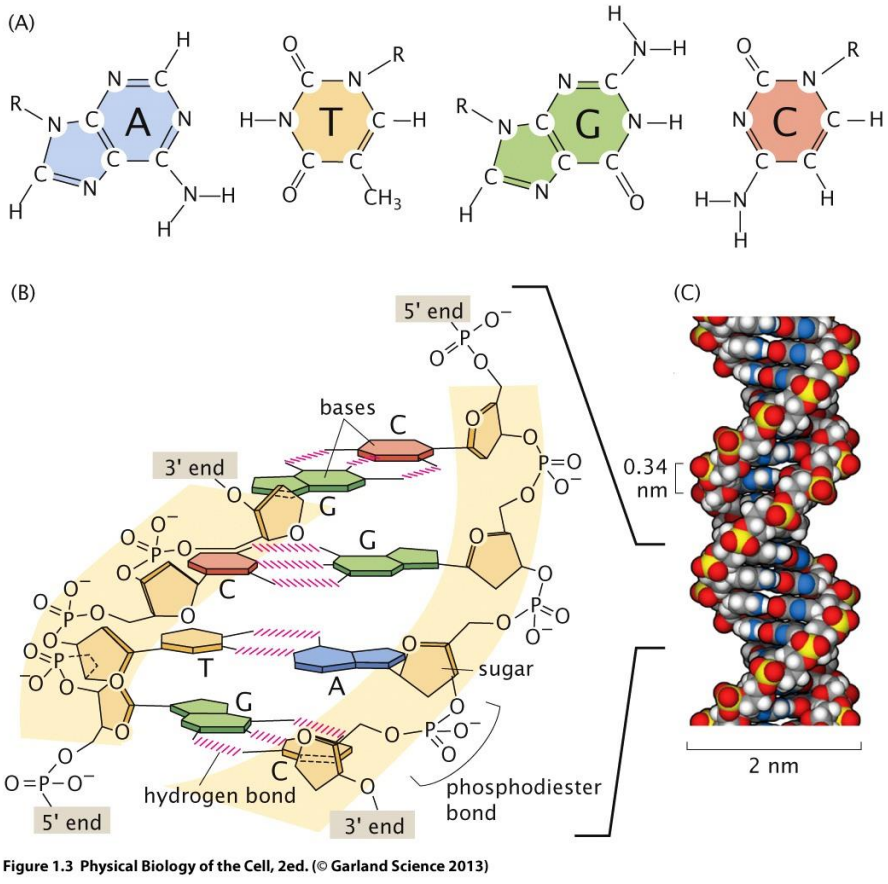

Figure 1.5 Schematic representation of double-stranded DNA [9].

Ionizing radiation can induce various types of lesions to the DNA macromolecule:

- *Base damage* occurs through the breaking of hydrogen bonds between complementary bases.
- *Single-Strand Breaks (SSBs)* represent discontinuities in one strand of the DNA double helix, usually accompanied by the loss of a single nucleotide and damage at the 5′- and/or 3′- ends of the break site. Chromosomal SSBs can have an impact on cell fate, such as the blockage or collapse of DNA replication forks during the S phase of the cell cycle, possibly leading to the formation of *Double-Strand Breaks* (DSBs). Cells can repair DSBs using mechanisms like homologous recombination (HR), but acute increases in cellular SSB levels might saturate this pathway, leading to genetic instability and/or cell death. In non-proliferating cells, cell death induced by SSBs might involve stalling of RNA polymerases during transcription. Alternatively, under certain physiological conditions, high levels of single-strand breakage might induce cell death through excessive activation of the SSB sensor protein poly (ADP-ribose) polymerase 1 (PARP1) [11]. SSB is a typical lesion caused by sparsely ionizing radiation, resulting in isolated damage.
- *Double-Strand Breaks (DSBs)*, mentioned above, are the most cytotoxic radiation-induced lesions, triggering a series of cellular DNA damage responses (DDRs). These responses include the activation of DNA damage sensing and early transduction pathways, cell-cycle arrest, and DNA repair, facilitating the recovery of cells from radiation injuries. Compared to simple breaks, complex DSBs are repaired more slowly and inefficiently, leading to genomic instability [12]. DSBs can result from the interaction of a single track or by the action of two tempo-spatially close single-strand breaks induced by the same or two different tracks. Various cell repair mechanisms,

such as homologous recombination (HR) and nonhomologous end-joining (NHEJ), exist to address these damages.

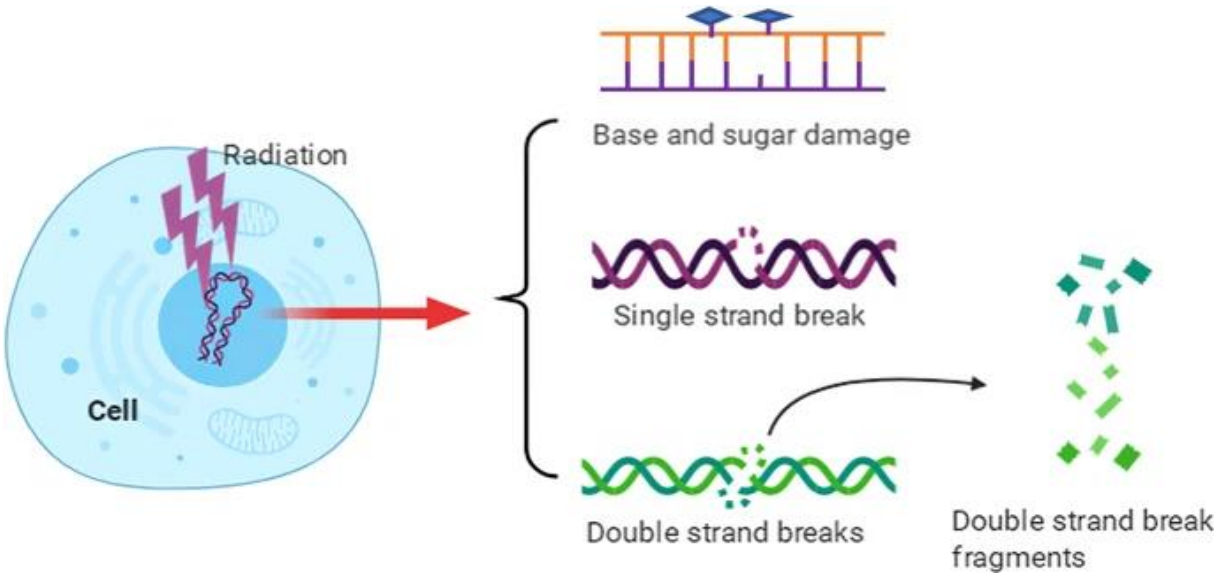

Figure 1.6 Representation of the main damages induced by ionizing radiation on the DNA [13].

Whether prevalently SSBs or DSBs are formed in the DNA varies depending on the type of ionizing radiation, particularly whether this is characterized by a low or a high LET. Studies have shown that the ratio of DSBs to SSBs is greater for densely ionizing (high LET) radiation, such as α-particles and neutrons, compared to sparsely ionizing (low LET) X-rays and γ-rays [12]. High-LET radiation, especially including heavy ions, has a propensity to induce clustered damage, resulting in a significantly higher number of closely spaced DSBs compared to low-LET irradiation [13].

1.2.3 DNA repair pathways

Mammalian cells have developed specialized pathways to sense, respond to, and repair the possible types of damage induced by ionizing radiations, specifically base damage, SSBs, DSBs, sugar damage, and DNA–DNA crosslinks. Some of best characterized repair pathways are described below.

Base Excision Repair (BER): base damage is repaired through the BER pathway. BER starts with a glycosylase excising the DNA base damage on the strand by hydrolysing the N-glycosidic bond between the base and deoxyribose. Removal of the base is followed by the removal of the sugar residue by apurinic endonuclease 1 (APE1) and the replacement with the correct nucleotide by DNA polymerase β and joined by DNA ligase III–XRCC1–mediated ligation.

Nucleotide Excision Repair (NER): it removes bulky adducts in the DNA such as pyrimidine dimers through two pathways, which are global genome repair (GGR or GG-NER) and transcription-coupled repair (TCR or TC-NER). The process of GG-NER can occur anywhere in the genome, while TC-NER only removes lesions in the DNA strands of actively transcribed genes [1].

Mismatch repair (MMR): it removes base-base and small insertion mismatches that occur during replication.

Since DSBs are the most lethal damage, cells have developed different mechanisms to repair them, the two predominant pathways being homologous recombination repair (HRR) and nonhomologous end-joining (NHEJ), as represented in Figure 1.7.

Homologous recombination repair (HRR) occurs primarily in the S/G_2 phase of the cell cycle because it requires an undamaged sister chromatid available to act as template. For this reason, HRR is considered an error-free process, because repair is performed by copying information

from the undamaged homologous chromatid/chromosome. The first step is the recognition of the lesion and processing of the double-strand DNA ends into 3′ DNA single-strand tails by the MRN (Mre11-Rad50-Nbs1) complex, which are then coated by RPA forming a nucleoprotein filament. HRR proteins (RAD51, RAD52 and BRCA1/2) are recruited to the nucleoprotein filaments. RAD51 mediates the invasion of the homologous strand of the sister chromatid, leading to the formation of the so-called Holliday junctions. The Holliday junctions are finally resolved into two DNA duplexes.

Non-homologous end-joining (NHEJ) occurs in the G_1 phase of the cell cycle, and it is an error-prone process. DNA strand breaks are recognized by the ATM and the MRN (Mre11-Rad50-Nbs1) complex, resulting in resection of the DNA ends. NHEJ starts with the binding of the ends at the DSB by the Ku70/Ku80 heterodimer. This complex then recruits and activates the catalytic subunit of DNA-PK (DNA-PKcs), whose role is the juxtaposition of the two DNA ends and the recruitment of the ligase complex (XRCC4/XLF-LIGIV/PNK) that promotes the final ligation step [1].

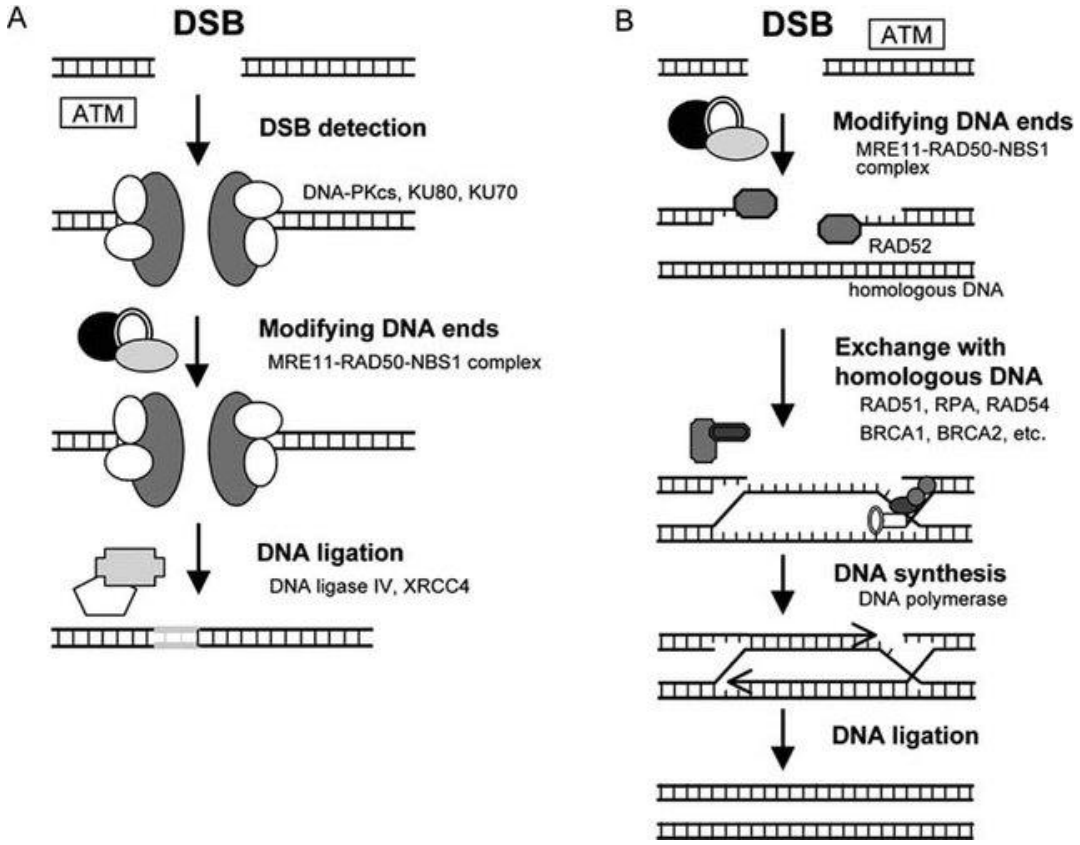

Figure 1.7 Repair of DNA DSBs by non-homologous end joining, NHEJ (A) and homologous recombination, HR (B) [14].

1.3 A combined γ-H2AX and 53BP1 approach to study the ionizing radiation-induced foci (IRIF)

Over the years, various techniques have been developed to study and quantify the response of cells to ionizing radiation-induced DSBs, such as the *foci assay* performed in this work.

DNA damage-induced nuclear foci represent complexes of signalling and repair proteins that localize to sites of DSBs in the cell nucleus.

This assay involves the visualization and analysis of specific proteins used as markers for foci formation. These proteins are γH2AX and 53BP1:

- *H2AX* is a histone protein, which is rapidly phosphorylated at its serine 139 residue in response to damage, occurring at the sites of nascent DSBs in chromatin, forming γH2AX. This phosphorylation is performed by members of the phosphatidylinositol-3-OH-kinase-like family of protein kinases, including ataxia telangiectasia mutated (ATM), ATM-Rad3-related, and DNA-dependent protein kinase. γ-H2AX interacts with numerous other proteins and protein complexes such as MDC1, MRN, 53BP1, and BRCA1/BARD1 to form foci in the region of DSBs [15].

  Histones are highly specialized proteins that form macromolecular complexes with DNA, known as nucleosomes. Histone H2AX acts as a tumour suppressor, helping to preserve genome integrity. Phosphorylated H2AX foci serve as platforms for the recruitment of DNA repair and chromatin remodelling factors, as well as factors involved in the cell-cycle checkpoints. They are also useful for detecting DSBs associated with cancer, senescence, and the radiation-induced bystander effect.
- *53BP1* becomes phosphorylated in response to stress and forms nuclear foci at the sites of DNA DSBs. The accumulation of 53BP1 at DSB sites is dependent on H2AX phosphorylation, and its role in the cell-cycle checkpoints may be explained by its ability to interact with p53 via its BRCT motifs. This interaction enables its

phosphorylation/activation by ATM at the DSB site. 53BP1 also contains two tandem Tudor domains that bind methylated histones H3 and H4, necessary for its accumulation at DSB sites. It is hypothesized that, in response to DSB formation, the accumulation of DNA damage response factors and the subsequent histone modifications in chromatin and nucleosome remodelling facilitate the accumulation of 53BP1 [16].

The combined analysis of γH2AX and 53BP1 by immunofluorescence microscopy is a reasonable approach for an accurate detection and quantification of DSB.

Technically, the cells are incubated with a primary antibody which is specific for γH2AX and for 53BP1. The binding of the primary antibody is then detected with a secondary antibody, which carries a fluorescent tag. Through fluorescence microscopy, it is possible to detect the position and intensity of the tag, allowing the foci to be quantified [1]. Dedicated computer software or manual counting are used to analyse the number, size, and intensity of γ-H2AX and 53BP1 co-localized foci within individual cell nuclei. Analysing the colocalization of γH2AX and 53BP1 signals can provide more reliable data on the presence of damage compared to the use of the sole γH2AX, for example (Figure 1.8).

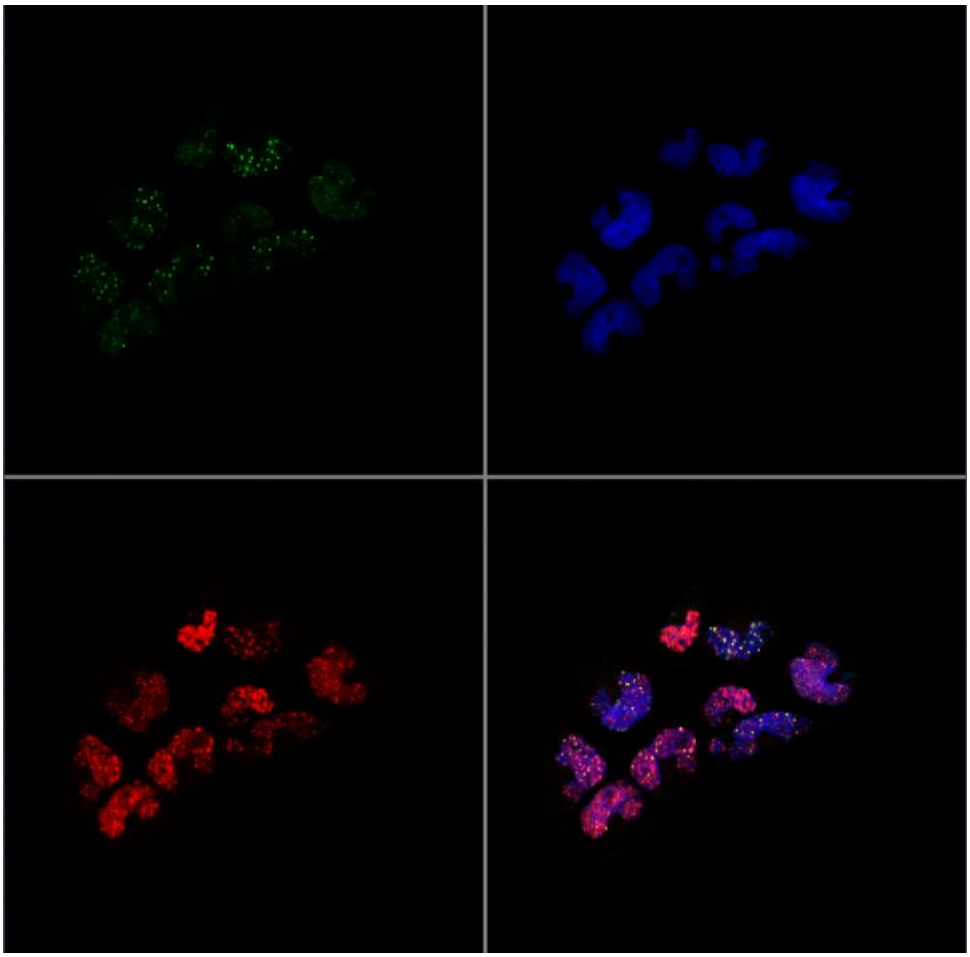

Figure 1.8 Photomicrograph of nuclear foci in cells as detected by staining with antibodies to 53BP1 (green) and γH2AX (red). Cells were also stained with the nuclear stain 4′,6-diamidino-2-phenylindole (DAPI) to show the location of nuclei. The last quadrant at the bottom shows the colocalization of the two signals (53BP1 and γH2AX). These images were obtained by confocal microscopy (Department of Biology, University of Naples Federico II) in the course of this thesis work.

2 Boron-Neutron Capture Therapy (BNCT)

BNCT is a treatment modality aimed at improving the therapeutic ratio[1] for difficult-to-treat tumours. The idea is to deliver borated agents to the patient to selectively deliver boron-10 to tumours. Subsequently, the patient is exposed to a beam of low-energy neutrons that interact with boron, generating two high-LET particles (an alpha particle and a lithium ion) that deposit all their energy inside the cell. Due to their short range, these particles preferentially affect the tumour while sparing more distant normal tissues [17]. To date, BNCT has been clinically studied in various disease sites, including glioblastoma multiforme and osteosarcoma, which are the subject of this *in-vitro* study.

The mechanism on which the BNCT is based is schematically presented in Figure 2.1.

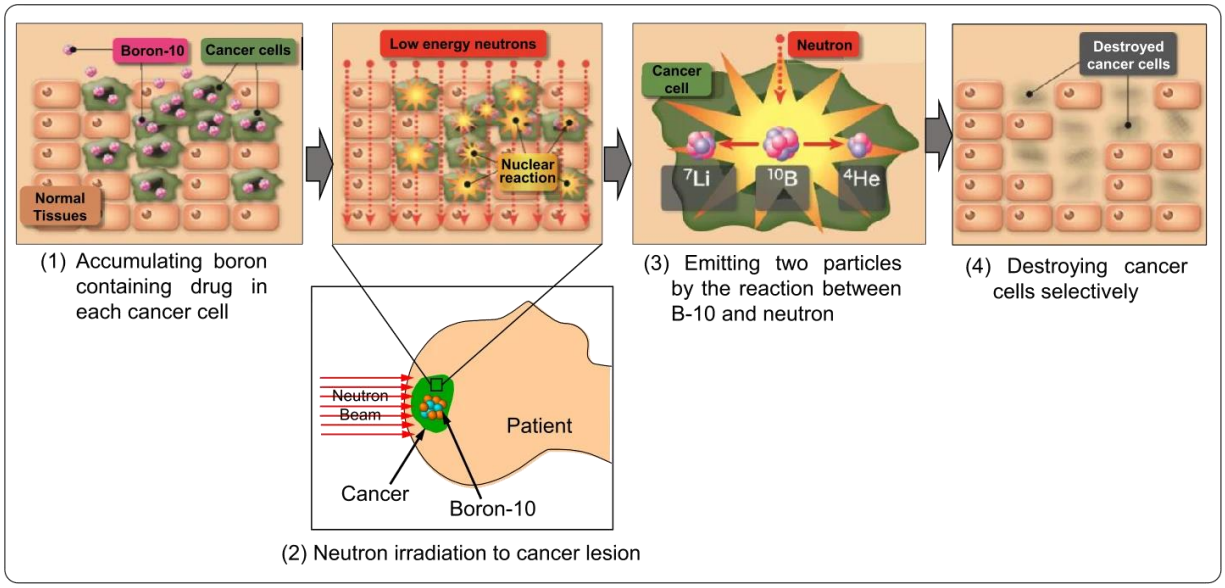

Figure 2.1 Principle of Boron-Neutron Capture Therapy [18].

[1] The therapeutic ratio, also known as the therapeutic index, is a measure that quantifies the relative safety of a drug. It is calculated by comparing the dose of a drug that produces a therapeutic effect to the dose that causes toxicity. The therapeutic ratio is expressed as a ratio of the two doses. The therapeutic ratio in BNCT is often expressed as the ratio of the absorbed dose in tumour tissue containing boron to the absorbed dose in normal tissue without boron.

2.1 Physical principles of BNCT: the $^{10}B(n,\alpha)^{7}Li$ nuclear reaction

BNCT is based on the nuclear capture following the irradiation of nonradioactive boron-10 atoms with thermal neutrons (<0.025 eV), which leads to the production of an alpha particle and a recoiling lithium-7 ion [17].

When irradiated by thermal neutrons, the ^{10}B atom captures the neutrons, leading to the following nuclear reactions:

$$^{10}B + {}^{1}n \rightarrow [^{11}B] \rightarrow {}^{4}He + {}^{7}Li + \gamma(0.48\ MeV) + 2.31\ MeV \quad (94\%) \qquad (Reaction\ 1)$$

$$^{10}B + {}^{1}n \rightarrow [^{11}B] \rightarrow {}^{4}He + {}^{7}Li + 2.79\ MeV \quad (6\%) \qquad (Reaction\ 2)$$

The nuclear reaction products, ^{4}He and ^{7}Li, are charged particles with high LET, contributing to 2.3 MeV of kinetic energy in 94% of the reactions and 2.8 MeV in the remaining 6%. These particles deposit their energy along a path of approximately 10-μm length (which is in the order of the dimensions of a human cell) [19]. Therefore, these particles release their energy exclusively in ^{10}B-loaded cancer cells tumour cells, effectively limiting radiation damage to non-tumour cells.

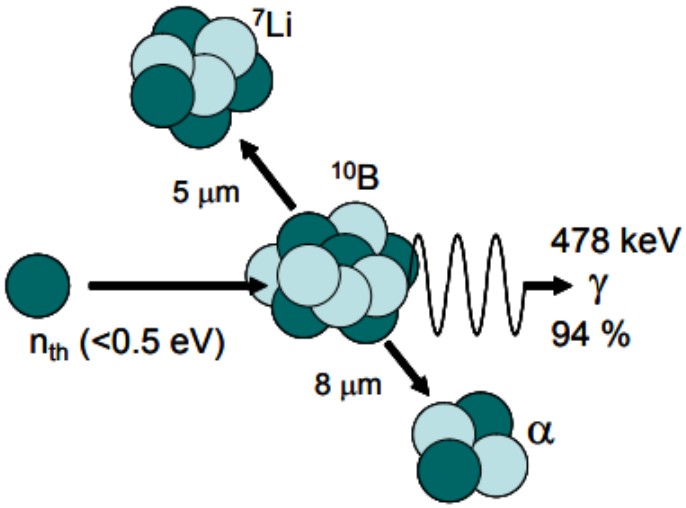

Figure 2.2 Nuclear reaction utilised in BNCT. A thermal neutron is absorbed by a ^{10}B nucleus and promptly emits a ^{4}He (alpha) particle together with the recoil ^{7}Li nucleus [20].

2.2 The boron carriers used in BNCT

The most challenging aspect of successful BNCT treatment is the selective delivery of boronated compounds to the tumour while minimizing uptake into normal tissues. The general requirements for successful boron delivery agents are:

- High tumour uptake.
- Low normal tissue uptake.
- Rapid elimination from the tissue after treatment.
- Low toxicity.

Studies on the production of the most suitable carrier are still ongoing [17].

Currently, there exist three generations of boronated compounds:

- **First-generation compounds:** Boric acid and its derivatives. These agents were used by Sweet et al. in the 1950s and 1960s; however, due to their poor selectivity and inadequate accumulation in the tumour, they did not yield significant clinical results in BNCT trials.
- **Second-generation compounds:** *p*-boronophenylalanine (BPA) and the sulphydryl borane ($Na_2B_{12}H_{11}SH$, or BSH). These compounds exhibited greater selectivity and lower toxicity. They became the agents of choice after the 1960s.

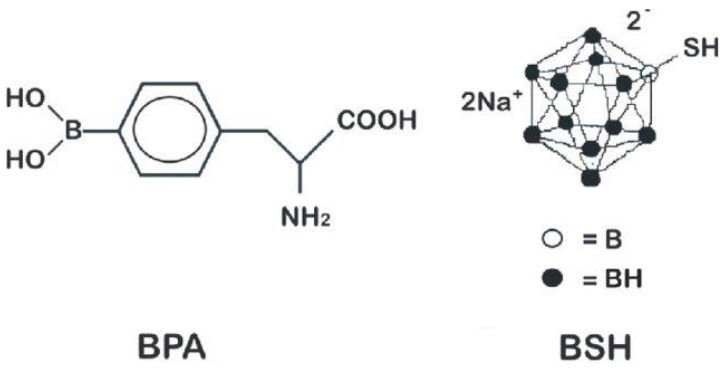

Figure 2.3 Chemical structures of BPA and BSH [21].

- **Third-generation compounds:** Polyamines, unnatural amino acids, peptides, proteins, nucleosides, sugars, porphyrins, antibodies, liposomes, and nanoparticles are conjugated with either BPA, BSH, or other boronated compounds to develop a more effective delivery system. Third-generation compounds are still in the experimental stage [22].

In this work, Boronophenylalanine (BPA) has been used as the boron delivery agent of choice.

2.2.1 Boronophenylalanine (BPA) as a boron delivery agent

Boronophenylalanine BPA is a derivative of the neutral amino acid phenylalanine, synthesized by Snyder et al. in 1958. It was first utilized as a boron drug for BNCT in 1986 [23].

In the context of BNCT, BPA has been investigated for its retention mechanisms and uptake pathways. It is localized to tumour cells through selective uptake mediated by transporters, such as LAT-1. This transporter, highly expressed in malignant tumours and tumour cell lines, has been associated with growth, proliferation, and tissue development [24].

BPA was originally used in BNCT to treat cutaneous melanoma, because it is involved in melanin synthesis and preferentially ingested by melanoma cells. BPA is also an effective boron carrier for brain tumours. It was demonstrated that BPA can carry a therapeutic concentration of ^{10}B to target a variety of tumour types, including rat glioma, and gradually it was extended to the treatment of other extracranial tumours, such as head and neck cancer [25].

2.2.2 ^{10}B concentration measurement in biological samples: neutron autoradiography

In BNCT, it is crucial to measure the concentration of boron captured by the irradiated cells. The absorbed dose depends on the number of interactions between the neutron beam and the boron inside the cells. Therefore, the quantification of the biodistribution of ^{10}B is essential for

calculating the dose of radiation absorbed by tissues during irradiation. One method used for quantifying the biodistribution of ^{10}B is *neutron autoradiography*.

Neutron autoradiography operates by detecting tracks left by alpha particles and ^{7}Li ions on passive nuclear track detectors after neutron irradiation. This method is based on the principle that high-LET particles traversing a dielectric material transfer a substantial fraction of energy per unit path, damaging molecules along their trajectory and creating a track. The chemical damage caused by these particles is on the order of nanometers, remaining invisible even under a microscope. Therefore, a chemical etching process is necessary to make the tracks visible. Once developed, the tracks can be counted using an optical microscope.

In this thesis work, boron measurements were conducted through neutron autoradiography at the Department of Physics and of Clinical-Surgical, Diagnostic and Pediatric Sciences, University of Pavia. To obtain the tracks, the solid-state nuclear track detector CR-39 was employed. CR-39 is an organic polymer well-suited for detecting particles resulting from nuclear reactions. In this case, the detector, in contact with the sample and exposed to a field of thermal neutrons, highlights the tracks of alpha particles and ^{7}Li nuclei produced as a result of the $^{10}B(n,\alpha)^{7}Li$ reaction in cells that have absorbed ^{10}B.

An image illustrating an example of track distribution obtained through neutron autoradiography is presented in Figure 2.4. Another option is the quantification of boron concentration through greyscale conversion into boron concentration by tuning the neutron autoradiography parameters to obtain an imaging of boron distribution in the samples.

More details will be provided in the Materials and Methods section (Chapter 3).

Figure 2.4 Track distribution obtained through quantitative neutron autoradiography of an irradiated and etched SSNTD of a tissue standard with 10 ppm of boron [26].

2.3 The neutron sources

BNCT clinical research began in the 1950s using research reactors at the National Brookhaven Institute and the Massachusetts Institute of Technology in the United States [18].

The main neutron source requirements for BNCT are:

- Neutron flux should be more than 10^9 cm^{-2}/s at the beam aperture.
- It is necessary to generate $\geq 5 \times 10^{13} n/cm^2/s$ neutron flux at the point of the neutron target.
- Neutron energy should be high enough to penetrate tumours.

Satisfactory neutron sources were exclusively produced by research nuclear fission reactors until recently [27]. This fact limited the application of BNCT to those Institutions already equipped with such installations. It is in fact difficult to install a new research nuclear reactor for clinical applications for different reasons among which the fact that they are not clinical devices, their cost, the difficult authorization process, the complex maintenance and, in some cases, social acceptability issues. Fission reactors produce neutrons across a spectrum that can be divided into three ranges: thermal neutrons (< 0.4 eV), epithermal neutrons (0.4 eV to 10 keV), and fast or high-energy neutrons (10 keV to 20 MeV).

By the end of the $20t^h$ century, reactor-based BNCT spread to Argentina, Taiwan, and China, treating malignant melanoma and brain tumours. Until the 1990s, irradiation was performed using thermal neutron beams (low-energy neutrons) [18]. However, superficial tissues, such as muscle and bone, attenuate the penetration of thermal neutrons through hydrogen capture reactions. Consequently, early BNCT studies required intraoperative irradiation to ensure an adequate thermal neutron flux within the tumour. Thus, the use of low-energy neutrons (< 0.4 eV) is beneficial for treating superficial tumours, such as melanoma.

Since the 1990s, epithermal neutrons (i.e., at higher energy levels, from 0.4 eV to 10 keV) have been used, allowing the craniotomy to no longer be used, and extend the use of BNCT to head and neck, lung, and breast cancer, which have deeper lesions. Today, almost all neutron beams used for clinical purposes are epithermal. This energy range represents a good compromise between beam penetration for treating deeper tumours and the radiation dose deposited in healthy tissues due to neutron scattering with hydrogen.

In recent years, attention has shifted towards accelerator-based BNCT, involving treatment with an accelerator-based neutron source [18]. In this case, neutrons are yielded by a nuclear reaction between accelerated protons with several tens of MeV and a beryllium or lithium target [28]. This technological innovation has allowed BNCT to know a new phase of clinical application, because accelerators can be certified as medical devices, enabling more structured clinical trials. In Japan, accelerator-based BNCT is already a clinical option covered by the National Health System [29] [30].

In this work, the TRIGA Mark II nuclear research reactor (University of Pavia) was used as the neutron source for BNCT irradiation of the cells. Inside the thermal column of the reactor, an irradiation facility was constructed to produce a sufficient thermal neutron flux with low epithermal and fast neutron components, and low gamma dose [31].

The TRIGA reactor was used for the first ex-situ BNCT application in the 2000s [32].

Figure 2.5 TRIGA Mark II research reactor (University of Pavia).

2.4 Medical applications of BNCT

Clinical investigations of BNCT have been conducted in various disease sites, including glioblastoma multiforme, meningioma, head and neck cancers, lung cancers, breast cancers, hepatocellular carcinoma, sarcomas, cutaneous malignancies, extramammary Paget's disease, recurrent cancers, paediatric cancers, and metastatic disease [18].

This *in-vitro* work focuses on the application of BNCT to two specific types of tumours: glioblastoma multiforme and osteosarcoma.

2.4.1 BNCT as a therapy for glioblastoma multiforme

Glioblastoma Multiforme (GBM) is the most common and aggressive primary brain tumour in adults. Key histopathologic features include necrosis and endothelial proliferation, resulting in the assignment of grade IV, the highest grade in the World Health Organization (WHO) classification of brain tumours [33]. Morphologically, GBM consists of small cells characterized by polymorphism and anaplasia, polygonal to spindle-shaped with acidophilic cytoplasm and indistinct cellular borders. Their nuclei are oval or elongated, and the chromatin is coarsely clumped hyperchromatic with multiply distinct nucleoli located centrally or peri-centrally. Vascularization is very high [34].

GBM poses a significant treatment challenge, with a median survival of approximately 14 months despite extensive resection, radiotherapy, and adjuvant chemotherapy. Consequently, BNCT has been proposed as a potential treatment approach, as boron can cross the blood-brain barrier and exhibit direct tumoricidal activity [18]. In 1968, in Japan, Hatanaka introduced sodium borocaptate (BSH) as a BNCT boron carrier, combined with pure thermal neutrons. Due to the limited penetration depth of thermal neutron beams in tissue, it was necessary to reflect the skin and to raise the bone flap to irradiate the exposed brain directly (intraoperative BNCT). However, results were unsatisfactory for patients with brain tumours in deeper regions

due to insufficient neutron delivery. Therefore, epithermal neutron beams were developed to improve neutron penetration, and in 2004, boronophenylalanine (BPA) was introduced as a new boron compound for GBM treatment [35].

BNCT has the potential to be effective in the treatment of GBM for three main reasons:

1. Better management of intrinsic radioresistance and heterogeneous radio-sensitivities of GBM compared to X-rays, as treatment is delivered by the high-LET radiation products of the neutron capture, resulting in densely clustered ionization damages.
2. The process of cell killing in BNCT is less susceptible to oxygen status (e.g. hypoxia, which is one of the main causes of conventional radiotherapy failure in tumour control).
3. BNCT can selectively deliver localized doses to tumour cells while minimising normal tissue toxicity. This is particularly advantageous for GBMs because it potentially enables the targeting of sub-clinical disease spread into normal brain tissue [36].

2.4.2 BNCT as a therapy for osteosarcoma

Osteosarcoma is the most frequent primary malignant bone tumour, with a higher incidence among children and adolescents, constituting over 10% of solid cancers in this age group [37].

It is characterized by the presence of malignant mesenchymal cells that generate immature bone and/or osteoid tissue. The tumour can arise in any bone, with the metaphysis of long bones (e.g., distal femur), v, and proximal humerus being the most prevalent primary sites. In rare instances, it may manifest in soft tissues [38].

Despite significant improvement in treatment success rates with the introduction of adjuvant and neo-adjuvant chemotherapy, aggressive surgery is still needed, and a considerable percentage of patients do not survive due to recurrences or early metastases.

The current standard treatment for osteosarcoma consists of preoperative (neo-adjuvant) chemotherapy, followed by the surgical removal of all detectable disease, including metastases

that are present in 80% of patients at the time of diagnosis, and postoperative (adjuvant) chemotherapy. The sequence of neo-adjuvant chemotherapy, surgery, and adjuvant chemotherapy proves effective in approximately 70% of patients with localized disease but, for patients with metastases, the long-term survival rate remains below 20%**.**

In recent decades, it has become important to avoid limb amputation and preserve the functional and aesthetic status of patients without decreasing the survival rate.

Osteosarcoma has traditionally been considered a radio-resistant tumour, but there have been suggestions that a large single fraction dose of radiotherapy may be effective. However, delivering high photon doses in a single fraction is complicated due to the tolerance of surrounding tissues. For this reason, recent treatments have employed charged particles such as protons and carbon ions, which allow for a highly conformed dose distribution.

BNCT has been investigated as a treatment option to facilitate less aggressive surgery by killing infiltrated tumour cells in the surrounding healthy tissues. Successful BNCT requires an intense neutron beam to ensure irradiation times on the order of 1 hour [37].

2.5 Dosimetry of BNCT

BNCT is characterized by a mixed radiation field consisting of high-LET alpha and lithium ions resulting from the thermal neutron capture by ^{10}B, intermediate LET protons originating from thermal neutron capture by ^{14}N and neutron elastic collision with H nuclei, and low-LET gamma-ray from the thermal neutron capture reaction by hydrogen and the gamma radiation in the irradiation beam. The energy released by high and intermediate LET particles induces a higher severity of biological damage compared to photons [36].

The clinical total dose is the sum of all the mentioned contributions, each to be calculated in both the tumour and the normal tissues involved in the irradiation:

$$D = D_t + D_f + D_\gamma + D_B$$

where:

- D_t = dose from thermal neutrons, mainly due to protons generated from the reactions $^{14}N(n,p)^{14}C$. The ^{14}N element in the tissue captures a thermal neutron, and a ~600 keV proton is emitted. The dose is obtained from locally delivered energy from the recoiling ^{14}C nucleus and the energetic proton.
- D_f = dose from fast neutrons, resulting from proton recoil following scattering, $^{1}H(n,n)^{1}H$.
- D_γ = dose from background photons and capture reactions $^{1}H(n,\gamma)^{2}H$.
- D_B = energy deposited by the $^{10}B(n,\alpha)^{7}Li$ reaction. ^{10}B captures a thermal neutron, and as result, an α-particle and a recoiling ^{7}Li ion are emitted.

This mixed field of radiation makes it difficult to predict the biological effect as a function of the absorbed dose because each component has its own effectiveness in producing damages. This prompted the necessity to translate BNCT absorbed dose into photon-equivalent units, i.e., to calculate the dose of a reference radiation (for example photons) that produces the same effect as the dose of BNCT. In the past, this was obtained using fixed RBE factors multiplying each component of the absorbed dose [39]. Recently, this approach was proven not precise enough to assess photon-equivalent dose in patients. New models have been proposed and are being applied to produce a more realistic dosimetry, able to explain the clinical results observed in the trials [40] [41].

3 Materials and methods

3.1 Experimental design

The experimental design presents six fundamental work phases:

1. **Preparation of U87 and UMR-106 cell cultures:**
    - Cultivation of U87 and UMR-106 cell lines.
2. **Administration of ^{10}BPA:**
    - Administration of ^{10}BPA to both cell lines.
3. **Quantitative neutron autoradiography to assess ^{10}B incorporation:**
    - The aim is to evaluate and quantify the cellular absorption of ^{10}B by the cell monolayers.
4. **Neutron irradiation for BNCT and X-ray irradiation:**
    - Neutron irradiation for BNCT of U87 and UMR-106 cell lines enriched in ^{10}BPA, and those without ^{10}BPA, conducted in the thermal column of the TRIGA Mark II nuclear reactor at the University of Pavia.
    - X-ray exposure of the above-mentioned UMR-106 cell lines performed at the Radiation Biophysics Laboratory, Physical Sciences Department, University of Naples Federico II, using a STABILIPAN 2 machine (Siemens, Munich, Germany).
    - X-rays treatment for the U87 cell line conducted at Istituto Nazionale Tumori "Fondazione Pascale", which utilizes the Linac Synergy Sgility Elekta accelerator for radiation therapy.

5. **In Vitro study of radiation-induced DNA damage using immunofluorescence:**
    - Application of an immunofluorescence assay for the in vitro study of radiation-induced DNA damage, utilizing γ-H2AX and 53BP1 as markers of DNA damage, specifically DNA double-strand breaks (DSBs).
6. **Data analysis using dedicated software for automatic identification and quantification of IRIFs:**
    - Data analysis conducted using a fluorescence microscope (Imager 1, Zeiss, Germany) connected to a computer equipped with the Metafer software (Metasystem, Germany) for automated image acquisition.

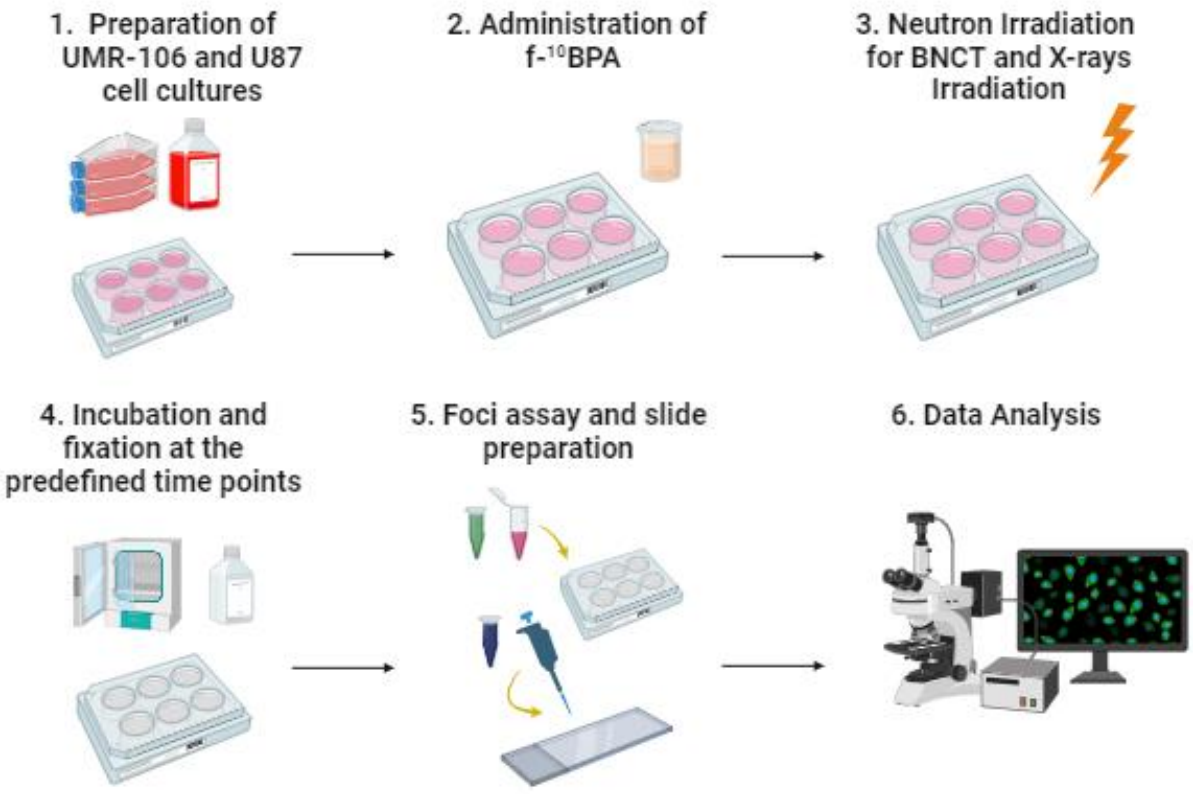

Figure 3.1 Schematic representation of the experimental design.

3.2 Preparation of the cell cultures

The effectiveness of BNCT, and its comparison with X-rays, has been studied on two tumour cell lines: U87MG (human glioblastoma cells), and UMR-106 (rat osteosarcoma cells). The following paragraphs will detail the growth and maintenance protocols for the two cell cultures.

3.2.1 Human glioblastoma multiforme cell line (U87MG): cell culture maintenance

U87 cell line is cultivated in adherent flasks and exhibits classical monolayer cell growth. Before reaching confluence, it initiates the formation of large-sized spheroidal structures (> 200 µm) that tend to detach from the monolayer to further grow and proliferate in suspension.

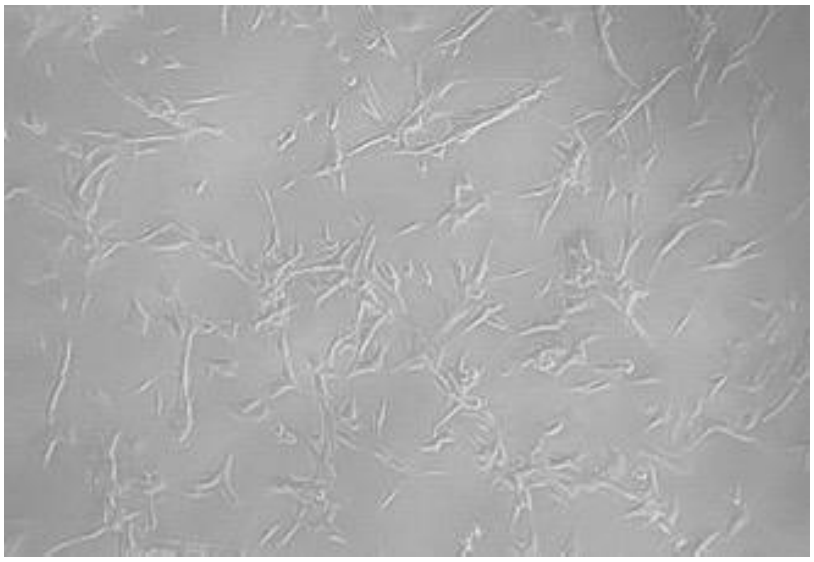

Figure 3.2 Microscopic image of the U87 cell line in monolayer culture.

For the cultivation of the U87 cell line, the protocol recommended by the American Type Culture Collection (ATCC®) was followed. U87 cells were therefore grown in standard tissue culture T-75 flasks using Dulbecco's Modified Eagles Medium (DMEM, Lonza), supplemented with 10% fetal bovine serum (Euroclone) and 1% gentamicin (Euroclone), and maintained in a humified atmosphere with 5% CO_2 at 37°C. For subculturing or harvesting prior to BPA treatment and/or exposure to radiation, following the removal of the culture medium, cells were washed with Ca++/Mg++-free Dulbecco's Phosphate-Buffered Saline (D-PBS). Subsequently,

they were detached by enzymatic treatment with trypsin-EDTA (Sigma) for 5 minutes at 37°C, and then resuspend in an appropriate amount of complete medium to quench the trypsin. The cells were then transferred to a new flask or processed further for irradiations.

For BNCT and X-ray experiments, U87 cells were seeded on glass coverslip (24 x 24 mm) in a 6-wells plate (35 mm) at a density of 4.0×10^4 cells two days before the treatment.

The plates were prepared considering control and irradiated samples, treated with two radiation doses (0.5 and 2 Gy). Cell fixation was performed 30 minutes and 24 hours post-irradiation. To ensure proper fixation and subsequent success of the immunofluorescence assay, different 6-well plates were used for samples fixed at 30 minutes and for samples fixed 24 hours post-irradiation.

Number of cells	Time	Dose (Gy)	Cells Fixation
4.0×10^4 cell	Two days before IR[2]	0; 0.5; 2	30 min and 24 h post IR

Figure 3.3 The scheme provides information on the number of seeded cells, the time of seeding before irradiation, the doses delivered in the radiation treatments, and the fixation time points for both experiments (BNCT and X-rays).

The samples for BNCT were prepared considering treatment both in the presence and absence of ^{10}BPA.

[2] Irradiation

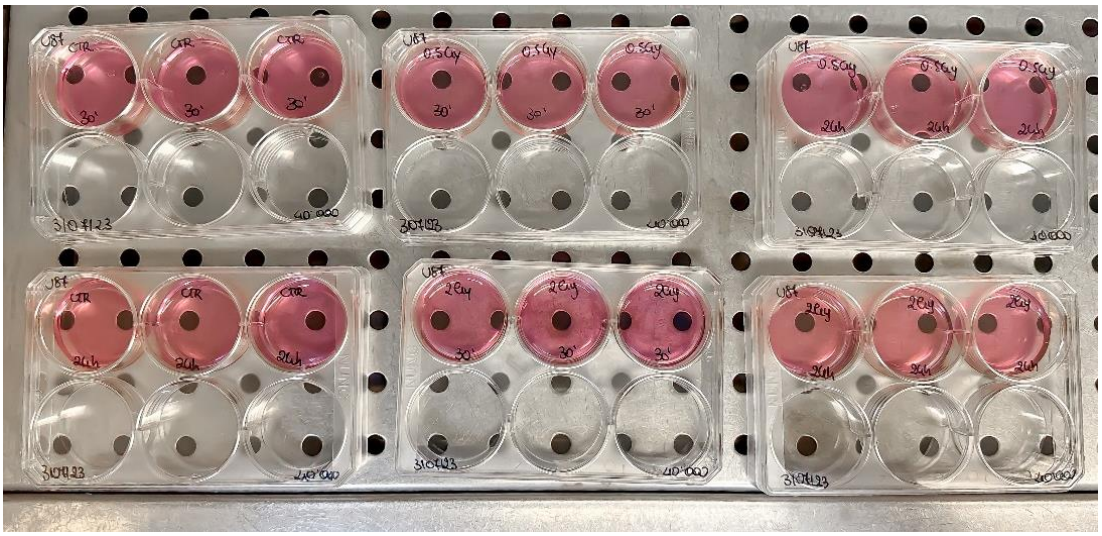

Figure 3.4 Preparation of the 6-well plates considering irradiation at 0.5 Gy and 2 Gy, with cell fixation at 30 minutes and 24 hours post-irradiation.

3.2.2 Rat Osteosarcoma cell line (UMR-106): cell culture maintenance

UMR-106 (provided by ECACC, Salisbury, Wiltshire, UK) was used as osteosarcoma cell line.

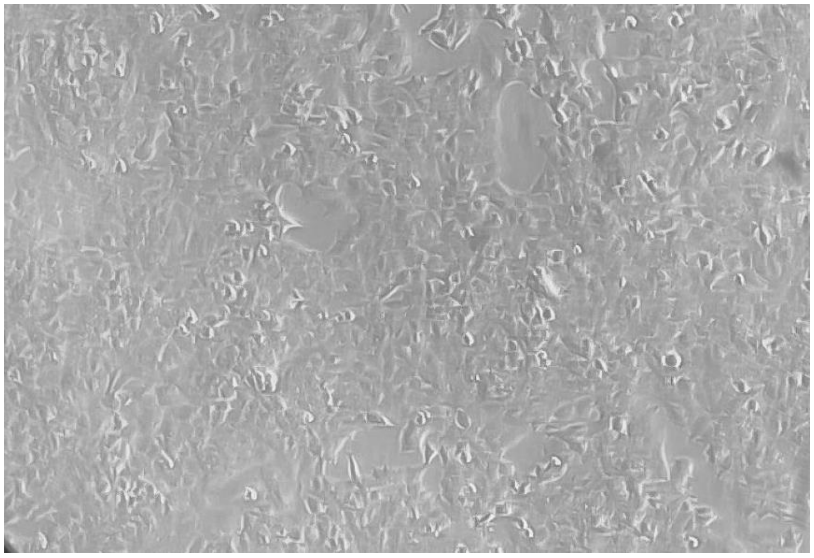

Figure 3.5 Microscopic image of the UMR-106 cell line in monolayer culture.

For the cultivation, the UMR-106 cell line was grown in T-75 flasks using DMEM medium (Dulbecco's Modified Eagles Medium, Lonza) supplemented with 10% of fetal bovine serum (FBS, Euroclone) and 1% gentamicin (Euroclone), and maintained at 37°C with 5% CO_2. For subcultures or harvesting, following the removal of the culture medium, cells were washed with Ca++/Mg++-free Dulbecco's Phosphate-Buffered Saline (D-PBS). Subsequently, cells were resuspended using enzymatic treatment with trypsin-EDTA (Sigma) for around 3 minutes at 37°C, and then resuspend in complete medium to neutralize trypsin. The cells were then transferred to a new flask containing ample medium.

For BNCT experiments, cells were seeded on glass coverslip (24 x 24 mm) in a 6-wells plate (35 mm) at a density of 3.0×10^4 cells two days before the treatment. The samples for BNCT were prepared considering treatment both in the presence and absence of ^{10}BPA.

Number of cells	Time	Dose (Gy)	Cells Fixation
3.0×10^4 cells	Two days before IR	0; 0.5; 2	30 min and 24 h post IR

Figure 3.6 The scheme provides information on the number of seeded cells, the times of seeding before irradiation, the doses delivered in the radiation treatments, and the fixation time points for both experiments (BNCT).

For X-ray experiments, cells were seeded on glass coverslip (24 x 24 mm) in petri dishes (35 mm) at a density of 1.5×10^4 cells ~18 hours before irradiation. The number of cells seeded in sample preparation differs in this case because the concentration was optimized for our X-ray experiments. After conducting various attempts, we found it necessary to increase the cell density for BNCT experiments to achieve a higher cell count.

Number of cells	Time	Dose (Gy)	Cells Fixation
1.5×10^4 cells	~18 hours before IR	0; 0.5; 2	30 min and 24 h post IR

Figure 3.7 The scheme provides information on the number of seeded cells, the times of seeding before irradiation, the doses delivered in the radiation treatments, and the fixation time points for both experiments (X-ray experiments).

The plates were prepared considering control and irradiated samples, treated with two radiation doses (0.5 and 2 Gy). Cell fixation was performed 30 minutes and 24 hours post-irradiation. To ensure proper fixation and subsequent success of the immunofluorescence assay, different 6-well plates were used for samples fixed at 30 minutes and for samples fixed 24 hours post-irradiation.

3.3 Intracellular absorption of ^{10}B and its quantification

For BNCT treatment, prior to neutron irradiation, cells were enriched with ^{10}B through the administration of the boron compound f-^{10}BPA.

3.3.1 Preparation of f-^{10}BPA solution

^{10}BPA is a substance with low water solubility. To enhance its usability, it must be complexed with fructose, obtaining a solution of f-^{10}BPA, hereafter simply denoted as BPA. The protocol involves the following steps:

- Weigh the powders of ^{10}BPA and fructose using an analytical scale.
- Mix the two powders and add the culture medium.
- Add 5 mol/L NaOH until a clear solution is achieved, maintaining a pH between 9.5 and 10.
- Adjust the pH back to values around 7.4 using 5 mol/L HCl and keep stirring for approximately 10 minutes.
- Attain the desired final volume by adding culture medium, considering the needed amount of BPA-enriched solution at 80 ppm.

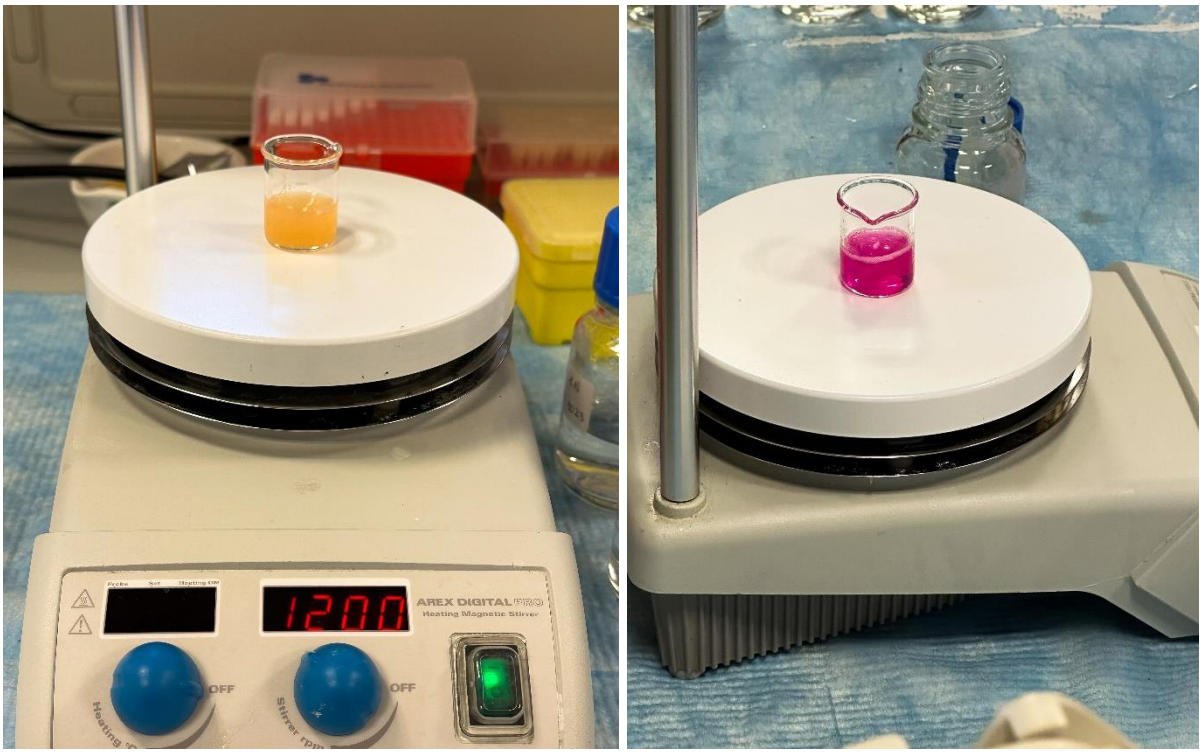

Figure 3.8 Preparation of f-^{10}BPA solution. These images show the colour shift resulting from the pH adjustment (Department of Clinical-Surgical, Diagnostic and Pediatric Sciences, University of Pavia).

3.3.2 Administration of f-^{10}BPA solution to U87 and UMR-106 cell lines

Before neutron irradiation, the cells were treated for 4 hours in the corresponding growth medium containing f-^{10}BPA, with a ^{10}B concentration of 80 μg/ml (80 ppm). Subsequently, the BPA-containing medium was removed before irradiation and, after three washes with PBS, was replaced with fresh medium.

These treatment conditions were experimentally determined based on previous studies related to the cytotoxicity and intracellular uptake cytokinetics of ^{10}BPA. For BNCT to be successful *in vivo*, a sufficient amount of ^{10}B must be selectively delivered to the tumour (~20 μg/g) and enough thermal neutrons must be absorbed by neoplastic cells [42]. In vitro, working conditions were optimized in the past to obtain at least this boron concentration in cells.

3.3.3 Evaluation of ^{10}B absorption: neutron autoradiography

It is crucial to determine the tumour cells' capacity to uptake and retain ^{10}B for a duration adequate for neutron irradiation to calculate the dose absorbed due to neutron irradiation. Neutron autoradiography was utilized to evaluate and quantify the intracellular boron absorption. The aim of this analysis is to confirm that, following exposure to ^{10}BPA, the cell line has assimilated a minimum of 25-30 ppm of ^{10}B, fundamental requirement for the success and efficacy of the treatment upon neutron irradiation and to provide the data for the determination of the radiation dose.

After BPA treatment as described above, the cells were detached by trypsin, counted, and centrifuged to obtain a pellet containing around $4x10^6$ cells. Pellets were then resuspended in the culture medium and deposited onto Mylar sheets. The same protocol was applied to control cells, cultured in a medium without BPA.

The cellular samples (control cells and cells treated with BPA) were thus allowed to completely dehydrate for at least 24 hours before irradiation on the mylar films.

Before irradiation in the thermal column of the nuclear reactor, the films were placed in contact to passive solid-state nuclear track detectors denominated CR-39 (allyl diglycol carbonate, C12H18O7). CR-39 is a plastic material that exhibits structural damage when exposed to charged particles. This "latent" damage becomes visible at a bright field microscope observation following a chemical etching process using a highly basic solution at high temperature. This results in the preferential erosion of the latent tracks along the path of the charged particles that have crossed the plastic material, making them appear as circular structures when inspected at the microscope.

The CR-39 films were irradiated in the TRIGA reactor at 20 kW for 30 minutes, positioned where the thermal neutron flux is 8 x 10^6 $cm^{-2}s^{-1}$ at 1 kW. For quantitative analysis, the CR39 were subjected to chemically etching in a PEW409 solution for approximately 10 minutes. The solution is maintained at a constant temperature (approximately 70°C) in a thermostated bath. As mentioned above, this process results in the enlargement of track diameters to the desired size. Once developed, the tracks have diameters ranging from 1 to 4 µm. Subsequently, CR-39 are analysed using a Leica stereomicroscope equipped with a motorized table for automatic scan of the surface. The images, representative of the entire sample area, are filtered, and specialized software is employed to count the tracks in each image. The track density serves as the parameter for calculating boron concentration based on a previous calibration curve. This curve is obtained using samples of the same nature, containing a known concentration of ^{10}B. The concentration-track density curve allows for the determination of the unknown concentration of the sample being measured based on the detected track density [27].

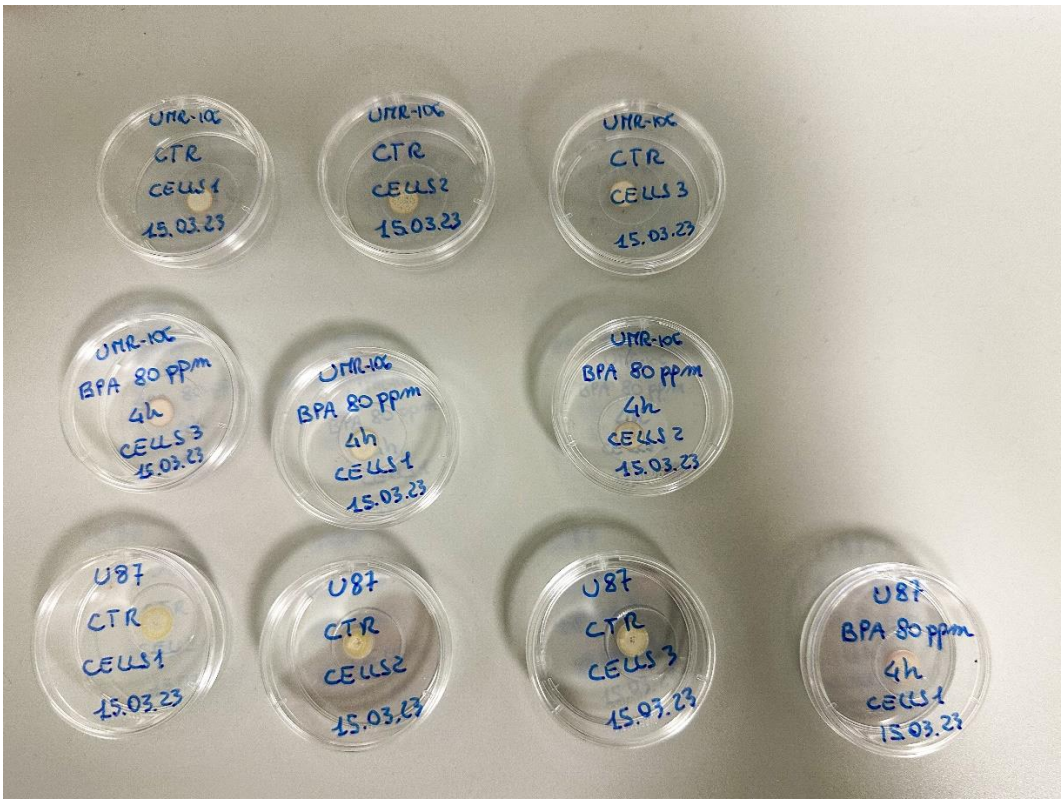

Figure 3.9 UMR-106 and U87 (control and treated samples) grown on Petri dishes containing Mylar films, prepared for the evaluation of ^{10}B absorption.

3.4 X-ray irradiation

3.4.1 Photon source for experiments on the UMR-106 and U87 cell line

The X-rays machine used for UMR-106 irradiation experiments was a STABILIPAN 2 machine (Siemens, Munich, Germany). X-rays were produced by a Thomson tube (TR300F) equipped with a tungsten anode at 250 kVp and filtered by 1-mm-thick Cu foil. Figure 3.10 shows the set-up with one of the petri dishes in the irradiation position. The cubic structure placed under the filter contains mobile shutters that can be used to delimit the radiation field. These shutters were kept completely open during our experiments, and the glass window from which the X-rays are emitted.

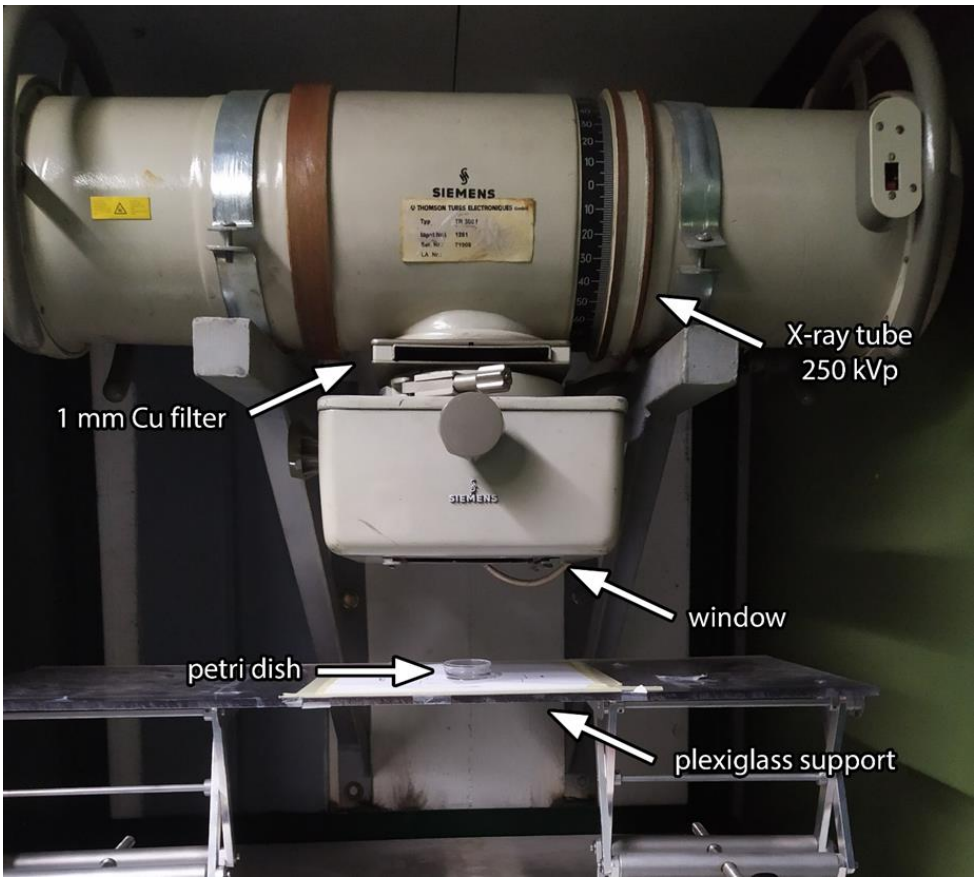

Figure 3.10 X-rays irradiation setup (Radiation Biophysics Laboratory, Physical Sciences Department, University of Naples Federico II).

Cells were seeded on 24x24mm^2 borosilicate glass coverslips placed inside a petri dish (Falcon®, diameter = 35mm, polystyrene (PS)), which is positioned on a height-adjustable surface composed of 6 mm thick plexiglass. Irradiation occurred from above through the petri dish cap (1 mm thick), an air gap inside the petri dish, and the volume of the culture media in which the cells were immersed. Further details regarding the distances and thicknesses of the various materials are provided in Figure 3.11.

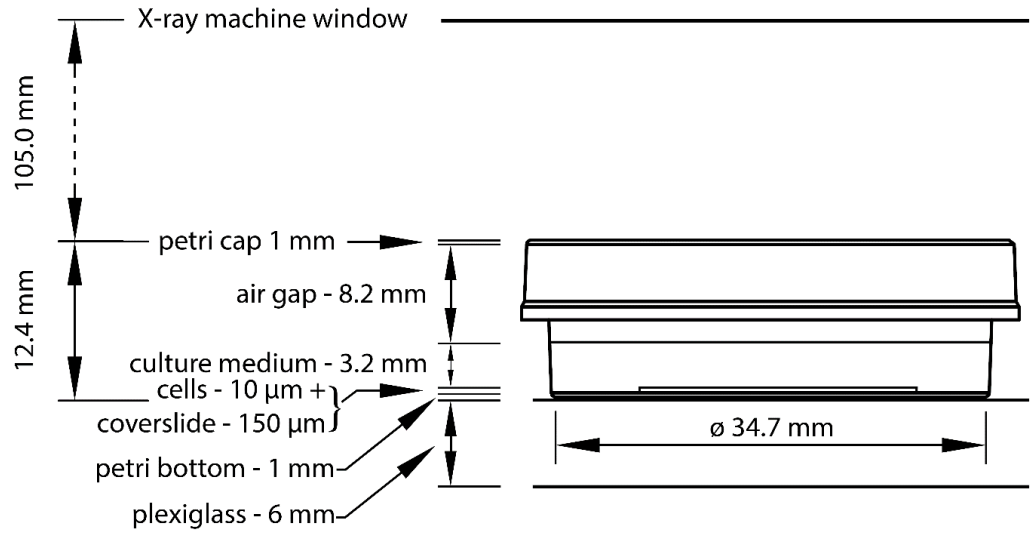

Figure 3.11 Details of the petri dish with cells during irradiation (courtesy of Valerio Ricciardi, Radiation Biophysics Laboratory, University of Naples Federico II).

The dose rate is measured using a RADCAL AccuPro Ionization chamber model (10X6-06) cantered in the position of the cell sample to be irradiated and, at the chosen height of the plexiglass support, resulted equal to $\dot{D}$=1.37 Gy/min. Since the ionization chamber is not flat, to obtain a dose rate measurement as accurate as possible at the position where the cells would be, the plexiglass support was lowered by an amount such that the centre of the sensitive volume of the ionization chamber would coincide with the position of the cell monolayer, that is approximately 1.2 cm. Therefore, after the dose rate measurement, the support was brought up by that amount and routine irradiations were carried out by setting on the tube control unit the

appropriate time as to deliver the desired dose. Thus, given the above-mentioned dose rate, to deliver 1 Gy, for instance, a time of 44 s was set, and so on.

3.4.2 Photon source for experiments on the U87 cell line

The X-rays irradiation for the U87 cell line was conducted at Istituto Nazionale Tumori "Fondazione Pascale" Naples which utilizes the Linac Synergy Sgility Elekta accelerator for radiation therapy, characterized by a maximum field of view of 40 x 40 cm², capable of generating photons at 4 and 6 MeV.

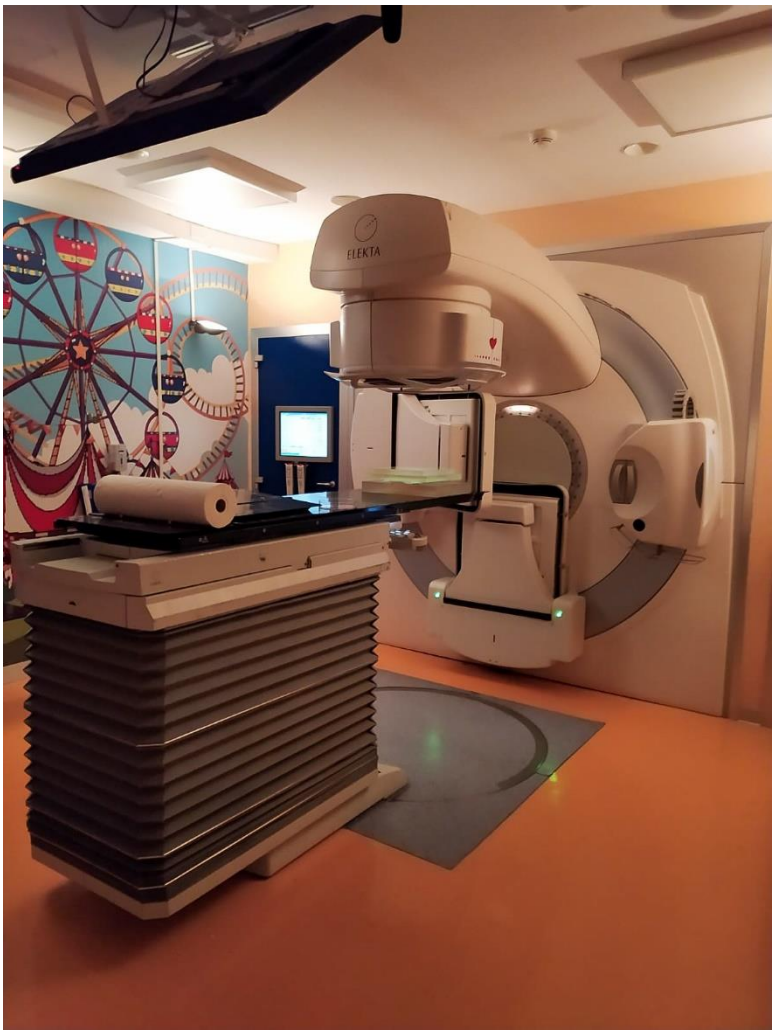

Figure 3.12 Photo of the LINAC accelerator “Synergy Agility” – ELEKTA, at the Istituto Nazionale Tumori “Fondazione Pascale” (courtesy of Rocco Mottareale).

3.4.3 Irradiation protocol

The experimental procedure involves comparing cell samples under different conditions:

- Control cells (not exposed to irradiation), to be fixed 30 minutes after irradiation.
- Control cells (not exposed to irradiation), to be fixed 24 hours after irradiation.
- Cells treated with X-rays at a dose of 0.5 Gy, to be fixed 30 minutes after irradiation.
- Cells treated with X-rays at a dose of 0.5 Gy, to be fixed 24 hours after irradiation.
- Cells treated with X-rays at a dose of 2 Gy, to be fixed 30 minutes after irradiation.
- Cells treated with X-rays at a dose of 2 Gy, to be fixed 24 hours after irradiation.

The time points for cell fixation post-irradiation and the doses are the same for both UMR-106 and U87.

The cells were exposed to different nominal dose values by adjusting the beam exposure time: 0.5 Gy and 2 Gy. Following irradiation, all flasks returned to the Radiation Biophysics Laboratory (Physical Sciences Department, University of Naples Federico II), and placed in the incubator, awaiting fixation at 30 minutes and 24 hours post-irradiation.

3.5 Neutron irradiation

The neutron irradiations for BNCT were performed for both cell lines (U87 and UMR-106) at TRIGA Mark II reactor of L.E.N.A (Laboratorio Energia Nucleare Applicata) in Pavia.

3.5.1 Neutron source for BNCT experiments

The neutron irradiation for in vitro study of radiation-induced DNA damage in the context of BNCT was carried out inside the thermal column of the Triga Mark II reactor (schematized in Figure 3.13).

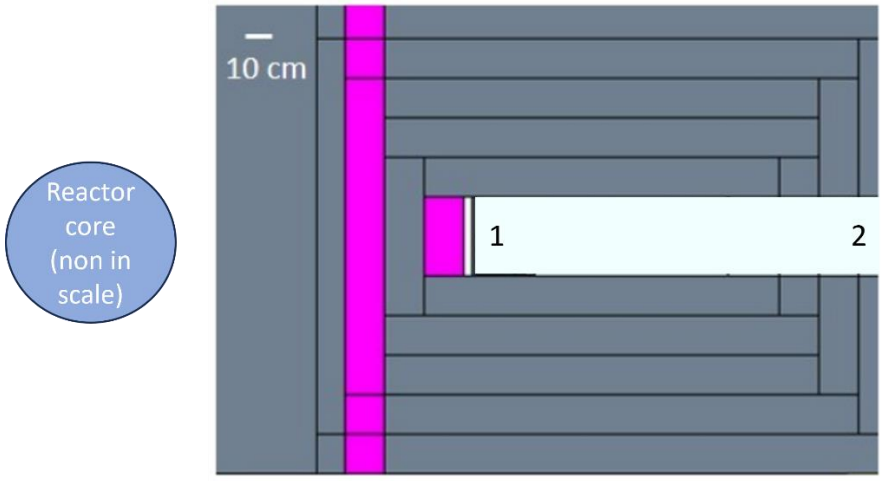

Figure 3.13 Geometrical representation of the reactor thermal column (longitudinal view) [31]. The irradiations for BNCT experiments and the neutron beam (without f-^{10}BPA) were performed by placing the petri dishes in position 1, while boron measurements were conducted in position 2.

The irradiation facility at the TRIGA reactor is a channel obtained inside the thermal column, towards the reactor core. Its dimensions are 100 cm of length, and 40 cm by 20 cm of cross section, illustrated in Figure 3.14 [31].

Figure 3.14 The TRIGA irradiation channel [42].

Irradiation of cells took place at a specific position where the thermal neutron flux measures approximately 8 x 10^7 $cm^{-2}s^{-1}$ at 1 kW (the neutron flux has a linear correlation with power).

The dose calculation was performed by the Pavia group, which determined a dose for BNCT that is isoeffective with 0.5 Gy and 2 Gy of photons. This was possible thanks to the previous work which determined the cell survival as a function of the dose for the two cell lines irradiated with photons, neutrons and neutrons in presence of boron (BNCT). The goal is to achieve the same effect in terms of DNA damage, and this is achieved with a lower neutron dose compared to the X-rays counterpart as both neutrons and BNCT are more effective in causing cell damages. The absorbed dose at the irradiation position for BNCT is the sum of the four components:

Component	Absorbed dose (Gy n^{-1}) 10^{-19}
$^{10}B(n,a)^{7}Li$	(0.667 ± 0.001)
$^{14}N(n,p)^{14}C$	(1.127 ± 0.001)
$^{1}H(n,n)^{1}H$	(0.397 ± 0.004)
Photons	(2.327 ± 0.004)

Figure 3.15 Parameters related to the four components of the dose [43].

Considering ideally 30 ppm of ^{10}B for 1 kW and 30 ppm, the total dose rate is:

7.6e13(30*0.667 + 1.127 + 0.397 + 2.327)*1e-19 = 1.81E-04 Gy/s*

While, for 1 kW and 0 ppm (dose calculated for samples without BPA, considering only the contribution of neutrons), the total dose rate is:

7.6e13(1.127 + 0.397 + 2.327)*1e-19 = 2.93E-05 Gy/s*

Based on previous studies conducted on U87 cells and analysing the survival curves, it has been observed that X-rays are more effective than gamma rays:

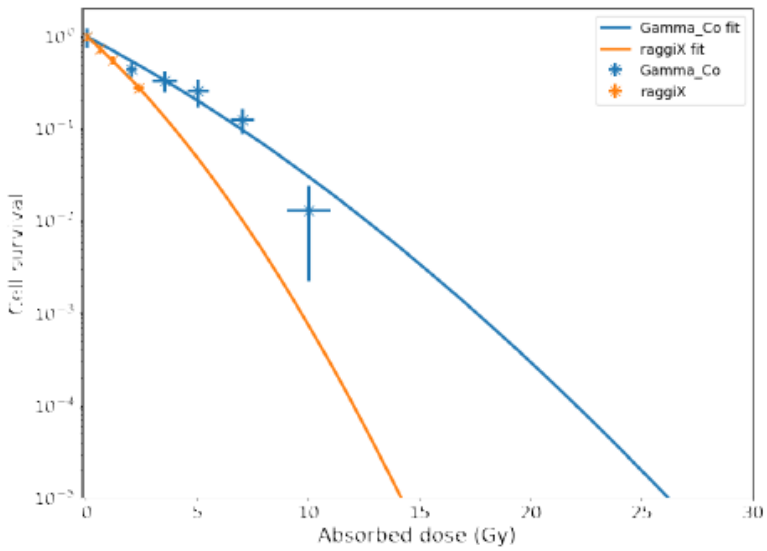

Figure 3.16 Survival curves of the U87 cell line as a function of absorbed dose for irradiation with X-rays (orange) and gamma rays (blue) [44].

Calculating the iso-effective dose for gamma rays compared to X-rays, we obtain that:

- 0.5 Gy of X-rays correspond to 0.85 Gy of gamma rays.
- 2 Gy of X-rays correspond to 3.5 Gy of gamma rays.

Hence, these values are employed to calculate the BNCT doses and neutrons required to achieve an equivalent biological effect. Utilizing the survival curves for BNCT, neutrons, and gamma rays (^{60}Co) in UMR106:

	Parameters of survival models	
	Alpha (Gy^{-1})	**Beta (Gy^{-2})**
^{60}Co source		
Reference radiation	0.14±0.05	0.05±0.01
ThC (TRIGA MARK II)		
Beam gamma photons	0.14±0.05	0.05±0.01
Neutrons	0.6±0.3	0.2±0.1
Boron (BPA)	2.3±0.2	0
ThC: Thermal column of the TRIGA MARK II reactor of University of Pavia (Italy);		

Figure 3.17 Fit parameters for the different dose components [43].

Survival log for 0.85 Gy of photons:

$$(0.14*0.85 + 0.05*0.85*0.85) = 0.155$$

Survival log for 3.5 Gy of photons:

$$(0.14*3.5 + 0.05*3.5*3.5) = 1.103$$

Equalizing the survival log, employing the BNCT fit:

0.155 = 2.3 D → D = 0.067 Gy = BNCT dose to achieve the same survival as 0.85 Gy of photons.

1.103 = 2.3 D → D = 0.479 Gy = BNCT dose to achieve the same survival as 3.5 Gy of photons.

Therefore, to achieve around 0.067 Gy (BNCT dose isoeffective with 0.5 Gy of X-rays), irradiation at 1 kW for 6 minutes is sufficient. Similarly, for approximately 0.479 Gy (BNCT dose isoeffective with 2 Gy of X-rays), irradiation at 4 kW for 11 minutes is needed.

Considering irradiation with neutrons only (samples without BPA):

$0.155 = 0.6\ D + 0.2\ D^2 \rightarrow D = 0.239$ Gy = dose required to achieve an equivalent survival as 0.85 Gy of photons.

$1.103 = 0.6\ D + 0.2\ D^2 \rightarrow D = 1.287$ Gy = dose required to achieve an equivalent survival as 3.5 Gy of photons.

Hence, to achieve approximately 0.239 Gy, irradiation at 10 kW for 14 minutes is required. Similarly, to obtain around 1.287 Gy, irradiation at 60 kW for 12 minutes is necessary.

3.5.2 Irradiation protocol

The experimental procedure involves comparing cell samples under different conditions:

- Control cells (without BPA and without neutron irradiation), to be fixed 30 minutes after irradiation (designated as B-R-).
- Control cells (without BPA and without neutron irradiation), to be fixed 24 hours after irradiation (B-R-).
- Cells treated with BPA, exposed to 1 kW for 6 minutes, to be fixed 30 minutes after irradiation (B+R+).
- Cells treated with BPA, exposed to 1 kW for 6 minutes, to be fixed 24 hours after irradiation (B+R+).
- Cells treated with BPA, exposed to 4 kW for 11 minutes, to be fixed 30 minutes after irradiation (B+R+).
- Cells treated with BPA, exposed to 4 kW for 11 minutes, to be fixed 24 hours after irradiation (B+R+).
- Cells treated with neutrons at 10 kW for 14 minutes (without BPA), to be fixed 30 minutes after irradiation (B-R+).
- Cells treated with neutrons at 10 kW for 14 minutes (without BPA), to be fixed 24 hours after irradiation (B-R+).

- Cells treated with neutrons at 60 kW for 12 minutes (without BPA), to be fixed 30 minutes after irradiation (B-R+).
- Cells treated with neutrons at 60 kW for 12 minutes (without BPA), to be fixed 24 hours after irradiation (B-R+).

The comparison between samples treated with BPA and neutron irradiation (BNCT), and samples treated only with neutron irradiation, is important to demonstrate that neutron irradiation, when combined with the administration of a boron compound, induces significantly greater lethality in cells compared to the individual elements.

UMR-106 and U87 were seeded on glass coverslip (24 x 24 mm) in a 6-wells plate (35 mm) two days before the treatment. Before the neutron irradiation, the medium containing BPA in each petri dish was replaced with 3 ml of fresh medium, after three washes with PBS. Then, the cells were irradiated with around 0.067 Gy (BNCT dose isoeffective with 0.5 Gy of X-rays), exposing the 6-well plates to 1 kW for 6 minutes, and approximately 0.479 Gy (BNCT dose isoeffective with 2 Gy of X-rays), exposing the 6-well plates to 4 kW for 11 minutes, for the samples treated with BPA. While, for samples treated with only neutrons, the cells were irradiated with around 0.239 Gy (dose isoeffective with 0.5 Gy of X-rays) exposing the 6-well plates to 10 kW for 14 minutes, and around 1.287 Gy (dose isoeffective with 2 Gy of X-rays) exposing the 6-well plates to 60 kW for 12 minutes. Nominal doses were estimated assuming 30 ppm of ^{10}B in the cells.

Fixation times have been calculated from the beginning of irradiation.

Figure 3.18 Extraction of the 6-well plates from the TRIGA irradiation channel.

3.5.3 Optimization of the irradiation protocol for BNCT experiments

Several experiments were conducted in Pavia for BNCT to identify the optimal irradiation protocol. The use of multi-well flasks allowed us to prepare triplicate samples, overcoming challenges related to the transportation and irradiation of individual petri dishes. Initially, issues arose due to low cell density, leading to a significant loss of cells in the initial experiments. This required a series of seeding protocols to determine the appropriate cell concentration. These attempts were conducted on both U87 and UMR-106 cell lines. The aim is to identify an optimal cell density for both irradiation (minimizing potential cellular loss caused by stress) and achieving an optimal distribution of cells (non-overlapping) to facilitate the subsequent visualization of fluorescence foci. This approach enables a precise examination of damage at the individual cell level.

Figure 3.19 Example of a seeding trial conducted for the U87 cell line. Various concentrations were compared (ranging from 2.0×10^4 cells to 1.0×10^5 cells) to determine the optimal condition for irradiation and the foci assay.

From the results of different seeding protocols, we have concluded that the optimal concentration for UMR-106 is 3.0×10^4 cells and for U87 is 4.0×10^4 cells.

However, initially, we placed the samples to be fixed at 30 minutes post-irradiation and the samples to be fixed 24 hours post-irradiation in the same multi-well (which would be treated with the same dose for both samples.)

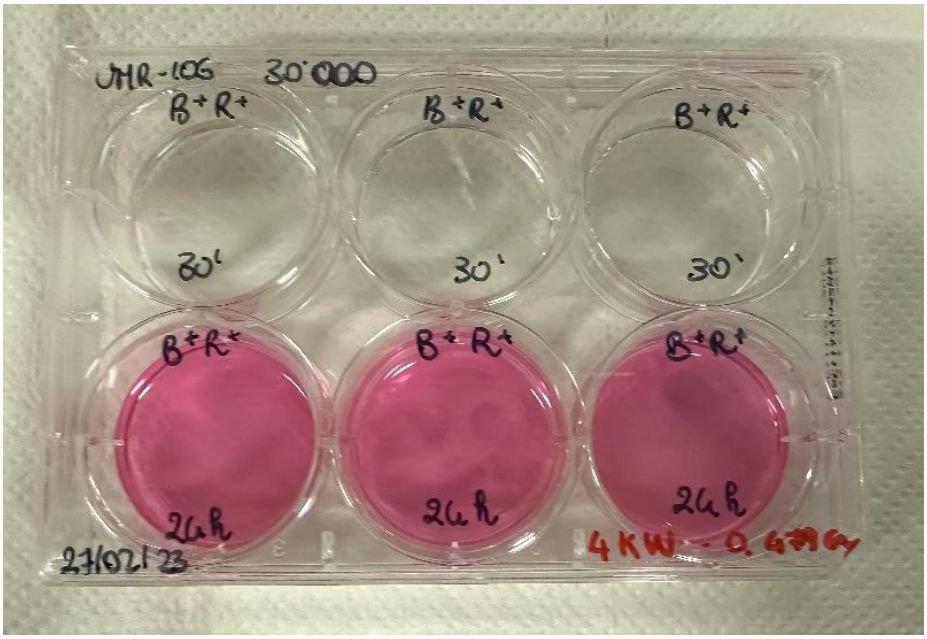

Figure 3.20 Example of a 6-well plate used in the first experiments. In this case, within the same multi-well, triplicate samples were prepared: those fixed 30 minutes post-irradiation (in the upper section of the multi-well plate) and those sample for fixation 24 hours post-irradiation (in the lower part, still with the culture medium to be placed in the incubator).

This arrangement was not appropriate, as the samples intended to be fixed 24 hours post-irradiation experienced stress due to the opening and closing of the petri dishes (for fixing the 30-minute samples). For this reason, in subsequent experiments, we employed different multi-well plates for the samples at 30 minutes and 24 hours post-irradiation, successfully mitigating any issues associated with BNCT irradiation.

3.6 Foci assay

3.6.1 Optimization of the protocol for the foci assay

After irradiating the samples, an immunofluorescence protocol was applied. This protocol relied on the use of specific antibodies directed against γH2AX and 53BP1, aiming to detect and visualize these proteins and quantify foci through fluorescence microscopy. Detailed protocols are provided in the subsequent paragraphs.

It is important to highlight that we optimized the protocol previously employed by the Naples group. Initially, slide flasks were utilized (illustrated in Figure 3.21) for studying DNA damage through the foci assay.

Figure 3.21 Example of slide flasks used in previous experiments.

In this study, we conducted experiments by seeding the cells onto glass coverslip (24 x 24 mm) in petri dishes (35 mm).

Figure 3.22 An example of a 6-well plate used in the experiments, where cells were seeded on glass coverslips (24 x 24 mm).

The aim of this change is to optimize the visualization of cells on glass coverslips with the Metafer software, aiming to obtain images as clear as possible.

3.6.2 Experimental protocol

To evaluate the radiation-induced DNA damage through the foci assay, cells were fixed with 4% paraformaldehyde (or 10% formalin) to preserve their structure after irradiation. Subsequently, permeabilization of cellular membranes was performed by treating them with agents that enhance permeability, allowing antibodies to penetrate in the cells. Permeabilization buffer was composed of 0.25 % Triton X-100 in PBS. A blocking solution was applied to prevent non-specific antibody binding, composed of 10 % goat serum, 1 % BSA, 0.3 M Glycine, 0.1 % Tween 20 in PBS. Cells were then incubated with specific antibodies targeting DNA damage markers, γH2AX and 53BP1. The primary antibodies used are anti-γH2AX, a murine monoclonal antibody that binds to the final amino acid sequence of 134-142 in the γH2AX histone, while anti-53BP1 is a rabbit polyclonal antibody that recognizes the region of 53BP1 between amino acids 350 and 400 (Ser/Thr-Gln sequences). After washing to remove unbound antibodies, cells were incubated with secondary antibodies labelled with fluorochromes, which bind to the primary antibodies. The fluorescent probes used are Alexa Fluor 555 (AF555, fluorophore for γH2AX) and Alexa Fluor 488 (AF488, fluorophore for 53BP1), respectively bound to the Anti-mouse and Anti-rabbit secondary antibodies. AF555 has an absorption spectrum with a peak at 555 nm (optimal excitation wavelength for visualizing γH2AX foci) and an emission spectrum with a maximum at 580 nm (γH2AX foci, under the microscope, will appear orange/red), while AF488 has an absorption peak at 488 nm (optimal excitation wavelength for visualizing 53BP1 foci) and an emission maximum at 525 nm (53BP1 foci, under the microscope, will appear green).

After the incubation period with secondary antibodies, additional washes were performed to remove excess secondary antibodies, and slides were mounted for analysis.

The detailed protocol is provided below:

1. **Fixation:**
    - Remove the medium from the petri dish.
    - Wash the cells twice with PBS (1.5 ml).
    - Add 1 ml of 4 % paraformaldehyde and leave for 15 min at room temperature (RT).
    - Wash the cells three times with PBS (1.5 ml) – at this point the cells can be stored in PBS at 4°C.
2. **Permeabilization:**
    - Remove the PBS and add 1 ml of permeabilization buffer to the petri dish and incubate for 15 min at RT.
    - Remove the permeabilization buffer and wash the cells with PBS.
3. **Blocking:**
    - Remove the PBS and add 1 ml of blocking buffer (BB).
    - Incubate for 1 h at 37°C in the incubator.
4. **Incubation with the primary antibody**:
    - Add 100 μL drop of 1 μg/ml primary antibodies mixture (1:1000) in BB on a petri dish covered with parafilm.
    - Incubate for 1 h at 37°C the glass coverslip (previously drained on paper) “faced down” on a 100 μl drop of primary antibodies mixture in BB (or overnight at 4°C in fridge).
    - Remove the blocking buffer BB from the petri dishes.
    - Remove the glass coverslips from the parafilm and place them back in each petri dish.
    - Wash the petri dishes 4 times with 1.5 ml of washing buffer (WB) – 5 min each wash.

5. **Incubation with the secondary antibody**:

- From now on work in dark (not under direct light).
- Add 100 μL drop of 1 μg/ml secondary antibodies mixture (1:1000) in BB on a petri dish covered with parafilm (2 μg/ml Anti-mouse (gH2AX) and 4 μg/ml Anti-rabbit (53BP1).
- Incubate for 1 h at 37°C in dark the glass coverslips (previously drained on paper) "faced down" on a 100 μl drop of primary antibodies mixture in BB.
- Remove the WB from the petri dishes.
- Remove the glass coverslips from the parafilm and place them back in each petri dish.
- Wash the petri dishes 4 times with 1.5 ml of WB – 5 min each wash.

6. **Posthybridization:**

- Remove the WB and add 1.5 ml of PBS to each petri dish.
- Place the glass coverslip (previously washed in dH20 to remove PBS salts prior to slide mounting and drained on paper) "faced down" on a drop of Prolong Gold antifade with DAPI on the slide (previously cleaned with ethanol).
- Leave the slides (lying flat) in the dark overnight at RT.
- Slides can be viewed (and acquired/scored) or stored in -20 °C in freezer.

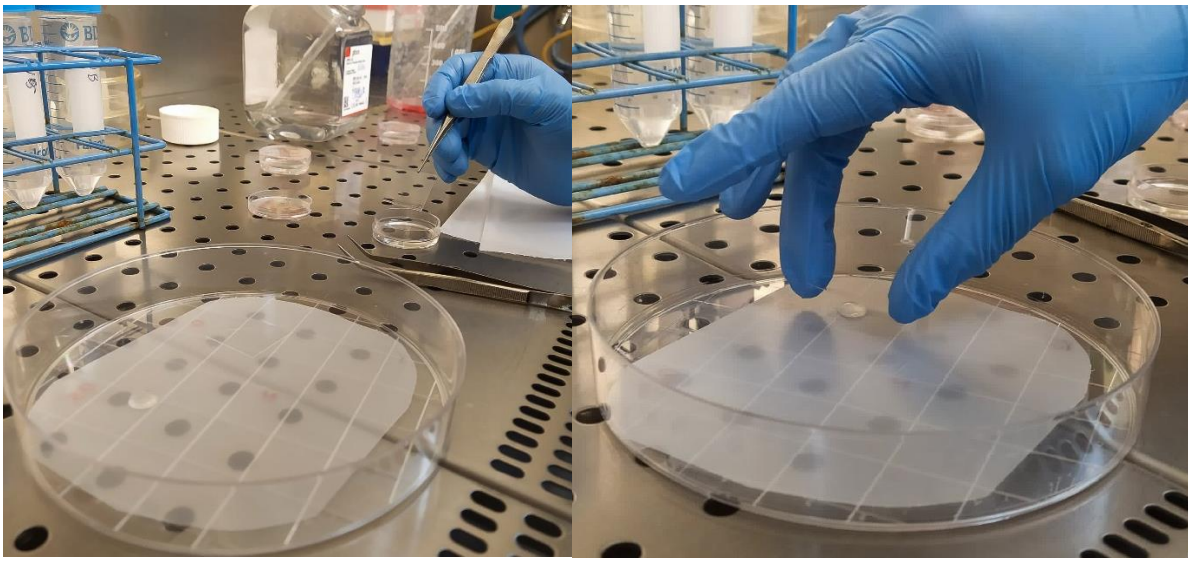

Figure 3.23 Image illustrating an example of how cells (fixed on glass coverslips 24 x 24 mm) were incubated with antibodies. Each glass coverslips were placed “faced down” on a 100 µl drop of antibodies mixture in BB.

3.7 Foci analysis

Data analysis was carried out at the Radiation Biophysics Laboratory at University of Naples Federico II, using a fluorescence microscope (Imager 1, Zeiss, Germany) connected to a computer equipped with the Metafer software (Metasystem, Germany) for automated image acquisition. The fluorescence microscope is utilized for observing and analysing samples using fluorescence imaging techniques. It is equipped with fluorescence light sources and optical filters that enable the excitation of specific fluorochromes within the sample, resulting in fluorescent signals. In this study, three types of fluorophores visible in the frequencies of blue (DAPI), red (γH2AX) and green (53BP1) light were used.

3.7.1 The Metafer software

Cell images were acquired with the automatic Metafer system, introduced by MetaSystems in 2004 and connected to a fluorescence microscope. The Axio Imager Zeiss is an epifluorescence microscope (excitation light is incident on the sample from above) equipped with a lamp emitting in the infrared and UV range. It features a touch screen interface for simplified operation, and the available microscope objectives for magnification are 10x, 40x, and 63x with oil immersion.

Figure 3.24 Image of the fluorescence microscope (Imager 1, Zeiss, Germany) connected to a computer equipped with the Metafer software (Metasystem, Germany) for automated image acquisition [45]. It consists of a Zeiss Axio Imager microscope, a scanning stage with a capacity for 8 slides, a high-resolution CCD camera connected to a frame grabber, a DVD-RAM drive for data storage, a PC, and a monitor.

Metafer can separately identify mononucleated cells by setting a series of parameters to create a “classifier”. To start a search on the Metafer system, up to 8 slides can be loaded on the stage of the microscope. The correct operation mode is selected, and in a slide set-up dialogue, the slide names are entered, the classifier is chosen, and the search window is defined (to determine the area to analyse on the slide) [45].

In particular, the initial parameters to select are:

- *Data path*: specifies where the files related to the slides, resulting from the scan, should be stored.
- *Name*: each slide should correspond to a file with a unique name.
- *Mode*: based on the events to be identified. For the foci assay, the MetaCyte module is chosen, which is utilized for detecting nuclei and quantifying fluorescent spots within them.
- *Classifier*: the classifier is a set of parameters that defines how the software processes and analyses the images. In the case of the foci assay, it determines how the system identifies cellular nuclei and the associated foci for both γH2AX and 53BP1. It is specific to the chosen magnification and the cell line used.
- *Maximum cell count*: establishes the maximum number of cells to be scanned.

After starting the search, the system automatically engages a 10x objective lens, adjusts the microscope lens according to the actual contrast and performs an autofocus. Subsequently, the complete search window is scanned, and positive objects are displayed in an image gallery [45]. Therefore, in the initial acquisition of slide images, a scan is conducted using a 10x magnification objective, employing the DAPI (blue) emission filter. This filter facilitates the identification of the region of interest on the slide and the nuclei within it. Subsequently, a high-magnification scan is performed with a 63x objective at various focal planes to capture high-resolution signals from individual nuclei previously detected in the RGB (red, green, blue)

channels. Upon completing the scan, Metafer generates a gallery for the acquired images of individual nuclei, also providing an estimate of the number of foci per cell for 53BP1, γ-H2AX, and colocalized signals.

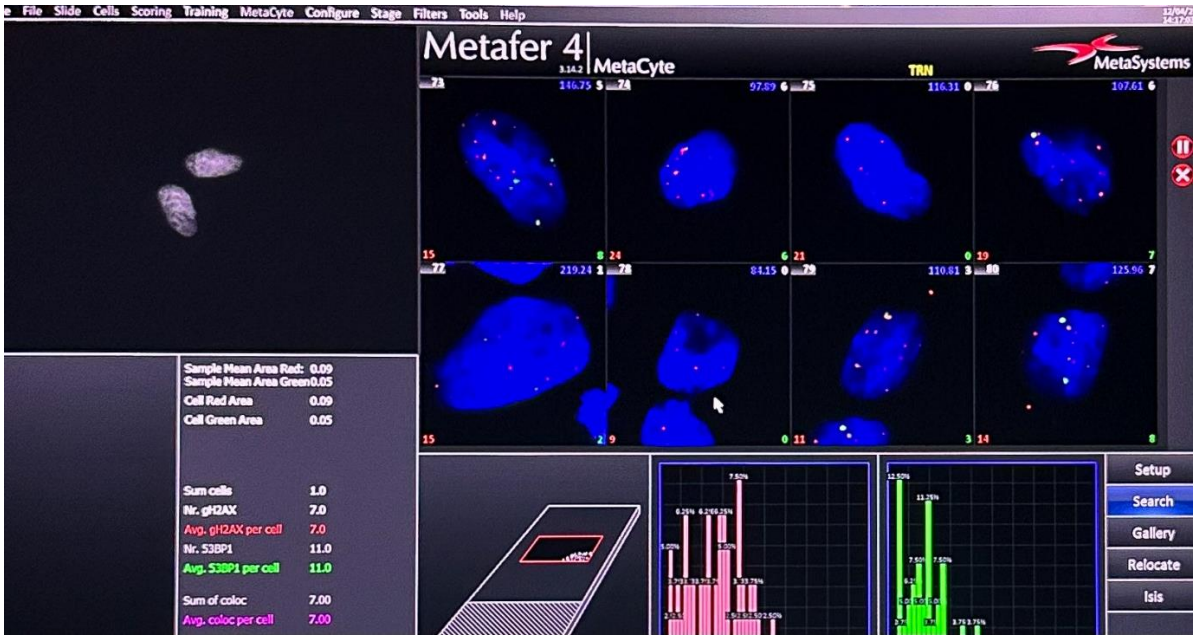

Figure 3.25 Example of a gallery produced by the Metafer software after scanning a slide.

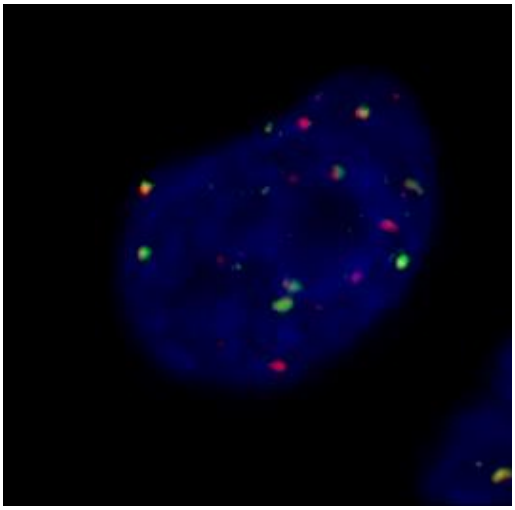

Figure 3.26 Example of a nucleus of a cell acquired by the Metafer software. The nucleus was stained with DAPI, hence visible in blue, while the other signals represent γ-H2AX (red) and 53BP1 (green), with some overlapping.

3.7.2 Optimization of the Metafer classifier

Utilizing the previously classifiers created by the earlier works of the Naples group, some parameters have been modified to improve Metafer's counting, also comparing with the manual counting. Taking inspiration from the research conducted by Zatsko et al. in 2022 [45] and adjusting the cell processing, specifically, we have introduced changes in:

- *Background*: SBLocMinAsy (Subtract background, Local Asymmetric Minimum) operation has been used. This operation is very efficient in removing a continuous variable background, analysing the background intensities on all four sides of the current pixel separately and then subtracting the highest of the four values.
- *Threshold:* SegThrAbs (Set Absolute Segmentation Threshold =129) has been used. This operation subtracts the segmentation threshold to the specified value.
- *Grey Levels*: StretchGL-NSP (Stretch Grey Levels, Number of Saturated Pixels = 10) was chosen as operation.
- *Number of Focus Planes*: 10.
- *Focus parameter set*: for FITC (53BP1) signal: Abs. Spot Meas. Area 20/100 µm, distance 3/10 µm, intensity 10%. For γH2AX signal: Abs. Spot Meas. Area 20/100 µm; Distance 2/10 µm; Intensity 5%. For fusion signals – Channel Mask 6; Max. Dist. 10/10 µm.

The use of this classifier allowed us to achieve an average number of foci per cell as close as possible to the manual count.

4 Results and discussion

In this section, the results of the study on the response of UMR-106 and U87 cells to DNA damage induced by exposure to X-rays and neutron irradiation (in the context of BNCT) will be presented through the application of the foci assay. Subsequently, a comparison between the treatments and relevant observations for each cell line will be provided.

Boron concentration in UMR-106 samples was measured to confirm that 30 ppm was a good assumption for dose calculation. Three pellets were prepared for neutron autoradiography and the result confirmed a concentration of 28 ± 2 ppm. Figure 4.1 shows the analysis of boron concentration in a representative sample.

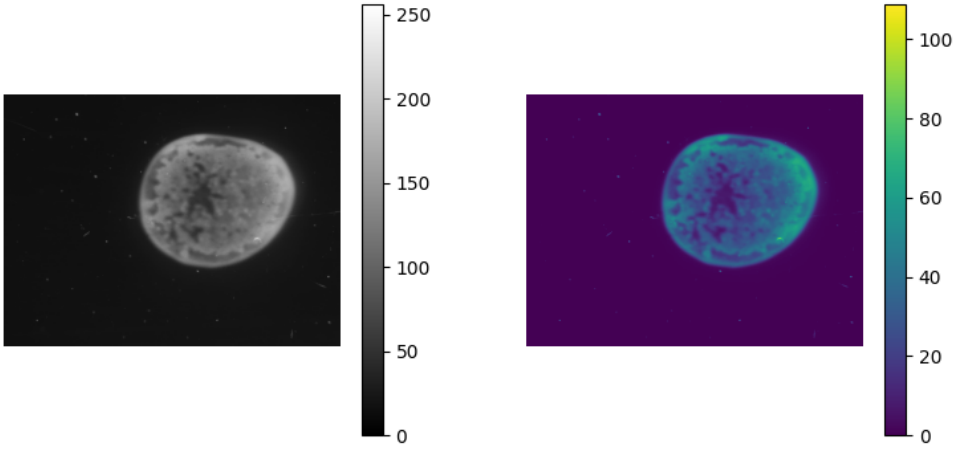

Figure 4.1 Neutron autoradiography of a cell pellet. In this case, neutron autoradiography (left) was optimized to obtain a map of boron distribution by a high-fluence irradiation and a long etching. The tracks on the CR-39 thus merge resulting in lighter areas where a higher number of boron captures occurred. On the right, the greyscale was converted in boron concentration values by a previous calibration. The average concentration in this sample was 30.2 ± 3.0 ppm.

The marker γH2AX indicates the presence of DSBs, while 53BP1 is a marker involved in the DNA damage repair. The analysis with Metafer provided an average number of γH2AX and 53BP1 per cell and, through the colocalization of the two signals, provided more robust data, reducing the possibility of having false positives. Indeed, colocalization occurs when both proteins are present at the same site within the cell nucleus. Specifically, when DNA is damaged, γH2AX accumulates around the damage site, indicating the presence DSBs. Simultaneously, 53BP1 also accumulates at DSB sites. The colocalization of both markers indicates coordinated activity in recruiting proteins involved in DNA repair.

The graphs presented in the following paragraphs have been created by analysing the data obtained by the Metafer software.

For statistical analysis, the average number of foci per cell was calculated in each experiment for each sample as the ratio of the sum of the counted foci (n) to the number of cells (N) in the sample (approximately 150 cells were acquired).

Assuming *f* as the average number of foci per cell:

$$f = \frac{n}{N}$$

The error (σ) is calculated according to the binomial distribution:

$$\sigma = \sqrt{\frac{f \cdot |f - 1|}{N}}$$

An exception concerns the error calculation for the experiments conducted on the UMR-106 cell line treated with X-rays. Since three different experiments were conducted, a weighted value was calculated as follows.

Given the weight (w), defined as the reciprocal of the square root of the standard error for each measurement:

$$w = \frac{1}{\sqrt{\sigma^2}}$$

and considering the weighted mean as given by:

$$\bar{X}_w = \frac{\sum_{i=1}^{3} f_i \cdot w_i}{\sum_{i=1}^{3} w_i}$$

The final error is calculated as a weighted error, that is:

$$\sigma_w = \frac{1}{\sqrt{\sum_{i=1}^{3} w_i}}$$

4.1 Results of radiation-induced DNA damage on UMR-106

In the following paragraphs, the results of the damage induced on UMR-106 following treatment with X-rays, BNCT and neutron treatment (without f-^{10}BPA) will be presented. Subsequently, a comparative analysis between BNCT treatment and X-rays treatment will be discussed.

4.1.1 Results of DNA damage induced by X-rays treatment

UMR-106 were seeded approximately 18 hours before the X-rays treatment on glass coverslip (24 x 24 mm) placed in petri dishes (35 mm) at a density of 1.5×10^4 cells. This cell density allowed a uniform distribution of cells on the coverslip, facilitating acquisition through fluorescence microscopy and subsequent quantification of DNA damage per individual cell using the Metafer software.

The following results for the X-rays treated UMR-106 line are reported below.

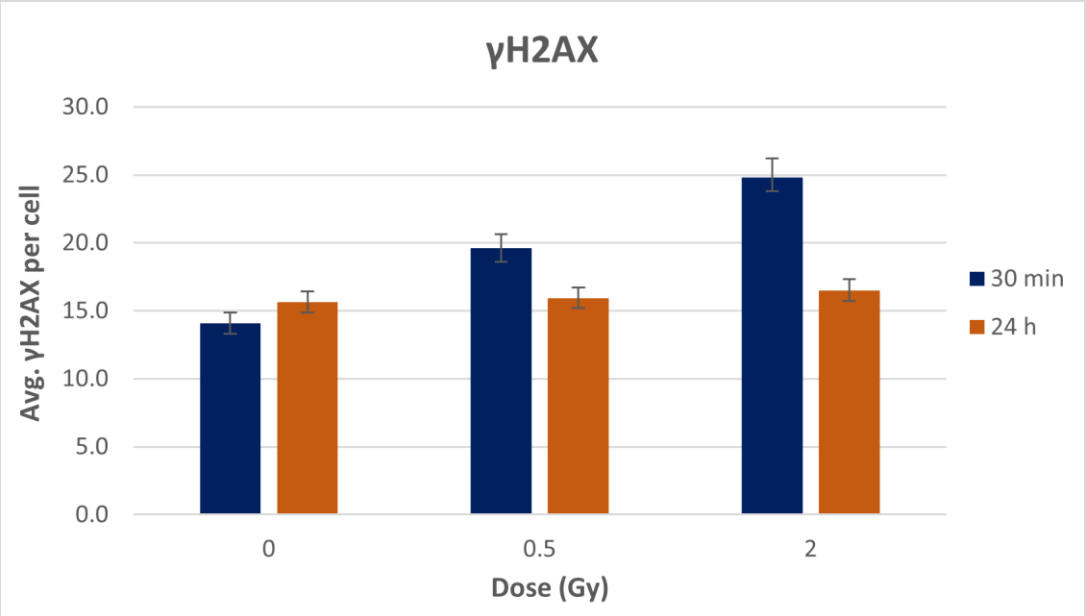

Figure 4.2 Average number of γH2AX foci per cell.

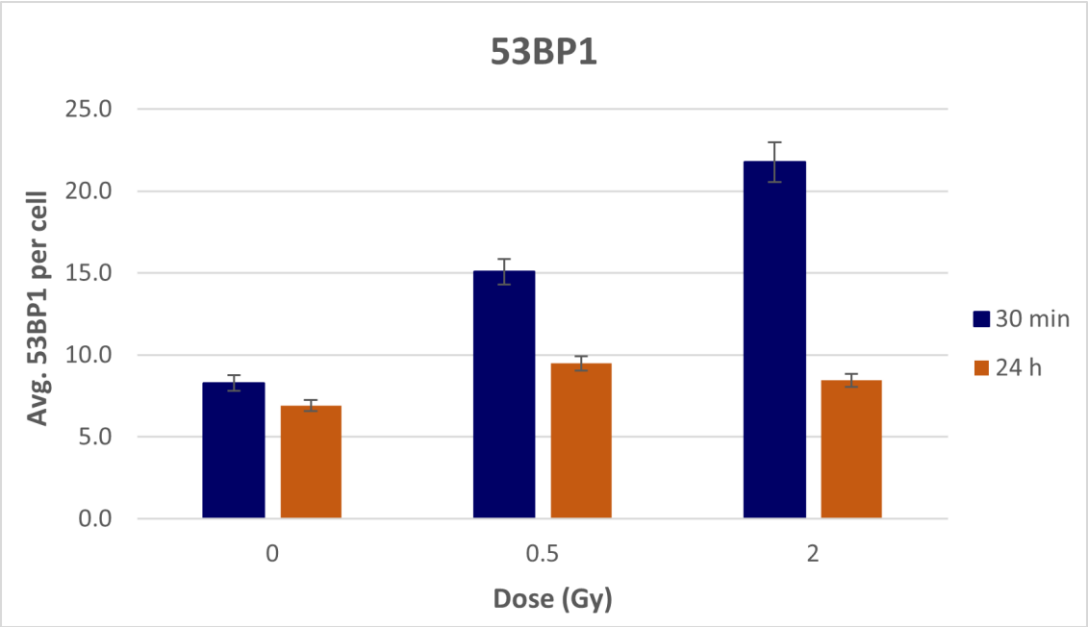

Figure 4.3 Average number of 53BP1 foci per cell.

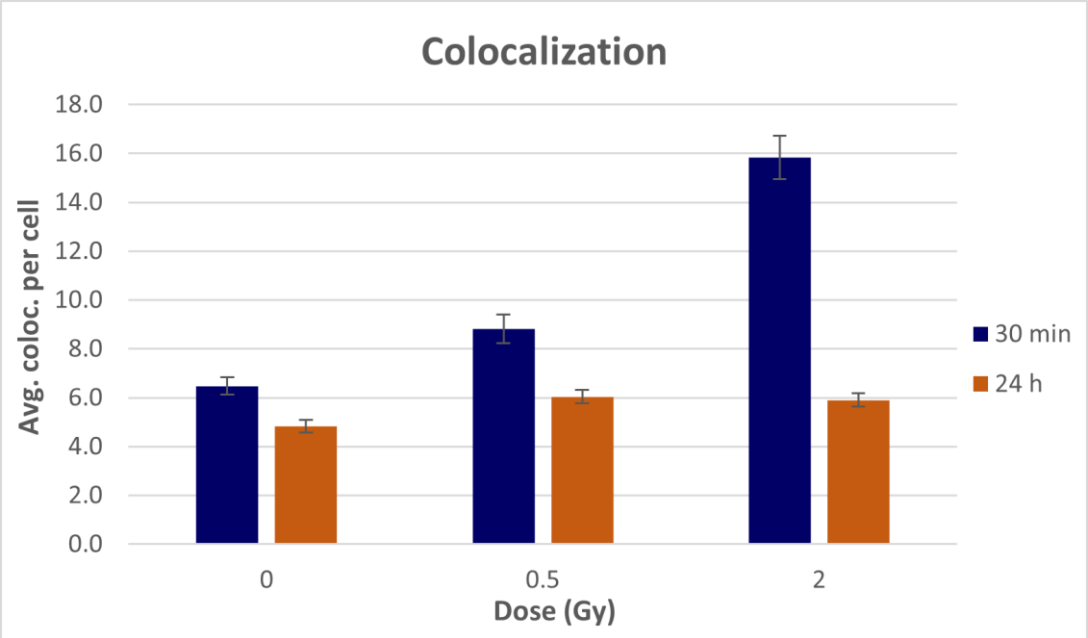

Figure 4.4 Average number of colocalized signals per cell.

For the X-rays treatment on the UMR-106 cell line, three distinct experiments were conducted, and the reported result is the average of these three experiments. Errors were calculated using the Weighted Standard Error of the Mean.

As shown in the graphs (Figure 4.2, 4.3 and 4.4), cells were exposed to 0.5 Gy and 2 Gy of X-rays, and the results were compared with the control sample (without irradiation) with fixation performed at 30 minutes (in blue) and 24 hours post-irradiation (orange). It can be observed that:

- At 30 minutes post-irradiation, there is a noticeable increase with time in the damage of the 0.5-Gy samples compared to controls, observed in both γH2AX and 53BP1 signals, as well as in colocalization signals.
- At 24 hours post-irradiation, an unexpected lower value was recorded for samples exposed to the higher dose (i.e., 2 Gy). This phenomenon could be caused by preferential elimination of more heavily damaged cells showing a greater frequency of foci via rapid interphase death (e.g., apoptosis) as to account for the apparent saturation/decline in the dose responses of residual foci at 2 Gy, as observed in the study by Marková et al. 2011 [46].

  Moreover, the number of foci is lower at 24 hours post-irradiation compared to samples fixed at 30 minutes, probably attributed to the activation of DNA repair processes or apoptosis by irradiated cells in response to radiation-induced damage. At 24 hours post-irradiation, some cells may have already completed these processes, resulting in a reduction in the number of foci. At the cellular level, the kinetics of formation or loss of γ-H2AX foci may reflect the rate or efficiency of DSBs repair. Additionally, there is evidence that DSBs assayed several hours after the initial radiation challenge that still remain unrepaired,

known as residual DNA damage, may be predictive of individual susceptibility to complex DNA lesions that can be lethal [47].

4.1.2 Results of DNA damage induced by BNCT treatment

For BNCT experiment, UMR-106 were seeded on glass coverslip (24 x 24 mm) in a 6-wells plate (35 mm) at a density of 3.0×10^4 cells two days before the treatment. The samples were prepared considering treatment both in the presence and absence of f-^{10}BPA (control sample). Neutron irradiations were conducted in the thermal column of the TRIGA Mark II nuclear reactor at the University of Pavia. The dose was calculated to be isoeffective at 0.5 Gy and 2 Gy of photons, corresponding to power levels of 1 kW and 4 kW, respectively, at the reactor. Two separate experiments were conducted for UMR-106 in the context of BNCT. The first experiment yielded unreliable data as the samples treated with BNCT showed lower damage compared to the control sample. For simplicity, only the graph relating to the colocalization of the γ-H2AX and 53BP1 signals is reported below.

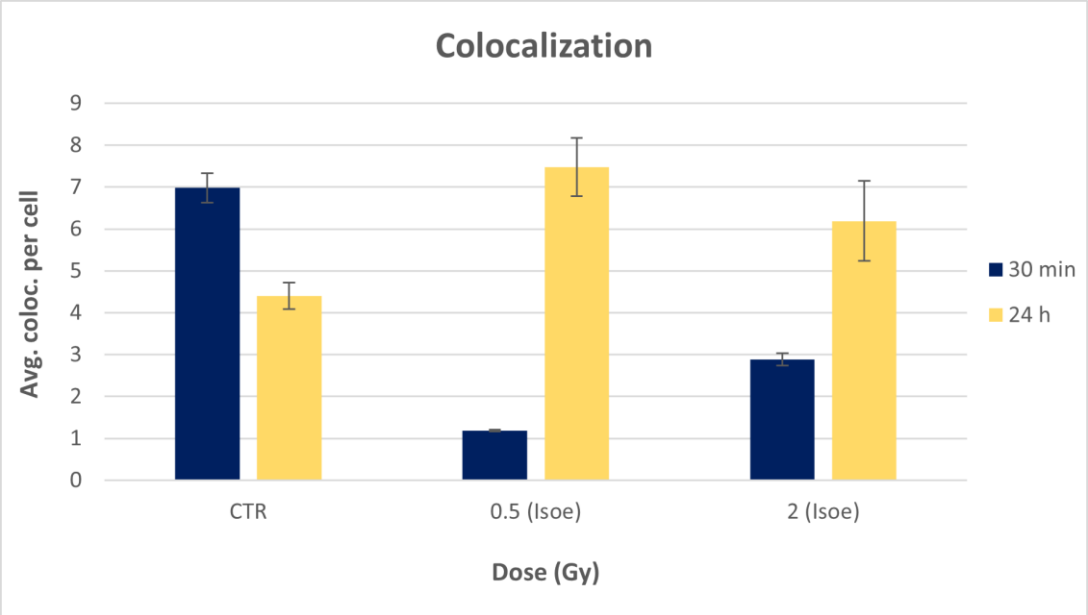

Figure 4.5 Average number of colocalized signals per cell: comparison between control samples (CTR) and samples treated with BNCT at doses isoeffective to 0.5 Gy and 2 Gy, fixed at 30 minutes post irradiation (in blue) and 24 hours post irradiation (in yellow).

The lack of reliability of the first experiment was further confirmed through the observation of cells via fluorescence microscopy (see Figure 4.6). The morphology of the cells, especially in the treated samples, exhibits noticeable alterations, with a significantly reduced size and irregular shape. This shrinkage could explain the observed decrease in the number of lesions. However, this change in shape and size appears not directly correlated to BNCT treatment, as a second experiment did not show such extreme morphological alterations. Instead, it could be associated with stress experienced during cell seeding or irradiation.

Furthermore, the 24-hour sample showed a severe cell loss, making it difficult to acquire images through fluorescence microscopy. Consequently, the data obtained with Metafer refers to less than 50 cells.

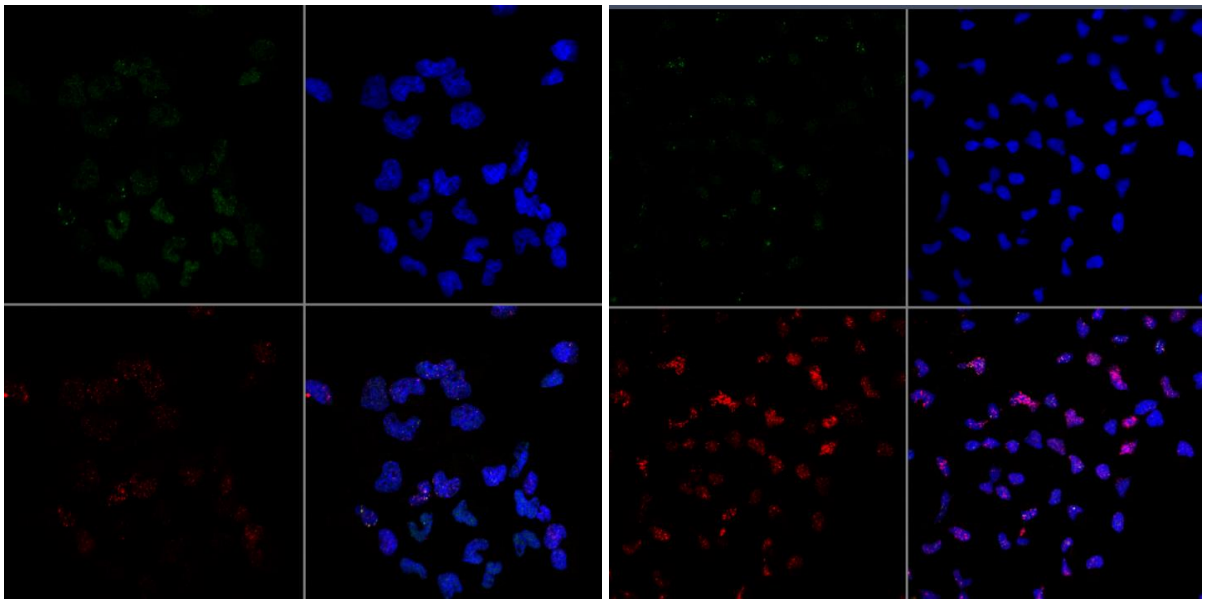

Figura 4.6 Comparison between CTR (on the left), and the sample treated with BNCT at 0.5 Gy (on the right). For both samples, cells were fixed at 30 minutes post irradiation. The images were obtained by confocal microscopy (Department of Biology, University of Naples Federico II). In blue, the signal detected by DAPI, in red, the signal of γ-H2AX, and in green, the signal of 53BP1.

In Figure 4.7, the graphs relating to the second experiment conducted on the UMR-106 treated with BNCT are presented.

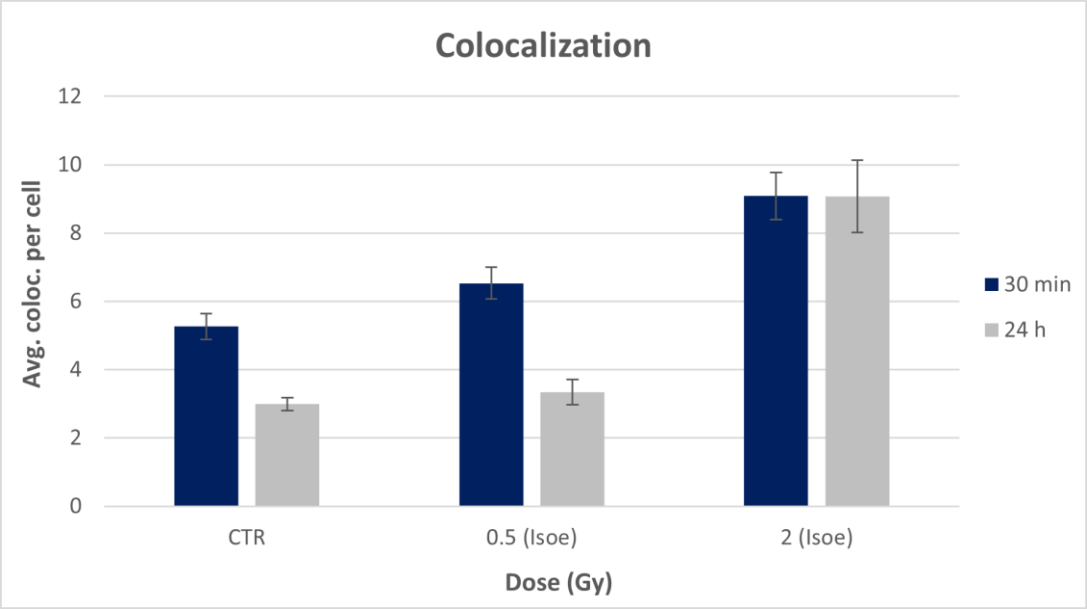

Figure 4.7 Average number of colocalized signals per cell.

Also for this experiment the cells were exposed to isoeffective dose values to the 0.5 Gy and 2 Gy of X irradiation, doses corresponding to the powers of 1 kW and 4 kW for the samples treated with BNCT. It can be noted that:

- At 30 minutes post-irradiation (samples in blue), an increasing trend is observed as a function of dose compared to the control sample. This suggests that an increase in radiation dose results in more significant cellular damage.
- At 24 hours post-irradiation, there was no significant increase in damage at the lower dose, possibly indicating a rapid activation of the activation of repair systems, while at 2 Gy the level of damage was similar to that recorded after 30 minutes, indicating again the possible elimination of more severely damaged cells. It is important to note that the response to DNA damage is also influenced by the cell cycle stage [48], so it is likely that cells are in a phase where DNA is not accessible to repair systems.

It is interesting to note that, at 24 hours post-irradiation, samples treated with BNCT show a significant loss of cells, which also complicated the acquisition of more robust data with the Metafer image acquisition software.

Regarding the doubts about the morphology of the cells in the previous experiment, the samples analysed by confocal microscopy relating to the second experiment are presented below, for which the data are considered reliable.

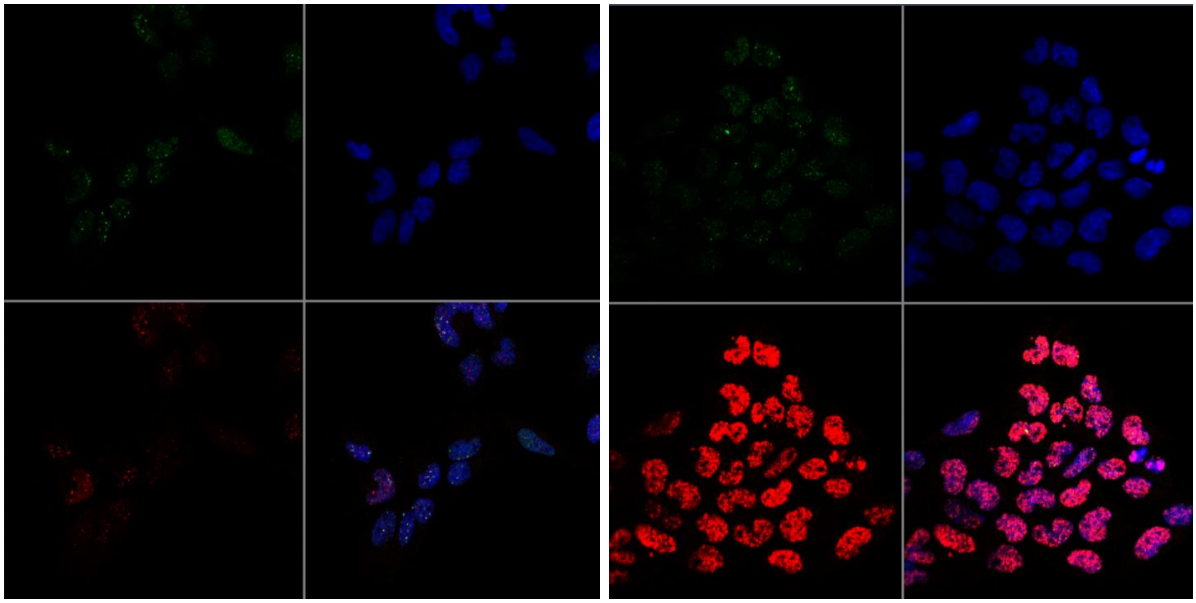

Figure 4.8 Comparison between CTR (on the left) and cells treated with BNCT at a dose isoeffective to 2 Gy. For both samples, cells were fixed at 30 minutes post irradiation. The images were obtained by confocal microscopy (Department of Biology, University of Naples Federico II). In blue, the signal detected by DAPI, in red, the signal of γ-H2AX, and in green, the signal of 53BP1.

In Figure 4.8, it is evident (via the blue DAPI signal) that the morphology of the cells in the treated samples is very similar to that of the control sample. This situation is significantly different from the first experiment and seems to confirm that irradiations at 1 kW and 4 kW do not significantly alter the morphology of the samples.

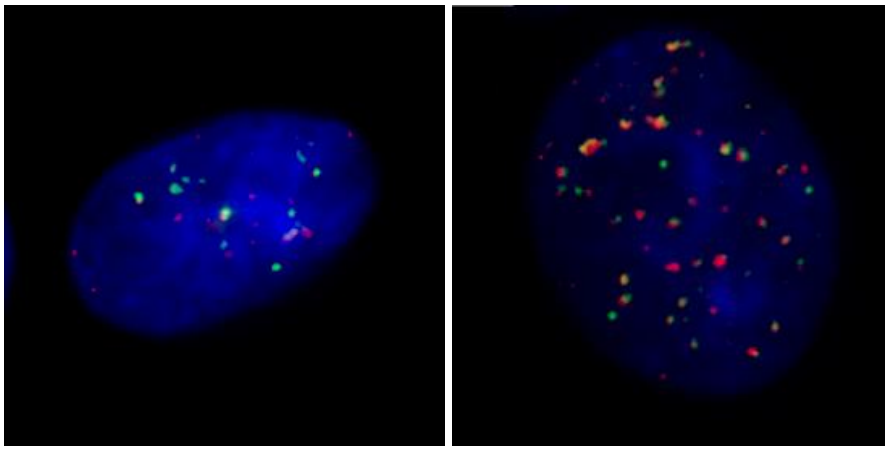

Figura 4.9 Cellular observation conducted using the Metafer system with a 63x objective. Comparison between the control sample (on the left) and a cell treated with BNCT (on the right).

Below is also reported an interesting qualitative evidence of the increase in the fluorescence signal of γ-H2AX (in red) and 53BP1 (in green) at 30 minutes post-irradiation, as a function of the dose (Figure 4.10).

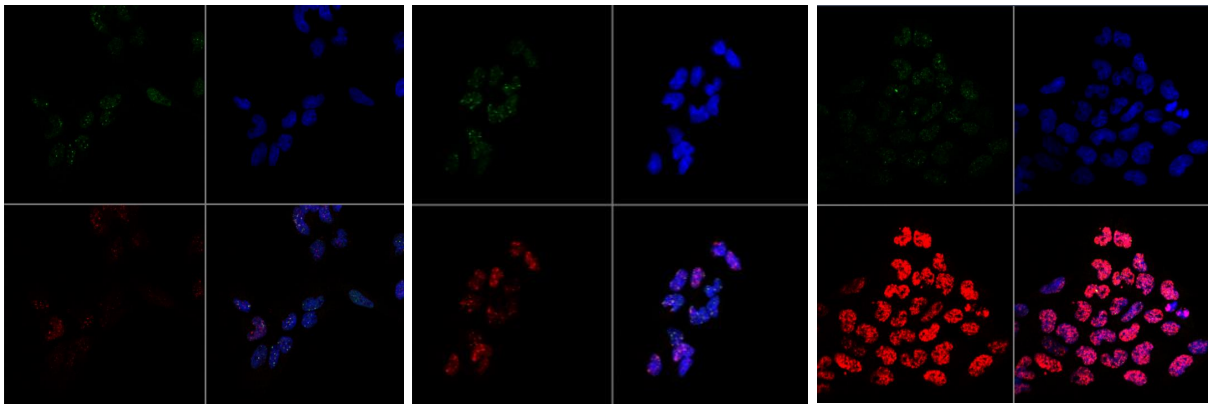

Figura 4.10 Comparison between CTR (first image), sample treated with BNCT at a dose isoeffective to 0.5 Gy (second image), sample treated at a dose isoeffective to 2 Gy, showing a significant increase in the signal of γ-H2AX (in red) and 53BP1 (in green) as dose increases.

On the other hand, in Figure 4.11, fluorescence-based evidence of the reduction of the γ-H2AX and 53BP1 signal at 24 hours post-irradiation is shown, as a function of the dose and compared to the samples fixed at 30 minutes post-irradiation. This is indicative of a decrease in damage.

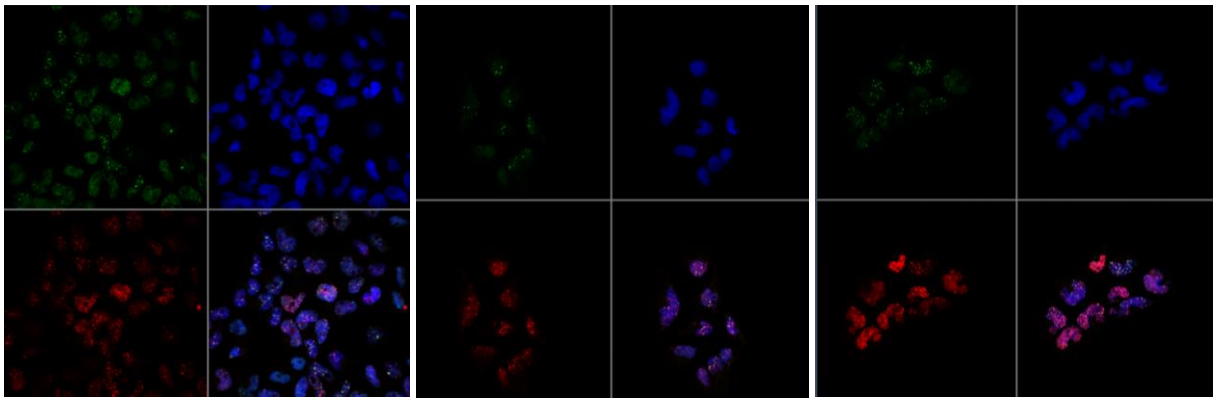

Figura 4.11 Comparison between CTR (first image), sample treated with BNCT at a dose isoeffective to 0.5 Gy (second image), sample treated at a dose isoeffective to 2 Gy. The images show a reduction of the γ-H2AX and 53BP1 signal at 24 hours post-irradiation but a higher damage signal is maintained at higher doses.

4.1.3 Results of DNA damage induced by neutron irradiation

The following results are meant to show the damage caused by neutron irradiation in samples without f-^{10}BPA (denoted as B-R+), in comparison with the damage induced by BNCT (samples treated with neutron irradiation but in the presence of f-^{10}BPA, denoted as B+R+). The dose was calculated to be iso-effective with regard to 0.5 Gy and 2 Gy of photons, which, considering only the contribution of neutrons, corresponds to power levels of 10 kW and 60 kW at the Triga reactor. In the case of samples treated with f-^{10}BPA, the calculated powers are 1 kW and 4 kW. For the sake of simplicity, only the graphs related to the colocalized signals of γ-H2AX and 53BP1 are reported (Figure 4.12).

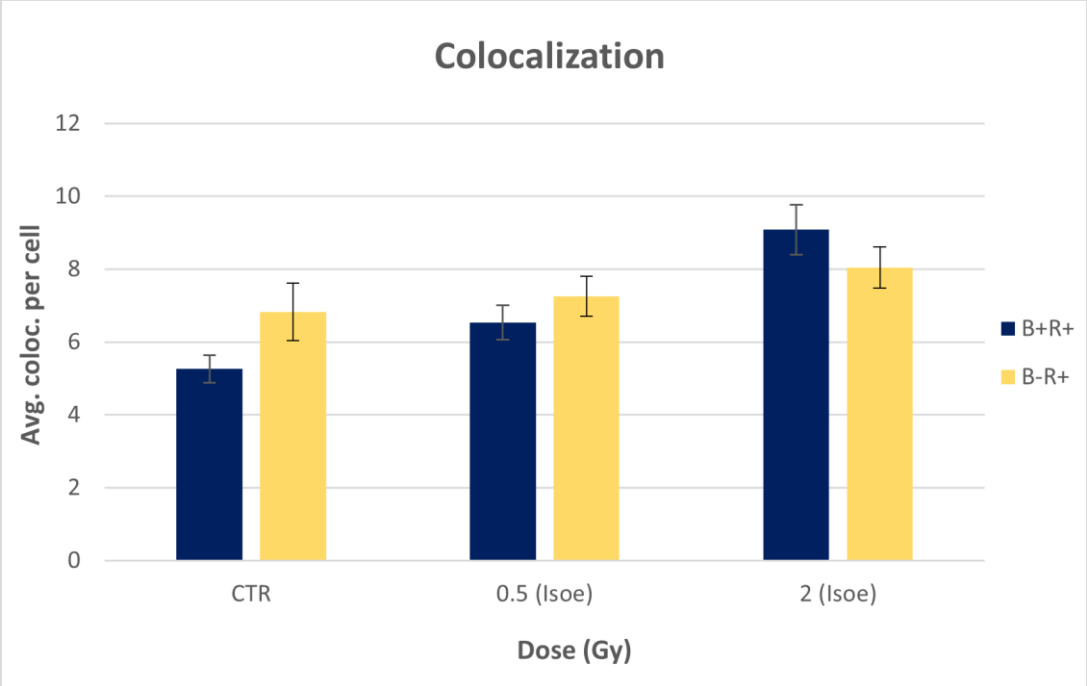

Figure 4.12 Comparison of the average number of colocalized foci between B+R+ (blue) and B-R+ (yellow) samples. The time point considered is 30 minutes post irradiation.

The neutron can interact with nuclei other than boron, through scattering reactions with hydrogen atoms and capture reactions with hydrogen and nitrogen atoms, whose products may damage the cellular DNA. This could lead to higher damage in B-R+ samples. In this context, damages are comparable within the errors for both doses, in line with the calculation of the iso-effective dose.

At 24 hours post-irradiation (Figure 4.13), a greater occurrence of damage is observed in B-R+ samples compared to the same samples fixed at 30 minutes post-irradiation. Instead, comparing with B+R+ samples (in blue), B-R+ samples (in yellow) show higher residual damage at 24 hours post-irradiation.

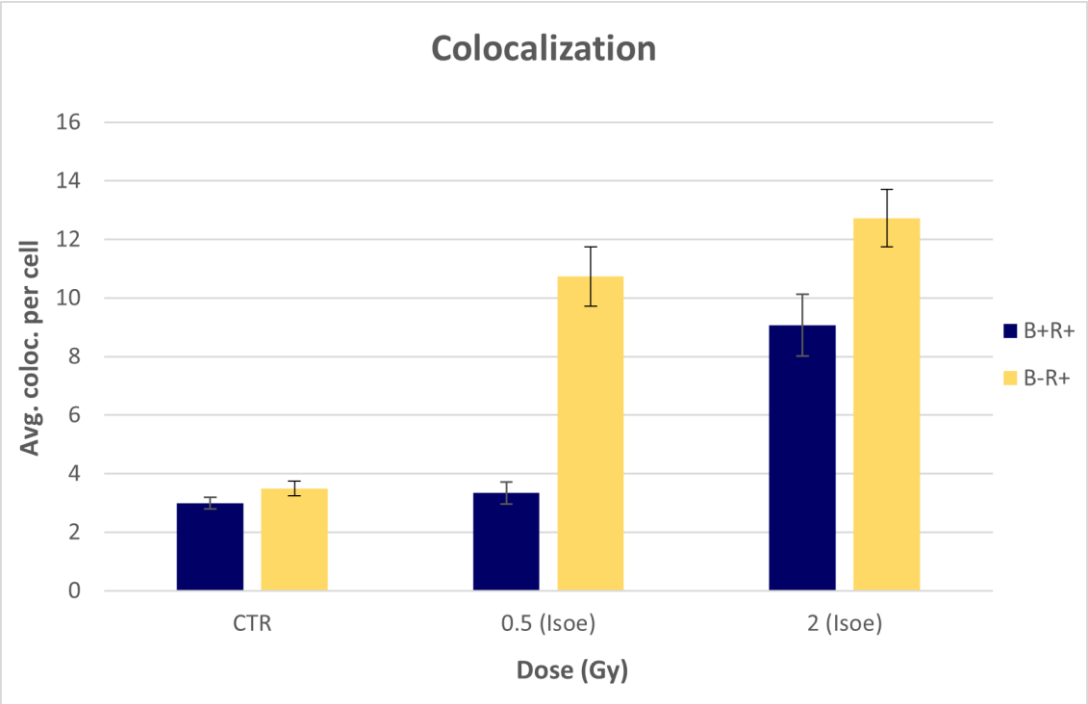

Figure 4.13 Comparison of the average number of colocalized foci between B+R+ (blue) and B-R+ (yellow) samples. The time point considered is 24 hours post irradiation.

4.1.4 Comparison between the treatments

Considering the second BNCT experiment conducted (of which the data are considered reliable), the experiment conducted with neutron beam without f-^{10}BPA and the X-rays experiment conducted on UMR-106, an appropriate comparison of the DNA damage induced by these different treatments is shown in Figure 4.14.

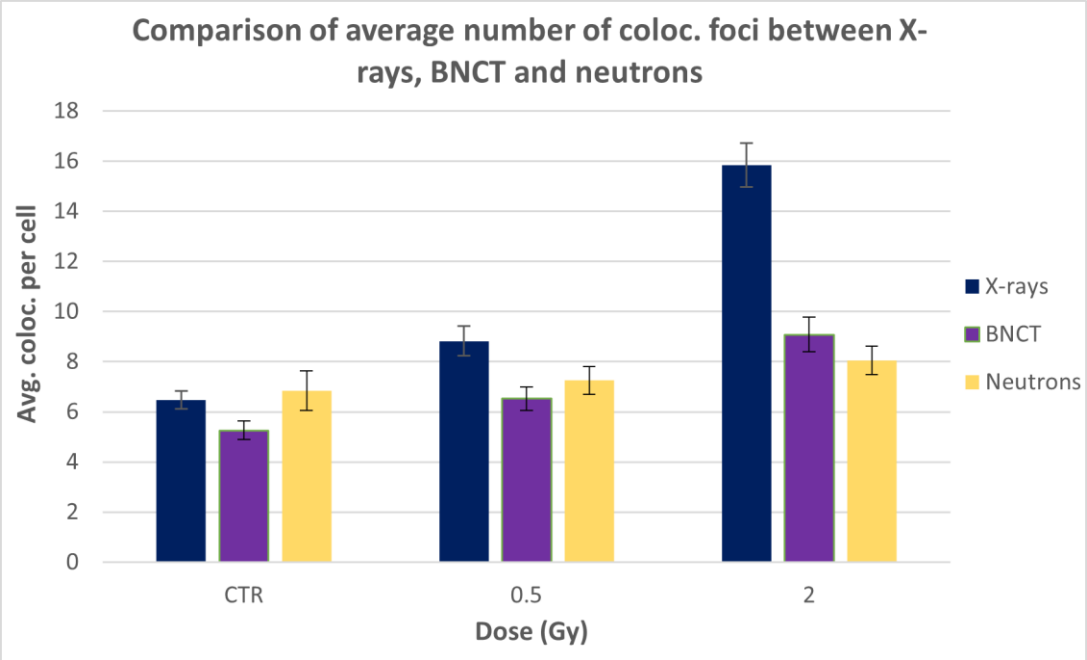

Figure 4.14 Average number of colocalized signals per cell**:** comparison between non-irradiated cells (CTR), cells irradiated with X-rays, cells without BPA irradiated with a neutron beam (Neutrons) and cells with BPA irradiated with a neutron beam (BNCT), at different isoeffective doses. The time point considered is 30 minutes post irradiation.

The quantification of foci per nucleus (Figure 4.14) demonstrated that the focus number was higher in cells irradiated with X-rays than in cells irradiated with neutrons (N) and BNCT. This is consistent with the findings reported by Rodriguez et al. in 2018, where a similar trend of higher damage was observed for the photon irradiation. However, when measuring the focus size, they observed that it was higher in the BNCT group. It is possible that the damage results in a higher number with X-rays treatment but is more complex in the case of BNCT because

DSBs induced by high linear energy transfer (LET) radiation are densely concentrated in clusters [49].

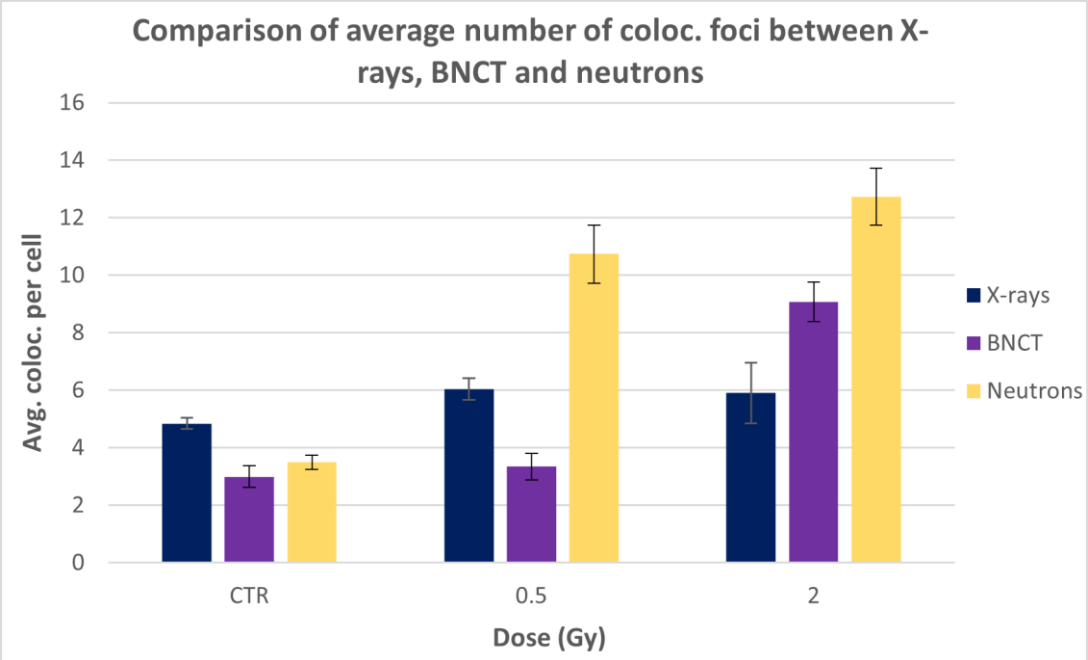

Figure 4.15 Average number of colocalized signals per cell: comparison between non-irradiated cells (CTR), cells irradiated with X-rays, cells without BPA irradiated with a neutron beam (Neutrons) and cells with BPA irradiated with a neutron beam (BNCT), at different isoeffective doses. The time point considered is 24 hours post irradiation.

After 24 hours the focus frequencies tended to decrease in all treatment groups, except for irradiation with neutrons beam, which shows a higher residual damage.

4.2 Results of radiation-induced DNA damage on U87

In the following paragraphs, the results of the damage induced on U87 following treatment with X-rays, BNCT and neutron beam (without f-^{10}BPA) will be presented. Subsequently, a comparative analysis between the treatments will be discussed.

4.2.1 Results of DNA damage induced by X-rays

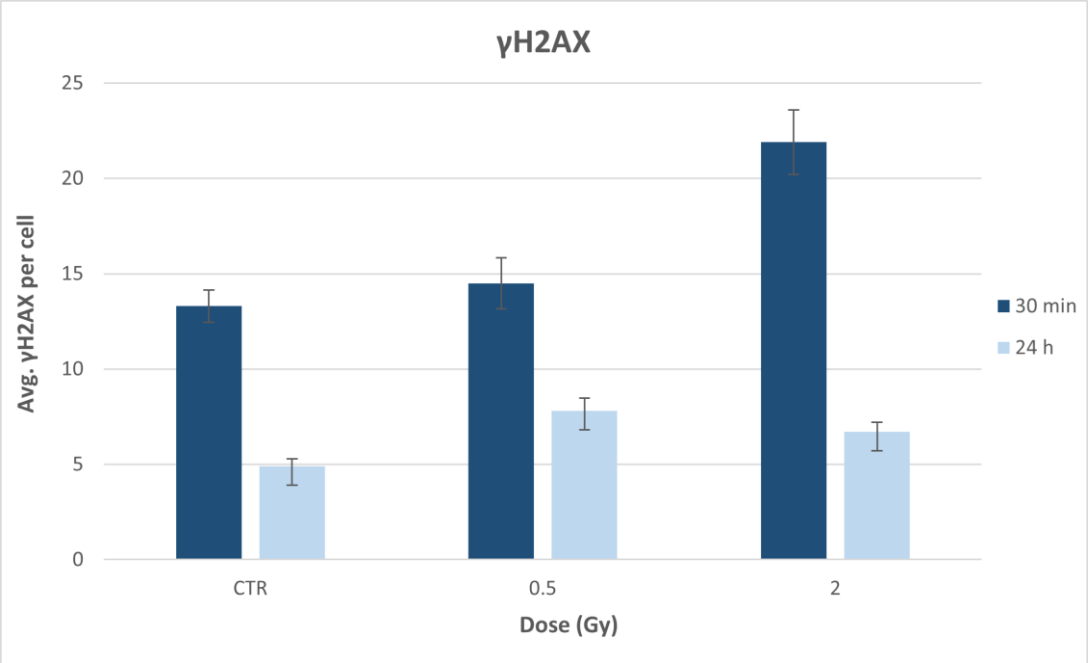

Figure 4.16 Average number of γ-H2AX foci per cell.

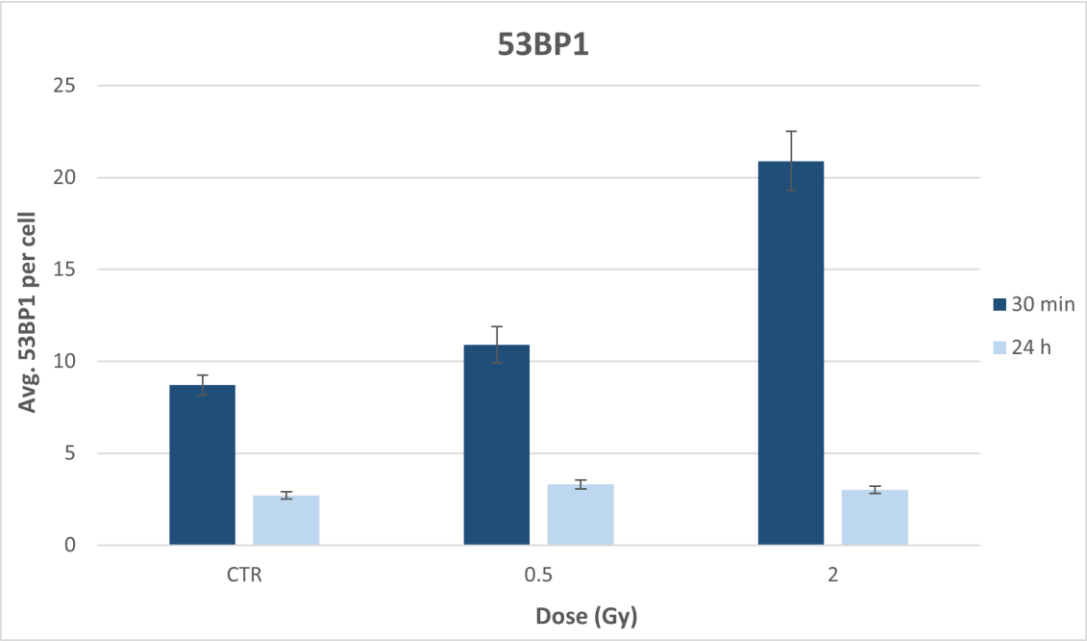

Figure 4.17 Average number of 53BP1 foci per cell.

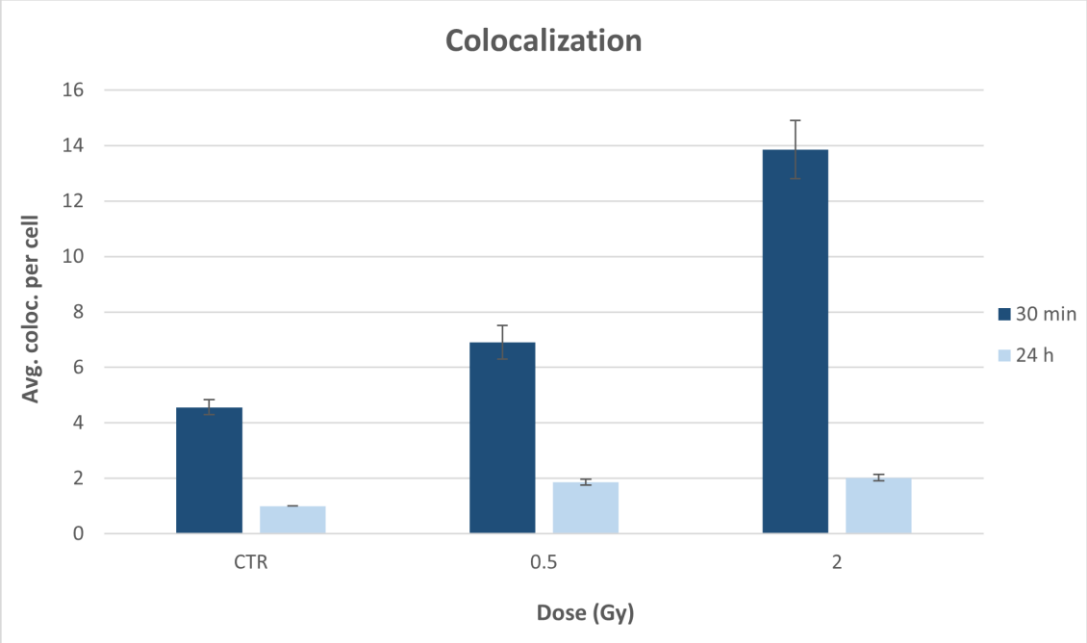

Figure 4.18 Average number of colocalized signals per cell.

As shown in the graphs (Figure 4.16, 4.17, and 4.18), U87 cells were exposed to 0.5 Gy and 2 Gy of X-rays, and the results were compared with the control sample with fixation performed at 30 minutes (in blue) and 24 hours post-irradiation (light blue). It is observed that:

- At 30 minutes post-irradiation, there is an increase in damage correlating with the dose, observed in both γH2AX and 53BP1 signals, as well as in colocalization signals, a trend similar to that obtained with the UMR-106 cell line. This finding is in line with the decrease in cell survival observed with increasing radiation dose in a previous study conducted at the Departments of Physics and Clinical-Surgical, Diagnostic, and Pediatric Sciences at the University of Pavia, in which survival curves obtained by irradiating U87 cells at different doses with X-rays clearly show that as the absorbed dose increases, cell survival decreases.
- At 24 hours post-irradiation, a situation comparable to that observed in UMR-106 is observed, with an unexpected lower value recorded for samples exposed to higher doses (2 Gy), probably correlated with the phenomenon observed in the study by Marková et al. 2011 [46]. Moreover, the number of foci is significantly lower at 24 hours, compared to the damage obtained at 30 minutes post-irradiation, probably attributed to the activation of DNA repair processes or apoptosis by irradiated cells in response to radiation-induced damage.

4.2.2 Results of DNA damage induced by BNCT treatment

For BNCT experiment, U87 were seeded on glass coverslip (24 x 24 mm) in a 6-wells plate (35 mm) at a density of 4.0×10^4 cells two days before the treatment. The samples were prepared considering treatment both in the presence and absence of f-^{10}BPA (control sample). Neutron irradiations were conducted in the thermal column of the TRIGA Mark II nuclear reactor at the University of Pavia and the dose was calculated to be isoeffective to 0.5 Gy and 2 Gy of photons, corresponding to power levels of 1 kW and 4 kW, respectively, at the reactor.

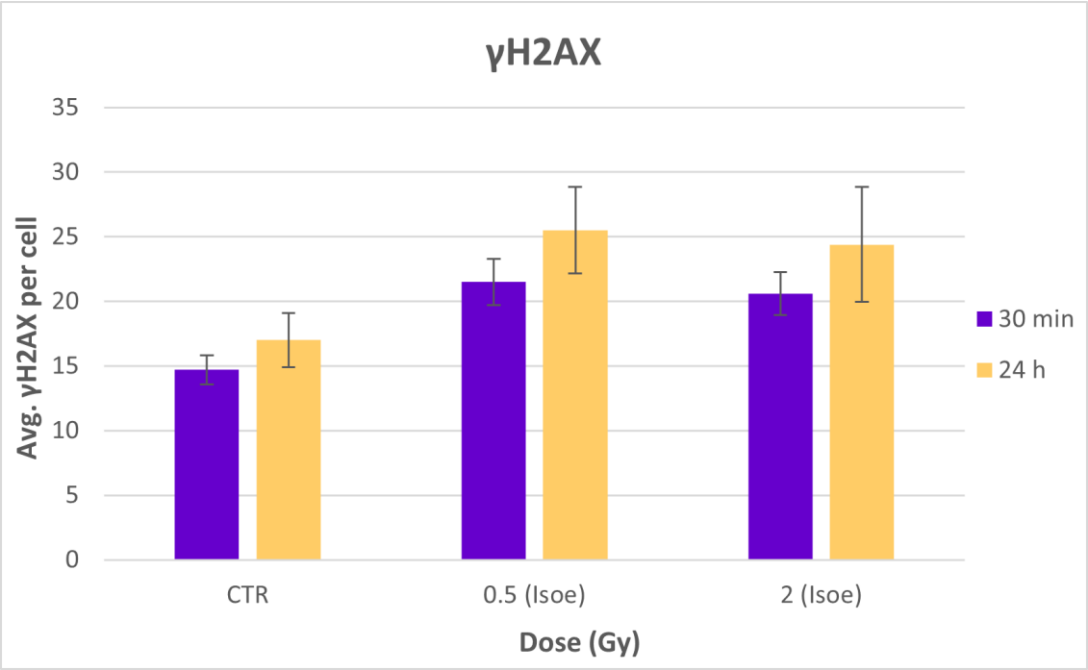

Figure 4.19 Average number of γ-H2AX foci per cell.

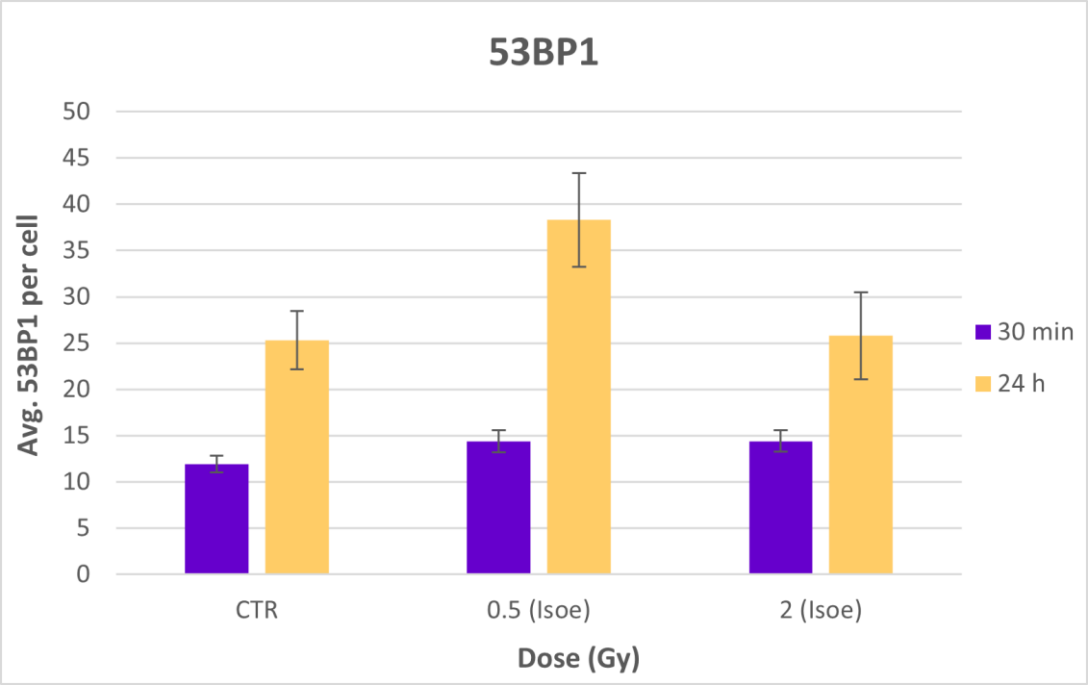

Figure 4.20 Average number of 53BP1 foci per cell.

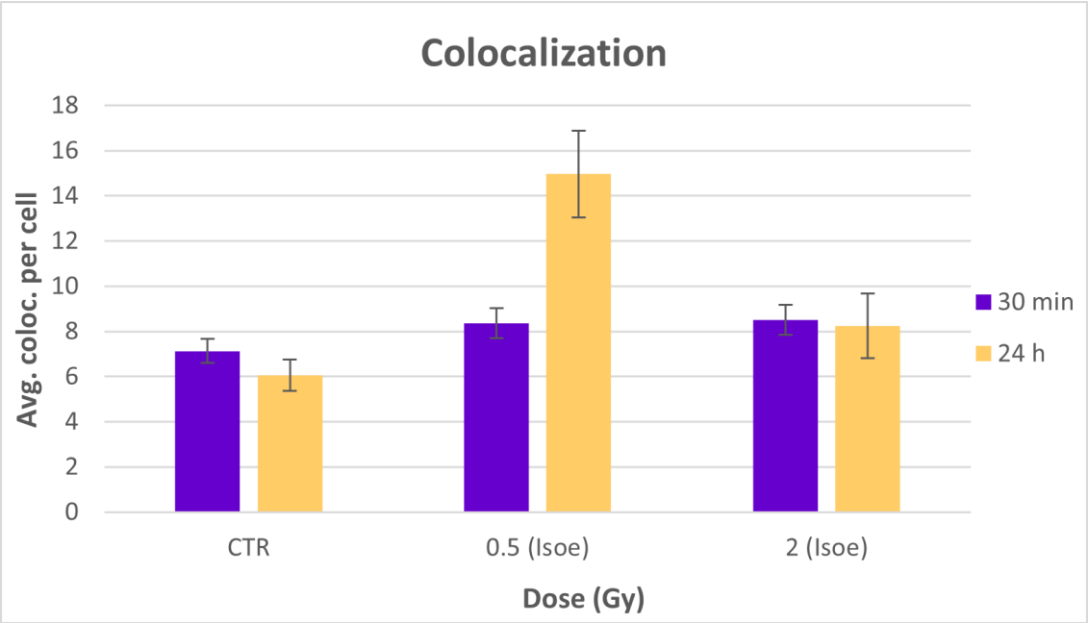

Figure 4.21 Average number of colocalized signals per cell.

As shown in Figures 4.19, 4.20, and 4.21, U87 cells were exposed to dose isoeffective to 0.5 Gy and 2 Gy, and the results were compared with the control sample with fixation performed at 30 minutes (in violet) and 24 hours post-irradiation (in yellow). For this treatment carried out on U87 cell line, the interpretation of the data obtained is not straightforward. It can be observed that:

- At 30 minutes after irradiation, the value of damage as given by foci frequency following the dose isoeffective to 2 Gy is very close to that obtained with with that isoeffective to 0.5 Gy treatment.
- At 24 hours after irradiation, it seems that the residual damage is greater than the data obtained after 30 minutes (especially at dose isoeffective to 0.5 Gy). Evidently, the cells do not repair immediately, given the strong initial damage. Additionally, the samples exhibit a significant loss of cells, complicating the analysis.

Moreover, under fluorescence microscopy examination, it was observed that cells fixed at 24 hours post-irradiation, including control cells, display evident signs of stress, the cause of which

remains unclear (Figure 4.22). Further experiments would be appropriate to fully understand the observed events.

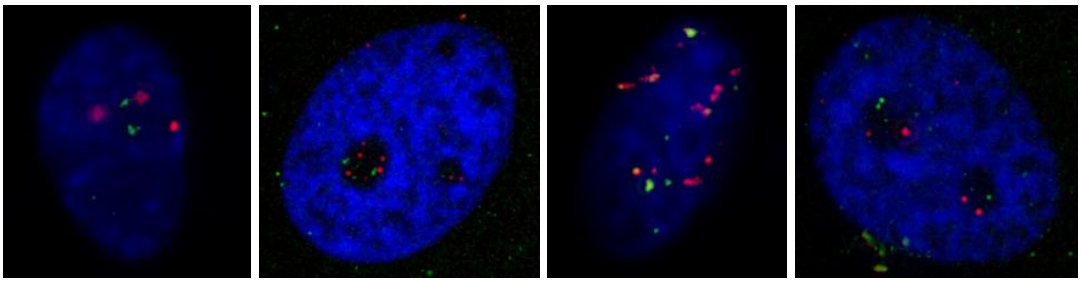

Figure 4.22 Comparison between a control cell fixed at 30 minutes post-irradiation, a control cell fixed at 24 hours post-irradiation, a cell treated with a dose isoeffective to 0.5 Gy and fixed at 30 minutes post-treatment, and a cell treated with a dose isoeffective to 0.5 Gy and fixed at 24 hours post-treatment. These images were obtained using the Metafer software with a 63x objective.

4.2.3 Results of DNA damage induced by neutron irradiation

The subsequent results show the damage caused by neutron irradiation in samples without f-^{10}BPA. The dose was calculated to be iso-effective at 0.5 Gy and 2 Gy of photons, which, considering only the contribution of neutrons, corresponds to power levels of 10 kW and 60 kW at the Triga reactor.

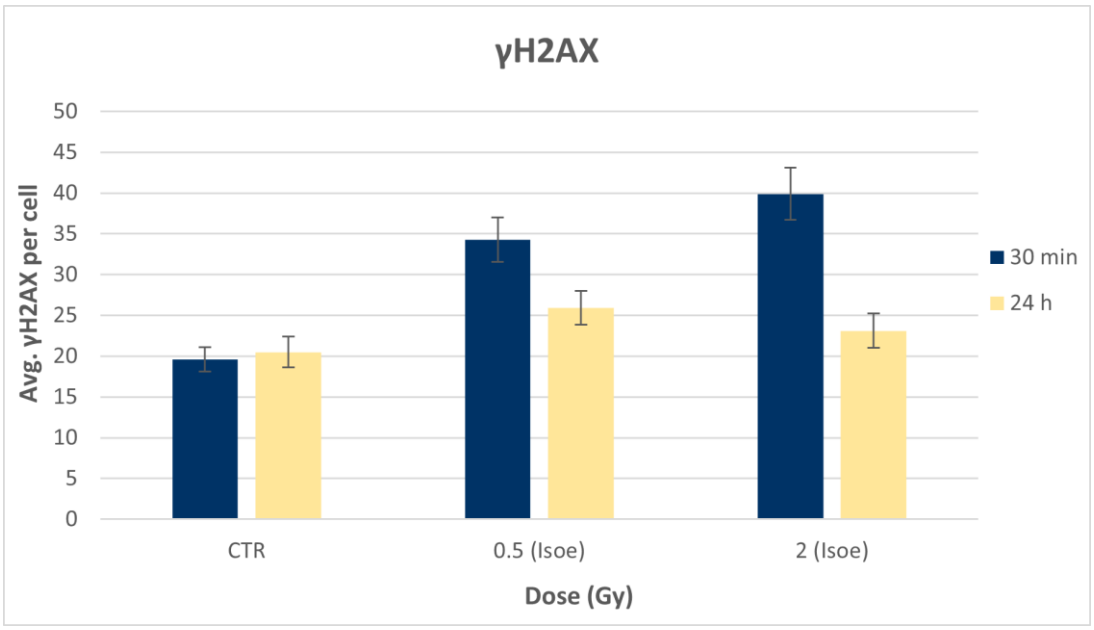

Figure 4.23 Average number of γ-H2AX foci per cell.

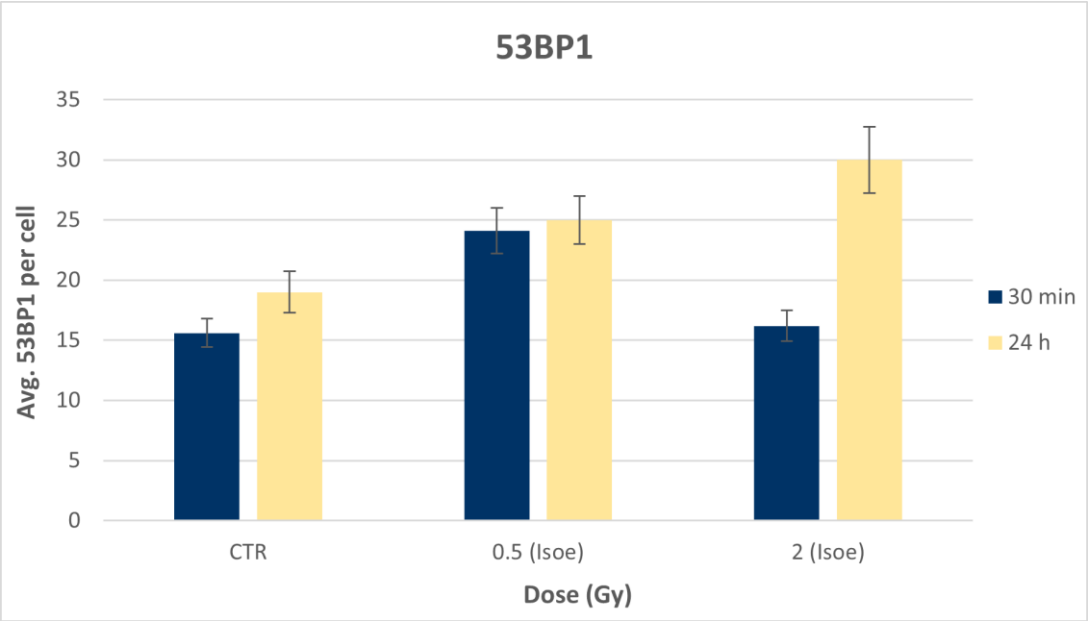

Figure 4.24 Average number of 53BP1 foci per cell.

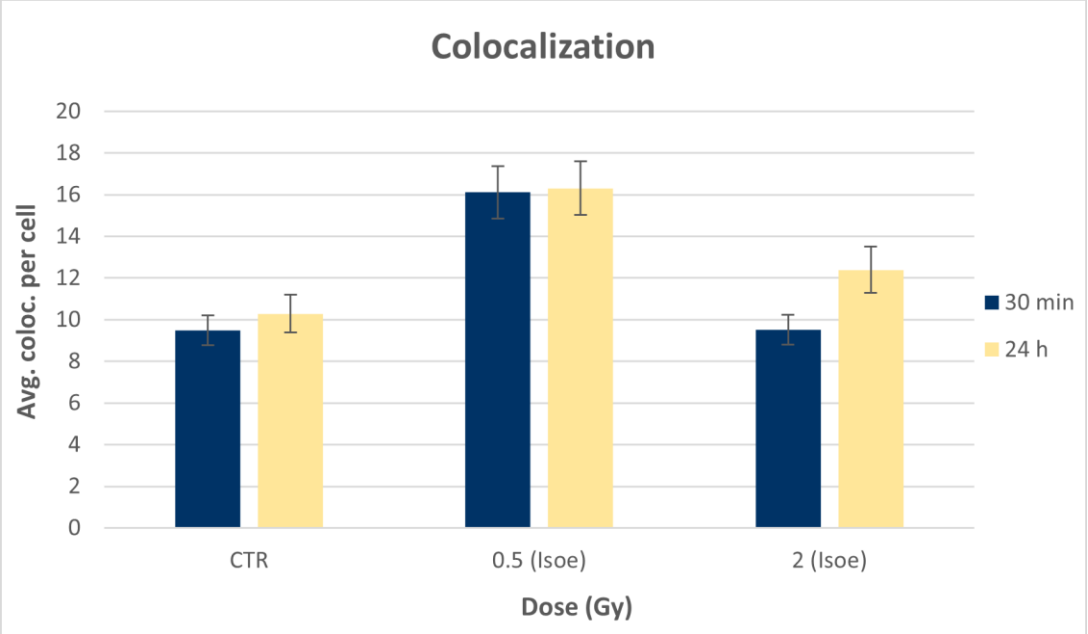

Figure 4.25 Average number of colocalized signals per cell.

U87 treated with neutron beam show very high damage, in particular from signals relating to individual markers. The residual damage at 24 hours remains very high, almost comparable to the damage observed at 30 minutes.

4.2.4 Comparison between the treatments

An appropriate comparison of the DNA damage induced by the three different treatments on U87 is shown in Figure 4.26 and 4.27.

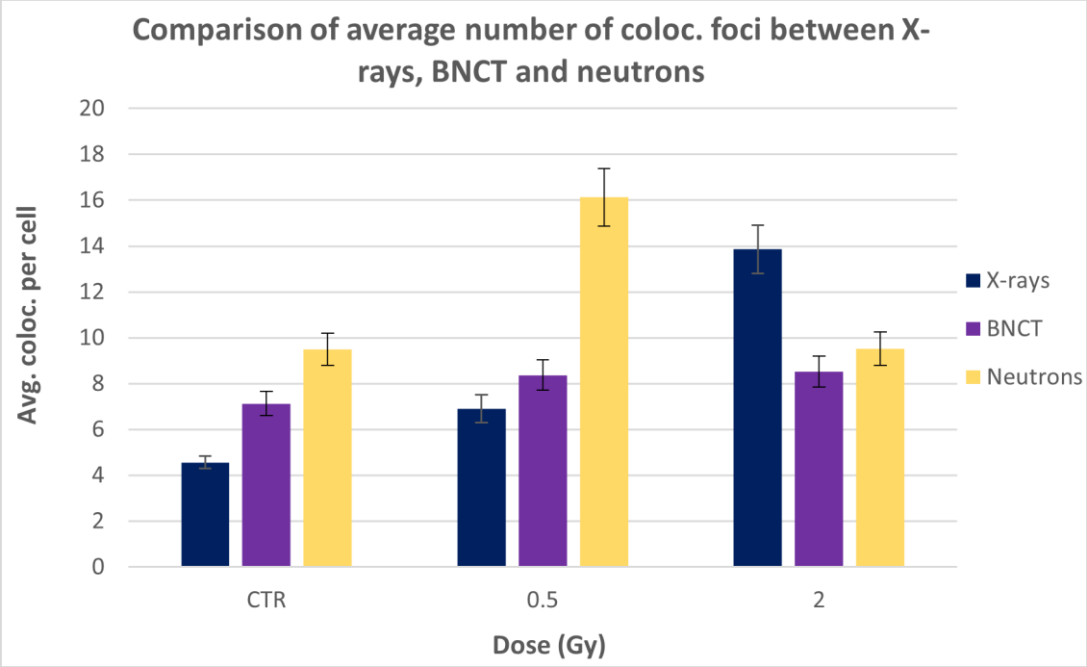

Figure 4.26 Average number of colocalized signals per cell: comparison between non-irradiated cells (CTR), cells irradiated with X-rays, cells without BPA irradiated with a neutron beam (Neutrons) and cells with BPA irradiated with a neutron beam (BNCT), at different isoeffective doses. The time point considered is 30 minutes post irradiation.

At 30 minutes, an increasing damage is observed as a function of the dose after the X-ray treatment, with a number of foci at a dose isoeffective to 2 Gy higher than the treatment conducted with BNCT and neutron beam alone. At a dose isoeffective to 0.5 Gy, particularly high damage was observed following treatment with neutrons (samples without f-^{10}BPA). However, as already mentioned, the data obtained with BNCT require validation through further experiments.

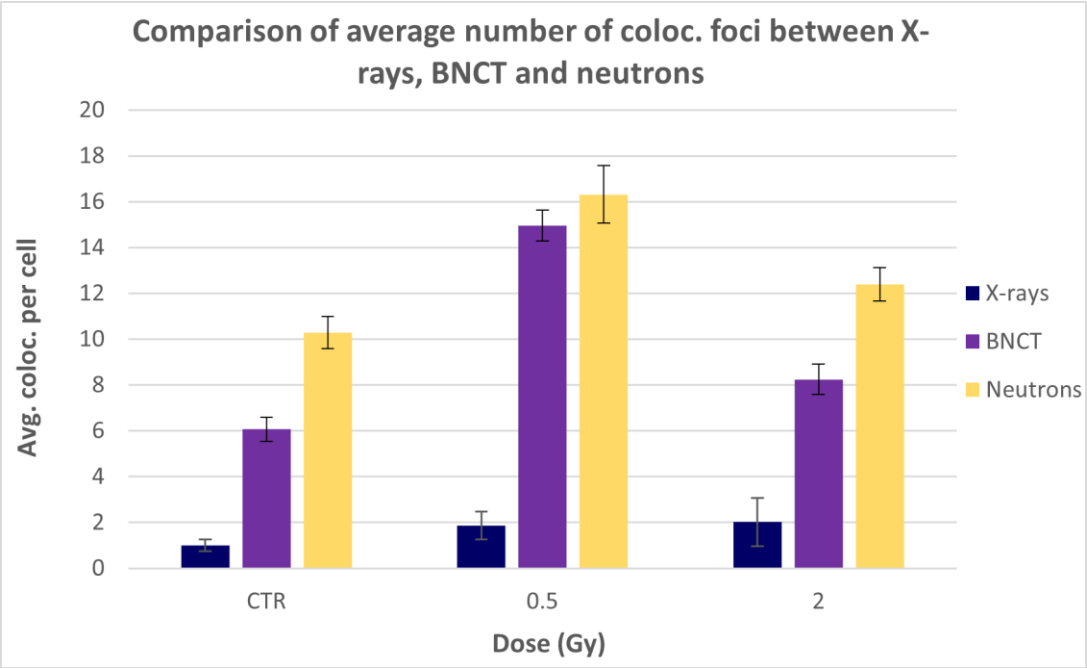

Figure 4.27 Average number of colocalized signals per cell: comparison between non-irradiated cells (CTR), cells irradiated with X-rays, cells without BPA irradiated with a neutron beam (Neutrons) and cells with BPA irradiated with a neutron beam (BNCT), at different isoeffective doses. The time point considered is 24 hours post irradiation.

At 24 hours, the damage observed with BNCT and neutron beam appears to be significantly higher compared to X-rays. This could suggest better repair at 24 hours after X-ray treatment, while damage resulting from BNCT and neutrons alone may be more complex to repair, resulting in greater residual damage.

CONCLUSIONS AND FUTURE PROSPECTIVES

This thesis work represents only a part of a broader study on the evaluation of the effectiveness of BNCT and its application in the treatment of glioblastoma multiforme and osteosarcoma.

Additional experiments, especially on the glioblastoma U87 cell line, are required due to the observed cellular stress, the cause of which remains unclear, as it was not observed in the case of treatment with neutron beams or X-rays on the same cell line.

In general, both U87 and UMR-106 cells exhibited a dose-dependent increase in damage 30 minutes after irradiation, with elevated damage compared to the control sample in all treatments. At 24 hours, the damage observed in U87 cells following BNCT and neutron beam treatments appears to be significantly higher compared to X-rays. This could be attributed to the fact that, at an equivalent dose, damages caused by BNCT and neutrons (high-LET radiation) may be more complex to repair than low-LET radiation (X-rays in this case), resulting in greater residual damage. For UMR-106 cells, after 24 hours, the foci frequency tended to decrease in all treatment groups compared to the samples observed after 30 minutes, except for irradiation with a neutron beam. However, further experiments are needed to confirm these results.

Another crucial observation is that, in samples where damage was observed 24 hours post-irradiation, both for UMR-106 and U87 cells, a severe loss of cells was observed following BNCT treatment. This has complicated the analysis of damage and the foci counting through the Metafer system. In contrast, no sample treated with X-rays or neutron beam (in the absence of f-^{10}BPA) exhibited such a severe loss of cells. This could be directly related to the efficiency of BNCT in terms of cellular damage and death.

A further optimization of this technique will be a deeper insight into the boron taken up in cells treated with BNCT in order to calculate the dose with higher accuracy to be sure of irradiating cells with Isoeffective dose values compared to photon irradiation.

In conclusion, this thesis work has contributed to a deeper understanding of the effects of BNCT on the U87 and UMR-106 cell lines. The results suggest that BNCT may have induced more complex damage and higher cellular mortality compared to treatments with X-rays or neutron beams. However, the understanding of certain observed phenomena, such as cellular stress in U87 or the significant loss of cells in all samples treated with BNCT, requires further confirmatory investigations. This study may pave the way for future research aimed at elucidating the molecular mechanisms involved in repair processes, understanding the complexity of damage, and cellular stress induced by BNCT, in order to support the efficacy of BNCT in the treatment of difficult-to-treat tumours.

This work represents just a chapter in this evolving story, with the hope of pioneering new frontiers in the fight against tumours resistant to conventional therapies.

BIBLIOGRAPHY

[1] Hall, Eric J., and Amato J. Giaccia. Radiobiology for the Radiologist. Vol. 6. 2006.

[2] Seneviratne, Danushka, et al. "Exploring the biological and physical basis of boron neutron capture therapy (BNCT) as a promising treatment frontier in breast cancer." Cancers 14.12 (2022): 3009.

[3] Hada, Megumi, and Alexandros G. Georgakilas. "Formation of clustered DNA damage after high-LET irradiation: a review." Journal of radiation research 49.3 (2008): 203-210.

[4] Nomoto, Takahiro, et al. "Poly (vinyl alcohol) boosting therapeutic potential of p-boronophenylalanine in neutron capture therapy by modulating metabolism." Science Advances 6.4 (2020): eaaz1722.

[5] Popp, Henning D., et al. "Immunofluorescence Microscopy of γH2AX and 53BP1 for Analyzing the Formation and Repair of DNA Double-strand Breaks." JoVE (Journal of Visualized Experiments) 129 (2017): e56617.

[6] Ogony, Joshua. "Effects of combined exposure to ethanol and ionizing radiation on the antioxidant status of in vitro and in vivo models." (2007).

[7] Iliakis, George, Emil Mladenov, and Veronika Mladenova. "Necessities in the processing of DNA double strand breaks and their effects on genomic instability and cancer." Cancers 11.11 (2019): 1671.

[8] Aggarwal, L. "Biological effects of ionizing radiation." Shodh Prerak 4.1 (2014): 342-348.

[9] Nakata, Akifumi, et al. "Cytogenetic Biodosimetry in Radiation Emergency Medicine: 3. The Basics of Chromosomes for Biodosimetry." Radiation Environment and Medicine 11.2 (2022): 82-90.

[10] Chaffey, Nigel. "Alberts, B., Johnson, A., Lewis, J., Raff, M., Roberts, K. and Walter, P. Molecular biology of the cell. 4th edn." (2003): 401-401.

[11] Phillips, Rob, et al. Physical biology of the cell. Garland Science, 2012. Caldecott, Keith W. "Single-strand break repair and genetic disease." Nature Reviews Genetics 9.8 (2008): 619-631.

[12] Van der Schans, Govert Paulus, M. C. Paterson, and W. G. Cross. "DNA strand break and rejoining in cultured human fibroblasts exposed to fast neutrons or gamma rays." International Journal of Radiation Biology and Related Studies in Physics, Chemistry and Medicine 44.1 (1983): 75-85.

[13] Huang, Rui-Xue, and Ping-Kun Zhou. "DNA damage response signaling pathways and targets for radiotherapy sensitization in cancer." Signal transduction and targeted therapy 5.1 (2020): 60.

[14] Lennartsson, Johan, Jorgen Carlsson, and Bo Stenerlow. "Targeting the epidermal growth factor receptor family in radionuclide therapy of tumors-signal transduction and DNA repair." Letters in Drug Design & Discovery 3.6 (2006): 357-368.

[15] Noubissi, Felicite K., et al. "Detection and quantification of γ-H2AX using a dissociation enhanced lanthanide fluorescence immunoassay." Scientific reports 11.1 (2021): 8945.

[16] DeWeese, Theodore L., and Marikki Laiho, eds. Molecular determinants of radiation response. Springer Science & Business Media, 2011.

[17] Malouff, Timothy D., et al. "Boron neutron capture therapy: a review of clinical applications." Frontiers in oncology 11 (2021): 351.

[18] Kumada, Hiroaki, Takeji Sakae, and Hideyuki Sakurai. "Current development status of accelerator-based neutron source for boron neutron capture therapy." EPJ Techniques and Instrumentation 10.1 (2023): 18.

[19] Castro, Vinícius A., et al. "MCNP to study the BF 3 detection efficiency." (2011).

[20] Kotiluoto, Petri. "Adaptive tree multigrids and simplified spherical harmonics approximation in deterministic neutral and charged particle transport." VTT Publications (2007).

[21] Porcari, Paola, Silvia Capuani, and Francesco Saverio Pastore. "Novel Pharmacological and Magnetic Resonance Strategies to Enhance Boron Neutron Capture Therapy (BNCT) Efficacy in the Clinical Treatment of Malignant Glioma." Management of CNS Tumors 267 (2011).

[22] Jin, Will H., et al. "A review of boron neutron capture therapy: Its history and current challenges." International journal of particle therapy 9.1 (2022): 71-82.

[23] Fukuda, Hiroshi. "Response of normal tissues to boron neutron capture therapy (BNCT) with 10B-borocaptate sodium (BSH) and 10B-paraboronophenylalanine (BPA)." Cells 10.11 (2021): 2883.

[24] Detta, Allah, and Garth S. Cruickshank. "L-amino acid transporter-1 and boronophenylalanine-based boron neutron capture therapy of human brain tumors." Cancer research 69.5 (2009): 2126-2132.

[25] He, Huifang, et al. "The basis and advances in clinical application of boron neutron capture therapy." Radiation Oncology 16 (2021): 1-8.

[26] Postuma, Ian, et al. "An improved neutron autoradiography set-up for B concentration measurements in biological samples." Reports of Practical Oncology and Radiotherapy 21.2 (2016): 123-128.

[27] Yuan, Tai-Ze, Shu-Qing Xie, and Chao-Nan Qian. "Boron neutron capture therapy of cancer: Critical issues and future prospects." Thoracic Cancer 10.12 (2019): 2195.

[28] Suzuki, Minoru. "Boron neutron capture therapy (BNCT): A unique role in radiotherapy with a view to entering the accelerator-based BNCT era." International journal of clinical oncology 25.1 (2020): 43-50.

[29] Kawabata, Shinji, et al. "Accelerator-based BNCT for patients with recurrent glioblastoma: a multicenter phase II study." Neuro-oncology advances 3.1 (2021): vdab067.

[30] Hirose, Katsumi, et al. "Boron neutron capture therapy using cyclotron-based epithermal neutron source and borofalan (10B) for recurrent or locally advanced head and neck cancer (JHN002): An open-label phase II trial." Radiotherapy and Oncology 155 (2021): 182-187.

[31] Bortolussi, S., et al. "Neutron flux and gamma dose measurement in the BNCT irradiation facility at the TRIGA reactor of the University of Pavia." Nuclear Instruments and Methods in Physics Research Section B: Beam Interactions with Materials and Atoms 414 (2018): 113-120.

[32] Zonta, A., et al. "Extra-corporeal liver BNCT for the treatment of diffuse metastases: What was learned and what is still to be learned." Applied Radiation and Isotopes 67.7-8 (2009): S67-S75.

[33] Urbańska, Kaja, et al. "Glioblastoma multiforme–an overview." Contemporary Oncology/Współczesna Onkologia 18.5 (2014): 307-312.

[34] Kageji, Teruyoshi, et al. "Boron neutron capture therapy (BNCT) for newly-diagnosed glioblastoma: comparison of clinical results obtained with BNCT and conventional treatment." The Journal of Medical Investigation 61.3.4 (2014): 254-263.

[35] Moghaddasi, Leyla, and Eva Bezak. "An Integrated Monte Carlo Model for Heterogeneous Glioblastoma Treated with Boron Neutron Capture Therapy." Cancers 15.5 (2023): 1550.

[36] Bortolussi, S., et al. "Understanding the potentiality of accelerator based-boron neutron capture therapy for osteosarcoma: dosimetry assessment based on the reported clinical experience." Radiation Oncology 12 (2017): 1-12.

[37] Delgrosso, Elena, et al. "3D bioprinted osteosarcoma model for experimental boron neutron capture therapy (BNCT) applications: Preliminary assessment." Journal of Biomedical Materials Research Part B: Applied Biomaterials (2023).

[38] Skwierawska, Dominika, et al. "Clinical viability of boron neutron capture therapy for personalized radiation treatment." Cancers 14.12 (2022): 2865.

[39] Coderre, Jeffrey A., et al. "Derivations of relative biological effectiveness for the high-LET radiations produced during boron neutron capture irradiations of the 9L rat gliosarcoma in vitro and in vivo." International Journal of Radiation Oncology* Biology* Physics 27.5 (1993): 1121-1129.

[40] González, S. J., et al. "Photon iso-effective dose for cancer treatment with mixed field radiation based on dose–response assessment from human and an animal model: clinical application to boron neutron capture therapy for head and neck cancer." Physics in Medicine & Biology 62.20 (2017): 7938.

[41] Sato, Tatsuhiko, et al. "Microdosimetric modeling of biological effectiveness for boron neutron capture therapy considering intra-and intercellular heterogeneity in 10B distribution." Scientific reports 8.1 (2018): 988.

[42] Colautti, Paolo, et al. "Microdosimetric measurements in the thermal neutron irradiation facility of LENA reactor." Applied Radiation and Isotopes 88 (2014): 147-152.

[43] Viegas, Ana Mailén Dattoli, et al. "Detailed dosimetry calculation for in-vitro experiments and its impact on clinical BNCT." Physica Medica 89 (2021): 282-292.

[44] Master's Thesis of Erica Simeone, "Studi dosimetrici per la BNCT del Glioblastoma Multiforme con acceleratore", Department of Physics, University of Pavia, 2022

[45] Lucian, Zastko, et al. "Classifier Spot Count Optimization of Automated Fluorescent Slide Scanning System." Acta Medica Martiniana 22.1 (2022): 24-33.

[46] Markova, Eva, Jesper Torudd, and Igor Belyaev. "Long time persistence of residual 53BP1/γ-H2AX foci in human lymphocytes in relationship to apoptosis, chromatin condensation and biological dosimetry." International journal of radiation biology 87.7 (2011): 736-745.

[47] Sharma, Preety M., et al. "High throughput measurement of γH2AX DSB repair kinetics in a healthy human population." PloS one 10.3 (2015): e0121083.

[48] Clay, Delisa E., and Donald T. Fox. "DNA damage responses during the cell cycle: Insights from model organisms and beyond." Genes 12.12 (2021): 1882.

[49] Rodriguez, C., et al. "In vitro studies of DNA damage and repair mechanisms induced by BNCT in a poorly differentiated thyroid carcinoma cell line." Radiation and Environmental Biophysics 57 (2018): 143-152.

ACKNOWLEDGEMENTS

Durante questi anni universitari, ho capito quale vorrei che fosse il mio posto nel mondo. Ho avuto l'opportunità di esplorare appieno il significato della ricerca, immergendomi in una realtà in cui la sete di conoscenza non ha mai smesso di crescere. Ringrazio il Prof. Lorenzo Manti per avermi fatto conoscere il campo della Biofisica e per avermi dato l'opportunità di partecipare a questa realtà, trasmettendomi tutta la sua passione per la ricerca.

Desidero ringraziare la Prof.ssa Silva Bortolussi per l'opportunità straordinaria che mi ha concesso di contribuire alla ricerca nel campo della BNCT, per la fiducia che ha posto in me sin dal primo momento e per la possibilità che mi ha dato di conoscere e partecipare a diverse realtà. Questo percorso mi ha insegnato non solo a lavorare in laboratori diversi e a collaborare con molte persone, ma anche ad accrescere sempre di più la mia passione per la ricerca. Per tutto questo, le sono sinceramente grata.

Ringrazio il gruppo dell'Università di Pavia: la dott.ssa Cinzia Ferrari, la dott.ssa Laura Cansolino ed Elena Del Grosso, per avermi seguito con dedizione durante il mio periodo a Pavia e per l'accoglienza calorosa ed il supporto che mi hanno fornito. Desidero, inoltre, ringraziare Ian Postuma per l'immenso aiuto, la pazienza ed il tempo che mi ha dedicato durante ogni esperimento effettuato a Pavia.

Ringrazio il gruppo del Laboratorio di Biofisica delle Radiazioni: Pavel Bláha, Valerio Cosimo Elia, Francesca Fede e Valeria Cardamuro per avermi aiutata e supportata quando ne avevo bisogno e per aver arricchito il mio percorso con la loro simpatia e originalità.

Ringrazio il Prof. Mimmo Turano per i preziosi consigli forniti durante lo sviluppo della mia tesi e per la piena fiducia per questo lavoro. Ringrazio, inoltre, la dott.ssa Concetta Di Lorenzo per l'aiuto ed il supporto che mi ha fornito.

Ringrazio Maria Paola e Marzia: senza di voi, la mia esperienza a Pavia non sarebbe stata la stessa cosa. Siete state sempre vicine, aiutandomi quando ne avevo bisogno e supportandomi in ogni momento.

Ringrazio Stefania, mia grande amica. Le tue parole mi hanno sempre dato forza nei momenti difficili, hai sempre avuto fiducia in me, spesso più di quanto ne avessi io.

Ringrazio Alessia, anche a distanza, hai dimostrato appieno cosa significhi essere un'amica. Grazie per il tuo tempo, per le parole spese con saggezza, e per avermi accompagnato fino alla conclusione di questo percorso.

Ringrazio Rossella; con te al mio fianco, non mi sono mai sentita sola, nemmeno a chilometri di distanza. Sei sempre stata come una sorella per me.

Ringrazio Sofia, Claudio e Dario; con voi ho rimesso i piedi in montagna, ho imparato a vedere le cose "in prospettiva", ed ho capito che si tratta non solo di raggiungere la cima di una montagna, ma di affrontare le difficoltà della vita con occhi diversi.

Ringrazio Umberta, Giusy, Sara e Marco per la vostra instancabile presenza, per avermi sempre ascoltata e supportata.

Ringrazio Alessandra per essermi stata sempre accanto e prontamente disponibile ogni qual volta ne ho avuto bisogno. La tua presenza costante è stata fondamentale durante ogni sfumatura di questi anni.

Ringrazio Sissi e Arcangelo ed i miei fratelli “acquisiti” Sara e Carmine: ognuno di voi ha saputo darmi il suo aiuto ed il proprio tempo quando ne ho avuto bisogno, siete sempre stati in prima linea per sostenermi.

Ringrazio Angelo, Greta, Andrea e Aurora. Ogni vostro sorriso, i vostri dolci abbracci e i momenti di leggerezza passati insieme hanno alleggerito il mio cuore durante questi anni.

Ringrazio mio padre per aver sempre sostenuto e supportato le mie scelte, senza mai contrastarle. La cosa più importante per me è stata comprendere quanto tu avessi fiducia in me in questi anni. Ti sono grata per i valori che mi hai trasmesso, come la perseveranza, la caparbietà e l’immensa passione che metti nel tuo lavoro. Questi valori hanno profondamente influenzato il mio ruolo in questa vita.

Infine, ringrazio la mia mamma. Nonostante sia stato un anno difficile per te, hai sempre cercato di starmi accanto e di farti in quattro per me. Senza il tuo aiuto non sarei andata avanti con la forza che sono riuscita a trovare. Mi sento grata di averti potuto abbracciare ogni volta che ne ho avuto bisogno. A te che stai lottando, dedico questo lavoro.